Design and Fabrication of MEMS Microheater for Gas Sensing Applications

A Thesis

Submitted in partial fulfillment of the requirements for the award of the degree of

Doctorate in Philosophy

in

Electronics & Communication Engineering Department

by

Manish Deshwal

Reg No: 901306008

Under the supervision of

Dr. Anil Arora

Assistant Professor, ECED

Thapar Institute of Engineering & Technology,

Patiala-147004, India

July, 2018

Candidate Declaration

I hereby certify that the work, which is being presented in the thesis, entitled Design and Fabrication of MEMS Microheater for Gas Sensing Applications, in partial fulfilment of the requirements for the award of the degree of Doctor of Philosophy in Electronics and Communication Engineering from Thapar Institute of Engineering and Technology, Patiala is an authentic record of my own work carried out during the period July 2013 to July 2018 under the supervision of Dr. Anil Arora. I have also cited the reference about the text(s)/figure(s)/table(s) from where they have been taken. The matter presented in this thesis has not been submitted elsewhere for the award of any other degree or diploma from any institution.

Date: 19th April 2019.

Manish Deshwal

Candidate

This is to certify that the above statement made by the candidate is correct to the best of my knowledge.

19/4/19

Date:

Dr. Anil Arora

Assistant Professor Supervisor

.....dedicated to

my parents, my wife

and my brother

Abstract

Recent technological advancements have adverse effects on mankind including environmental (air) pollution due to rapid industrialization, chemical pollution due to increased use of pesticides in agriculture and some unforeseen effects of genetically modified food stuff affecting the health of living organisms as well as the ecosystem. Hence, efficient sensors are essentially required to detect these pollutants at the first step only. Nowadays, efforts are continuing towards the realization of smart and intelligent systems which combine sensors with necessary electronics to make a portable or wireless sensor.

Acetone vapours/gas having a pungent and irritating smell is toxic if inhaled directly. Acetone is released in environment both by the natural and anthropogenic (man-made) sources. The main sources of acetone emission are industrial sources as a result of chemicals manufacturing, non-ferrous materials, plastic products, printing processes, and sewage and drainage services and also from coal mining. The other natural sources are volcanic gases and forest fires. The acetone is also present in the vehicle exhausts and also from railway operations, and even from tobacco smoke. Acetone being highly flammable and/or explosive in nature when mixed with some peroxides or strong oxidants, is also present in the consumer products such as paint and varnish removers, thinners, paints and primers etc. Thus, there will always be need to detect the leakage of the acetone in any form within a premises or environment. As acetone is heavier than air, it may travel along the surface to a hot equipment or flames which can caught fire causing distant ignition even in lowered concentrations. Hence, to prevent a disastrous situation the acetone sensor must be installed to detect any leakage.

Sensors of this kind have a simple design that makes mass production feasible and is strongly linked to the availability of better sensing materials with improved functional properties. The phenomenon of change in the resistance of semiconducting sensing element in the presence of a reducing or an oxidizing gas while being operating at elevated temperatures is the basic principle of operation of semiconducting metal oxide gas sensors. Later, demand for enhanced sensitivity and fast response speed led to the development of thin film based sensing devices. Currently, worldwide efforts are focused in both the basic as well as applied areas and there is continued interest in developing new sensing materials along with novel design structures for obtaining improved sensing response characteristics.

The fabricated sensor is then tested with a newly designed coplanar architectured for inter digitated electrodes and the microheater for improving the sensing efficiency of the sensor by improving the increased uniform area for heating of the sample. Finally the results are discussed for each sensor fabricated in respective sections.

List of Publications

Published:

- ✓ ***Springer Nature:***

  Journal of Materials Science: Materials in Electronics

  Title: Enhanced acetone detection using Au doped ZnO thin film sensor

  M. Deshwal and A. Arora Enhanced acetone detection using Au doped ZnO thin film sensor *Journal of Materials Science: Materials in Electronics* pp. 1-6 (2018).

- ✓ ***NISCAIR:***

  Indian Journal of Pure and Applied Physics

  Title: Enhanced Sensitivity with Thickness Optimization of ZnO based Acetone Sensor

  A. Arora and M. Deshwal Enhanced sensitivity with thickness optimization of ZnO based acetone sensor *Indian Journal of Pure & Applied Physics (IJPAP)* 56 pp. 367-372 (2018)

Under Review:

- ✓ **Indian Journal of Pure and Applied Physics**

  Title: Annealing Temperature Optimization for Highly Sensitive ZnO based Acetone Gas Sensor

  Present Status: Under Review

Other Scopus Indexed or International Journals:

- ✓ **American Scientific Publishers**

  Sensor Letters

  Title: Thermally Efficient Coplanar Architecture of Microheater and Inter-Digitated Electrodes for Nanolayered Metal Oxide based Hydrogen Gas Sensor

  Status: Accepted

- ✓ **IEEE Explore Digital Library**

  Conference Proceedings of "International Conference on Emerging Trends in Computing and Communication Technologies 2017"

  Paper Title: A highly sensitive Pt-doped ZnO based Ethanol sensor
  Authors: Manish Deshwal, Anil Arora

List of Conference Publications

- ✓ **Proceedings of National Conference of "Advances in Metrology"** (AdMet 2014)at Thapar University, Patiala (February 19-21, 2014).

  Paper Title: Uniform Temperature Distribution of MEMS Micro-heater for Efficient MEMS based Gas Sensors

  Authors: Palak Bhatt, Manish Deshwal, Anil Arora

- ✓ **Proceedings of 2nd National Conference on "Multifunctional Advanced Materials"** from May 11-13, 2016 at Shoolini University –Solan, Himachal Pradesh

  Paper Title: ZnO thin film based Acetone Sensor

  Authors: Manish Deshwal, Monika Tomar, Vinay Gupta, Anil Arora

- ✓ **Proceedings of 4th National Conference on "Nanoscience and Instrumentation Technology**" (NCNIT-2016) during June 04-05, 2016 at Department of Physics, National Institute of Technology, Kurukshetra

  Paper Title: ZnO thin film based Acetone Sensor

  Authors: Manish Deshwal, Monika Tomar, Vinay Gupta, Anil Arora

- ✓ Presented at **3rd ISSE National Conference – 2017, National Conference on Complex Engineering Systems of National Importance: Current Trends & Future Perspective** OCTOBER 12–13, 2017, Indian School of Business, Mohali Organised by ISSE - Chandigarh Chapter & Semi-Conductor Laboratory, Department of Space

  Paper Title: A Coplanar Microheater And Inter Digitated Electrodes Structure For Zno Based Hydrogen Gas Sensor

  Authors: Manish Deshwal, Anil Arora

- ✓ Presented a Poster at **International Symposium on Integrated Functionalities (ISIF) 2017**, 10-13 December 2017, Shangri-La's Eros Hotel, New Delhi, India.

  Paper Title: VOC's Sensor using ZnO thin film on prefabricated IDE using Silicon as substrate

  Authors: Manish Deshwal, Anil Arora

- ✓ Conference Proceedings of **"International Conference on Emerging Trends in Computing and Communication Technologies 2017"** at GEHU Dehradun, IEEE Explore Digital Library

  Paper Title: A highly sensitive Pt-doped ZnO based Ethanol sensor

  Authors: Manish Deshwal, Anil Arora

Acknowledgement

Pursuing for Ph.D was an idea to me planted by the enthusiasm of dreams. Persevering for 5 years and 150 yards to the Electronics & Communication Engineering Department, Thapar Institute of Engineering & Technology; has made it possible to accomplish my work and producing this piece of thesis after conducting several trials and finding the new perspective in form the research work. A keen interest in toxic gas/vpors sensing led the drive in me to push hard for this critical work. Guiding my path was encouragement from my family and constant faith of my mentor ***Dr. Anil Arora****.*

It wasn't been without the guidance of my supervisor ***Dr. Anil Arora****, Assistant Professor who portrayed my dream into the substantial research and paved the pathway in a sequential phased manner, this work would have left to be completed. Whenever there is a need of inducing a fresh effort, whenever there is a need of fresh perspective, whenever there is a need to overview the research activities, the tall and respectable stature of Dr Anil Arora bails me out. This piece of thesis is encrypted by the colossal efforts of Dr. Arora. It's very difficult to thank him in words for being the source of my pillar strength and in every other aspect.*

I would like to express my gratitude towards ***Dr. Alpana Agarwal****, Professor and Head of Department for she made sure that the infrastructure surely should suffice with our requirements.*

I would also like to thank ***Dr. Rajesh Khanna*** *and* ***Dr. Sanjay Sharma****, as most of my practical work was completed under their tenure of heading the department. I am extremely overwhelmed for showing a great trust in my conduct and supporting me during critical situations. Their student friendly decisions always helped me grow and overcome all the technical hiccups.*

Besides my mentor, ***Dr. Sanjay Kumar****,* ***Dr. Bhaskar Mohanty, Dr. D.P. Singh, Dr. Mukesh Kumar*** *and* ***Dr. Mayank Kumar Rai*** *played a pivotal role for being a source of inspiration during all the years. They enlightened me and provided a valuable support while overcoming various challenges. They also gave me precious words of conviction and always believed in my abilities.*

I am grateful to ***Prof. Vinay Gupta****, Dean Examination & Professor, Department of Physics & Astrophysics, University of Delhi (North Campus), New Delhi who gave this opportunity to have access to the laboratory and encourage research work in this field. He is a great human being and his conduct always inspires me to good great work for humanity. He enabled us to carry all the sampling work in the EMDL (Electronic Devices & Materials Laboratory). The collection of data and other information from University of Delhi and IIT Delhi would not have been possible without his presence. Besides, helping in the research activities he has been a great inspiration for me. His passion and grounded nature is a quality I look forward to. His support has been impeccable all through this journey. I have learnt so much being around him and for that I cannot thank him enough.*

My sincere gratitude to ***Dr. Monika Tomar****, Assistant Prof, Department of Physics, Miranda House, University of Delhi (North Campus), New Delhi. Her contribution to this research work is immense.*

The other staff members of ECED, TIET, Patiala and DPAP, University of Delhi (North Campus), New Delhi, provided me envisions to carry my research work to the ground level. ***Mr. Vinod Kumar Bhatt & Mr. Puran*** *was always helpful.*

I would like to thank fellow researchers & faculty members ***Dr. Anjali Sharma, Dr. Surbhi, Dr. Aarti Arora, Dr. Ayushi Paliwal, Dr. Reema Goyal, Dr. Punit Tyagi, Dr. Prakash Sati, Lokesh Kumar, Avneet Singh, Sujit Kumar, Shaan, Gurpreet, Sheetal Dewan, Surbhi Gupta and Krishna Sir*** *for guiding me frequently and sharing the latest techniques and development in the scientific world.*

I would like to express the sincere gratitude to the fellow research inmates who became my strength during tough times ***Prerna Arora Khanna and Daljeet Singh****, for inculcating the research oriented habits. Both of them constantly stood beside me and guided me. They took care of me as family and always boosted my confidence. They guided a lot during thesis writing process and helped me catch trivial errors.*

I like to express my deep joy to work with all the M.tech students who gave a chance to learn more about my field. Their presence kept my enthusiasm high and my passion for this field grew during all these years. Palak Bhatt, Mayank Dhull, Roohi Singh, Amit Kumar Bhatt with whom I share a good repertoire and a deep mutual understanding.

No matter how did and what kind of work is completed, the supporting role of the well-wishers and friend played the fulcrum role. To begin with; ***Dr. Gaurav Madhu, Dr. Pradeep Kumar Teotia, Dr. Balveer, Jitendra Singh Virk, Atul Sharma, Gittaly Dhingra, Dr. Amandeep Sharma, Chandanpreet Kaur, Dr. Amrita Singh and Rajnish Garg*** *who have been a source of huge motivation when and always encouraged carrying out my endeavours.*

I imbibe the virtue of relaxing in the company of my brothers ***Er. Gaurav Ahlawat and Er. Vaibhav Deshwal*** *always gave me the necessary motivation whenever I felt devastated.*

My parents ***Dr. Rajendra Kumar and Mrs. Renu****, for whom I am dedicating my research work. It was their dream and this dream along with their love gave me strength to overcome all the hurdles and accomplish this. Their blessings are the sole reason of my successful completion of this much awaited milestone of my life.*

My Wife ***Mrs. Anshu Tomar****, who provide me an encouragement and valuable support to carry out my dreams. Her love has been unconditional for all my life.*

Date: ***Place: Patiala***

List of Contents

List of Figures

List of Tables

Notations

°	*Degrees*
μ	*micro*
P	*resistivity*
Θ	*Theta (angle)*
Y	*Optical frequency*
nm	*nanometres*
cm	*centimetres*

Abbreviations

AC	*Alternating current*
AFM	*Atomic force microscopy*
CMOS	*Complementary metal oxide semiconductor*
CSD	*Chemical solution deposition*
CVD	*Chemical vapor deposition*
DC	*Direct current*
DMM	*Digital multimetre*
e-beam	*Electron beam*
EDX	*Energy dispersive x-ray spectroscopy*
Eg	*Energy band gap*
FESEM	*Finite element scanning electron microscopy*
FWHM	*Full width half maxima*
GC	*Gas chromatography*
GCTS	*Gas calibration and testing apparatus*
HRTEM	*High resolution transmission electron microscopy*
IDE/IDT	*Inter digitated electrode/transducer*
IPA	*Iso-propyl alcohol*
IR	*Infra red*
MEA	*Monoethanol amine*
MH	*Microheater*
PL	*Photoluminescence*
Ppb	*Parts per billion*
Ppm	*Parts per million*
PR	*Photoresist*
Ra	*Resistance in air*
RF	*Radio frequency*
Rg	*Resistance in gas*
SAW	*Surface acoustic wave*
SEM	*Scanning electron microscopy*
SILD	*Successive ionic layer deposition*
SPR	*Surface plasmon resonance*
TCE	*Tri-chloro ethylene*
TEM	*Transmission electron microscopy*
UV	*Ultra violet*
UV-vis	*Ultra violet visible range*
VOC	*Volatile organic compounds*
XRD	*X-ray diffractometry*

Chapter 1

Introduction

"This section introduces to the modern world gas sensing technologies and materials that are used for their fabrication. The various types of gas sensing technologies that can be used for gas sensing with their advantages and limitations. Also the need of the gas sensors in the present scenario with the recent technological findings is also discussed with a thorough literature survey. The later portion of the section deals with the shortcomings identified from the presented literature and formulation of the problems. Later, the brief overview for the present thesis is highlighted".

1.1 Gas/Vapor sensors and its obligation: An Introduction

With the advancement in science and technology, different equipments have been invented which cater to the needs of mankind making everything effortless and simpler. However, these technological developments also have some negative effects such as air as well as chemical pollution due to rapid industrialization [1], an increased pesticides usage in farming [2] and some unanticipated effects of genetically modified foods distressing the health condition of organisms as well our ecosystem [3]. Hence, efficient sensors are fundamentally required for the detection of such pollutants. Nowadays, efforts are continuing towards the realization of sensors with digital systems to make a portable or wireless sensor that can be used with wireless sensor networks [4], [5]. Nano-technological research is extensively focused towards the invention of sensing materials that could be exploited for wide range of applications as various types of sensing [6-8]. Some of the applications for such sensors may be space antenna applications [9], [10], gas alarms [11], medical analytics [12-14], vehicular pollution control check [15], nutritional industries, with environmental as well as chemical waste monitoring systems [16] etc. Various incidents had been reported till date, where the damage to life and property could have been prevented if any gas sensing systems had been installed for crucial sites monitoring. As a result, a high performing sensing systems with low detection limits have become an essential for monitoring and the quantification of various kinds of toxic and other harmful chemicals and gases etc. In today's era, where each country is designing and developing its own chemical warfare agents along with various explosives, the reliable and accurate sensors are required for their early detection. With the early detection and warning of such compounds will prevent huge loss to life of soldiers as well as innocents.

Acetone, Toluene, CO and SO_2 are major toxic gases with rapidly increasing concentrations at an alarming rate in the atmosphere [17], [18]. Acetone is released in many ways, such as, industrial waste, chemicals manufacturing, degreasing in industries, adhesives manufacturing industries etc [19], [20]. Also, acetone is a highly inflammable clear and a colorless liquid. Consequently, it has now become important for the fabrication of efficient gas sensors with high sensitivity and selectivity with fast response times for detection of toxic and harmful gases/ vapors that can detect the presence of acetone leakage in any industrial plant or as an environmental hazard. However, only few efforts have been done towards the detection of acetone vapors, thus the focus of present work is the efficient detection of acetone vapors. The present research work details about the efficient sensing of volatile organic compounds

(VOC's) vapors especially acetone vapors by optimizing the heating uniformity of sensing layer by microheaters, thickness of sensing layer, annealing temperature of sensing layer with dopant variations for high selectivity as well as sensitivity with quick response and recovery times for the sensor.

1.2 Acetone as vapor or gas

Acetone vapors/gas having a pungent and irritating smell is toxic if inhaled directly. Chemical formula of acetone is CH_3COCH_3 [21]. The chemical structure of acetone is as shown in Figure 1.1. Acetone also known as propanone or 2-propanone is highly flammable when either in liquid or in gas phase and can be ignited from distance. The melting point is 178.5 K with the boiling point of just above the room temperature at 329.20 K. It is miscible in water as well as other organic products and even plastics [22].

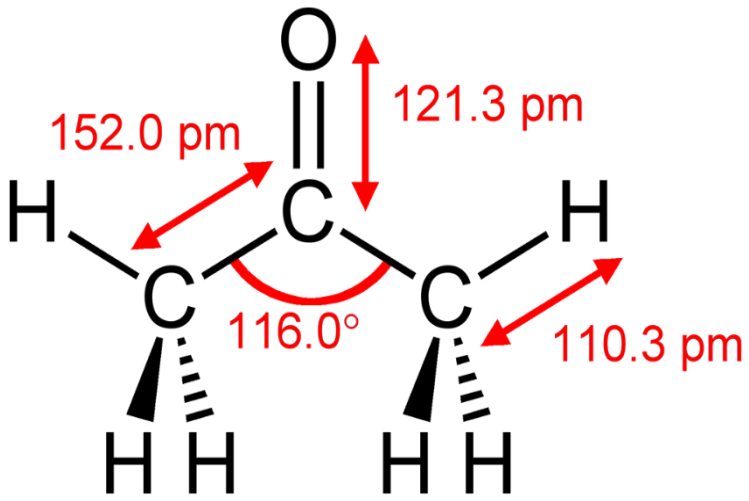

Figure 1.1: *Structure of acetone.*

1.2.1 Sources of Emission

Acetone is released in environment both by the natural and anthropogenic (man-made) sources. The main sources of acetone emission are industrial sources as a result of chemicals manufacturing, non-ferrous materials, plastic products, printing processes, and sewage and drainage services and also from coal mining. The other natural sources are volcanic gases and forest fires. The acetone is also present in the vehicle exhausts and also from railway operations, and even from tobacco smoke. Acetone is also present in the consumer products such as paint and varnish removers, thinners, paints and primers etc [23].

1.2.2 Effects of Acetone

Inhalation of acetone directly or indirectly ranging from mild to higher levels may cause serious injuries to human health. After exposure, the acetone enters the blood stream which exposes all our internal organs to the substance. The exposure results in damaged skin, damaged nervous system, damage to cornea/blurred vision, kidney and liver dysfunctionality [24].

Also if accidentally acetone is flushed with hydrogen peroxide, the acetone forms a byproduct as acetone peroxide which is a highly explosive derivative of acetone in nature. Acetone may pose a significant risk of oxygen depletion due to microbial consumption in aquatic systems.

1.2.3 Need for Detection of Acetone

As discussed earlier, acetone is used in almost all manufacturing industries, fabrication laboratories, as a degreasing agent in automobile industry and much more. Besides its use in industrial applications, the acetone is highly flammable and/or explosive in nature when mixed with some peroxides or strong oxidants [23]. Thus, there will always be need to detect the leakage of the acetone in any form within a premises or environment. As acetone is heavier than air, it may travel along the surface to a hot equipment or flames which can caught fire causing distant ignition even in lowered concentrations. Hence, to prevent a disastrous situation the acetone sensor must be installed to detect any leakage.

Moreover, in terms of medical use, the acetone breathe analyzer can detect higher glucose levels in the bloodstream, which in turn can be concluded for a diabetic person. As a biomarker application acetone sensor can be used to immediately detect the glucose levels of a diabetic patient [25].

Hence, acetone sensors shall be useful in aspects of pertaining health and environment, work place safety by detecting and controlling levels of acetone.

1.3 Acetone Vapor/Gas Sensors

Table 1.1 summarizes various sensing techniques used for the detection of various toxic gases along with their detection principles. Amongst all the sensing techniques, electrochemical, optical and surface acoustic wave (SAW) based techniques are mostly preferred for acetone detection due to the fast response speeds and relatively low operating temperature. However,

the major drawbacks of these sensing techniques include (i) poor selectivity, (ii) poor response, (iii) difficulty in miniaturization, and (iv) bulky and expensive equipment [26]. To overcome all these issues, semiconductor based conductometric gas sensors are in great demand for the detection of acetone vapor/gas since last few decades due to their small size, relatively simple device structure and low cost. The detection principle relies on the change induced in sensor conductivity upon adsorption of gas molecules on its active surface. However, their high operating temperatures make the power consumption of the device to be very high and selectivity is also an important issue.

Table 1.1: *Various techniques for toxic gases detection.*

Technique	**Principle of detection**
Optical	Variation in intensity of light or refractive index
Semi-conductor (Conductometric)	Resistance variation
Electro-chemical	Emf/current variation
Piezoelectric	Change in frequency
Field effect transistors	Voltage variation
Chemocapacitive	Capacitance variation
Surface Acoustic Wave	Change in frequency
Cantilevers	Change in frequency
Mass spectroscopy	Variation in molecular weight

1.4 Sensor Attributes

Sensor is a transducer which converts one energy into another one by measuring their physical, chemical or biological quantity that can be measured by an observer/instrument. Hence, it can be said that a sensor is a device which converts a non-electrical value to another measurable value like an electrical signal. Figure 1.2 shows the basic schematic for a typical sensor.

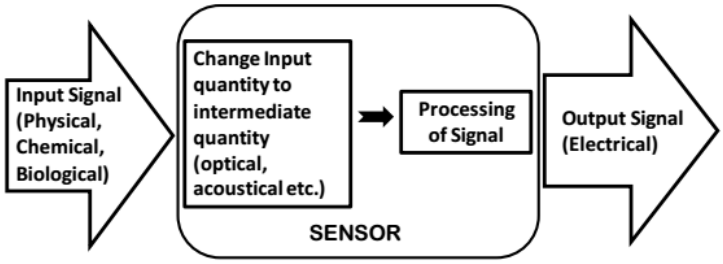

Figure 1.2: *Workflow schematic for sensor.*

Typically, a good sensor must possess the following characteristics:

- high sensitivity towards input stimulants
- must be insensitive towards other interferences means having good selectivity
- must be able to measure low concentrations for stimulus means lowered detection limits
- must be able to provide results in least possible time means having faster response and recovery times
- sensor must be embedded such that it will be portable and wireless
- must be insensitive towards harsh environments means high stability
- must provide similar results for repeated cycles (repeatability)
- must be power efficient (low operating temperatures)

Now, while designing of a sensor, several above mentioned characteristics must be taken into consideration. There are various sensor architectures that have been designed for the detection of various stimuli and some are also available in the market. For the present work, the main focus is for the development of gas sensors where stimuli are gas molecules.

1.5 Gas Sensing Platforms

Various approaches and techniques have been employed till now for quantification and monitoring of gases/ vapors which includes, (a) Semiconductor sensors, (b) Infrared (IR) spectroscopy, (c) Chromatography, (d) Electrochemical sensors, (e) Surface plasmon resonance (SPR) sensors, (f) Surface acoustic wave (SAW) based sensors. A brief description for the gas/vapor sensors is presented below:

1.5.1 Semiconductor sensors

The semiconductor gas sensors is a class of sensors that are basically working on chemo-resistive principle where change in conductivity or resistance of the semiconducting sensing element changes after its interaction with the target gas. As stated by Jaaniso, et al.,(2013) [27] , this semiconducting sensing element is any form for thin/thick films, pellets or other capable nanostructured architectures. As the semiconducting metal oxide is exposed to either oxidizing or reducing gas, the surface potential gets changed due to gas molecules adsorbed over the surface. This resulted for the variation in conductivity of the sensing element which can be easily detected by electronic instruments.

Such gas sensors are mostly preferred due to their ease of fabrication, ruggedness and low cost for commercial fabrication. The Figures 1.3 (a) and (b) present the schematic of the semiconductor based sensor and thin films, respectively. As shown in Figure 1.3 (a), the basic architecture for bulk semiconductor gas/vapor sensor with electrodes on either sides that are used for measuring the real time resistance values for the sensor. The same semiconducting materials need to be heated by either external heater or an in-built microheater which aids the sensor in achieving an optimized sensing at an optimum temperature. A bulk semiconductor sensor is fabricated by dipping a metal coil in a paste of the sensing material prepared using a colloidal solution of metal hydroxides as precursors.

The schematic of Figure 1.3 (b) represents the semiconductor thin film based gas sensor where substrate is wisely chosen for the sensor as base with pre-fabricated comb-like planar electrodes known as Inter-Digitated Electrodes/Transducers (IDE/IDT's) with the under-placed heater, are deposited with semiconducting thin films. The main disadvantage of semiconducting metal oxide gas/vapor sensors is the higher operating temperatures resulting in higher power requirements. The efforts are continuing worldwide in the development of either reduced operating temperatures for the fabricated gas sensors or having an alternate approach for efficient gas sensors.

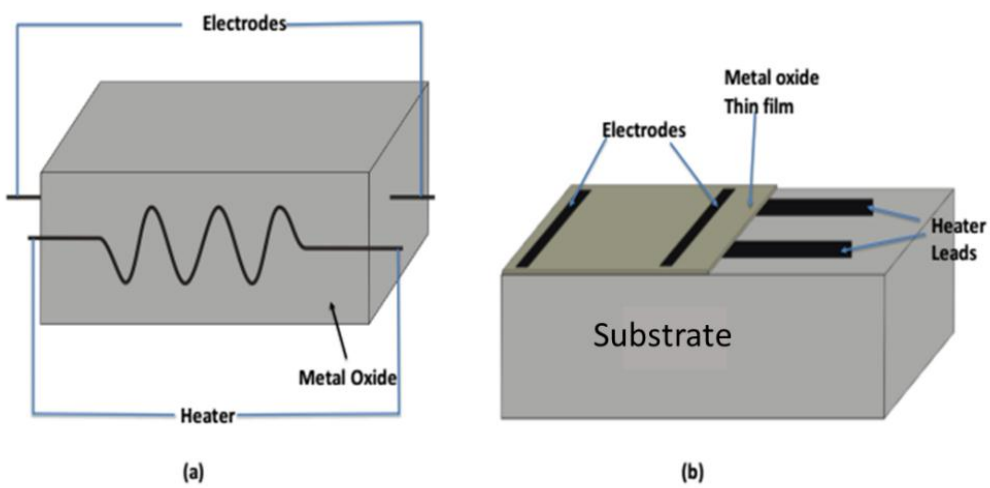

Figure 1.3: *Metal oxide gas sensor with (a) bulk and (b) thin film sensing element.*

1.5.2 Infrared (IR) Spectroscopy

Infrared(IR) spectroscopy, as explained by Tittel, et al.,(2003) [28] , is also one of the sophisticated technique that is used for the analysis and detection of gases/vapors. The IR source induces some molecular vibrations for the excitation of higher energy levels within the

range for wave numbers of 4000 to 200 cm^{-1} which further provides a rise to the absorption bands due to chemical bonds present in the test samples as shown in Figure 1.4 (a). The Figure 1.4 (a) represents the IR waves travelling through two adjacent (reference and sample) cells. In the reference cell, the IR waves travel through the IR filters and directly reach the filters whereas at the sample side, IR waves got absorbed when passing through the gas molecules present inside and then reaches to the IR filters.

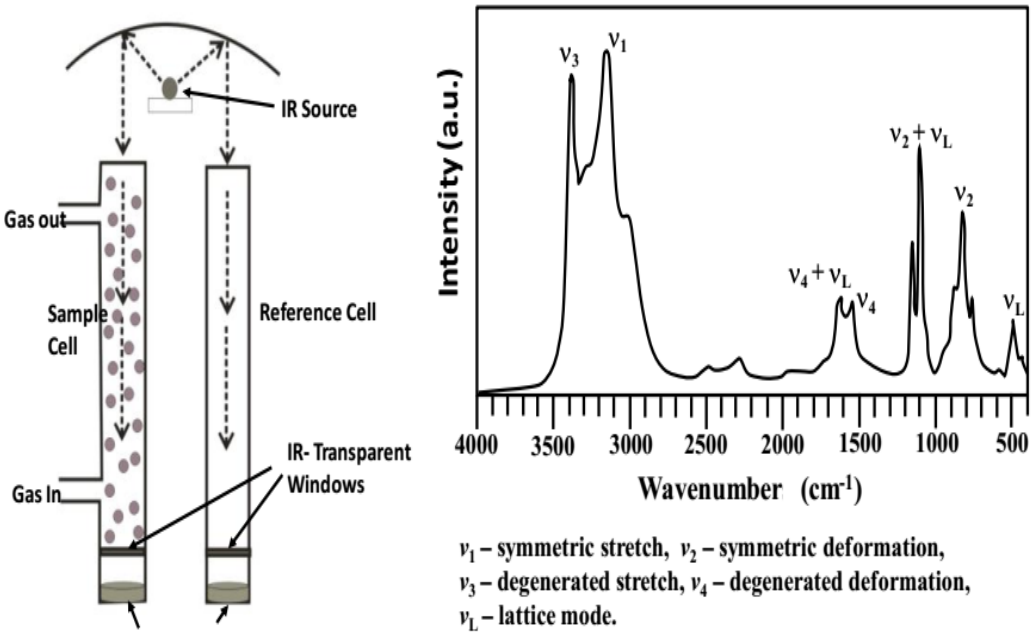

Figure 1.4: *(a) IR Sensor schematic, (b) IR Spectra for ammonia (NH3) gas (Dubost, et al.,(1972) [29]).*

Every compound is having a unique characteristic spectrum where the absorption bands occur at specific frequencies providing the indication for the presence of gas molecules. As shown in Figure 1.4 (b), an example for the NH_3 gas IR spectrum [29]. The present spectrum shows the characteristic bonds for the NH_3. But the main disadvantage for the present technique is its inability for monitoring all gases like hydrogen and the results can easily get fluctuated with the presence of different humidity levels.

1.5.3 Chromatography for Gases

Gas Chromatography (GC) technique is one of the most popular technique that was introduced in early 1950's which is used for the separation and analysis of a mixture of compounds. Adahchour, et al.,(2006) [30] and Snow, et al.,(2002) [31] explained that presently this technique is widely used in applications like identification and analysis of drugs, characterization of polymers and gases/vapor sensing. The GC works according to the

principle that whenever a mixture of compounds is passed through a narrow tube (also known as columns) at higher temperatures with a coating with some suitable material (known as stationary phase), the compounds present in the mixture got separated and eluted at different times. The elution time of different compounds is different depending upon the affinity towards the particular gas/vapors as shown in Figure 1.5 (a). This separation of compounds is detected by the output detector. The GC schematic is as shown in Figure 1.5 (b). The columns are fabricated usually with fused silica and the materials present inside the columns which are responsible for the separation of compounds are generally inorganic salts and other materials. There are several disadvantages of using this technique such as bulk in nature, high power consumptions, and other portability issues.

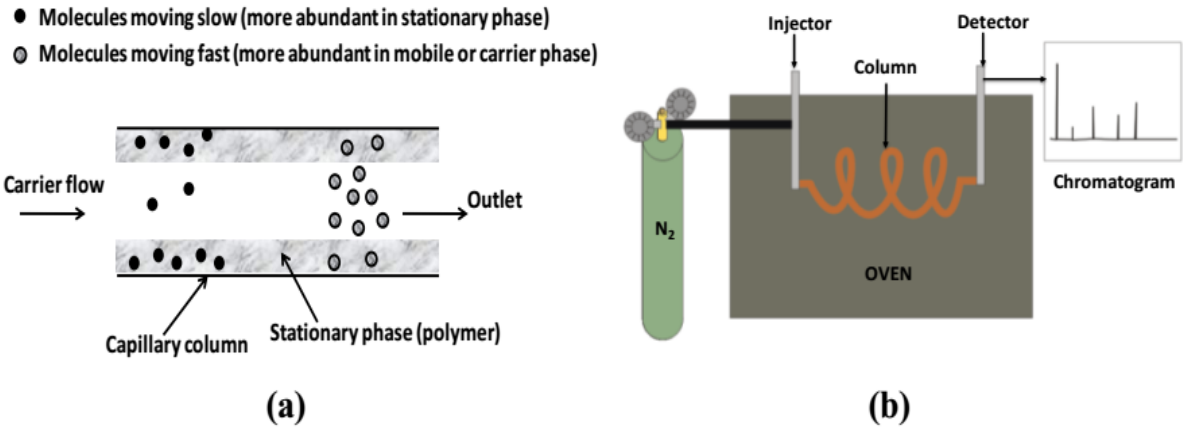

Figure 1.5: *(a) Gas molecules retention in column, (b) GC Setup.*

1.5.4 Electrochemical Gas Sensor

The electrochemical sensors generally relies over the principle of change in electrochemical properties (like redox potentials, conductivity/resistivity etc.) for working of electrode during the interaction with the gas /vapor molecules. A basic setup is as shown in Figure 1.6 for the electrochemical sensor. In general, there is a three electrode system viz. a counter electrode, a reference electrode and a measuring electrode shown in Figure 1.6. The target gas is diffused into the electrolyte enclosures through a hydrophobic permeable membrane. These sensors are used for determining the partial pressure of oxygen molecules in the ambient air or the concentration of toxic gases.

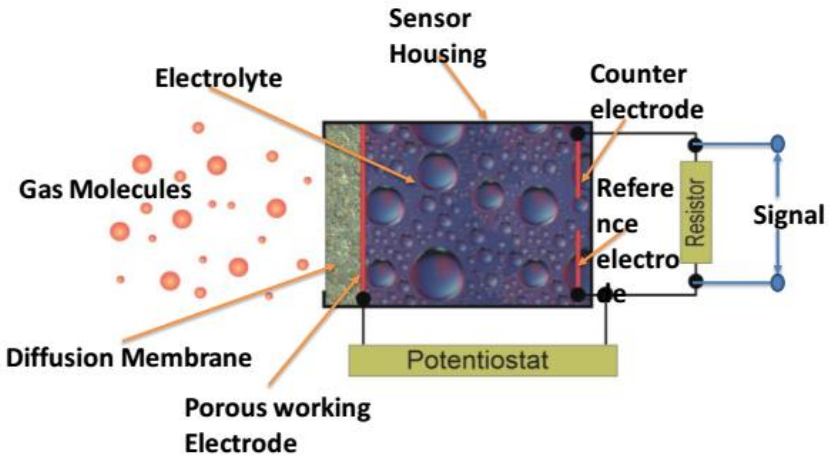

Figure 1.6: *Electrochemical gas sensor (Tyagi, et al.,(2017) [32]).*

A constant voltage is applied between the reference electrode and the working electrode with the help of a potentiostat connected with the sensor (Figure 1.6). Choice of electrode material, electrolyte and working potential is based on the nature of the target gas (oxidizing/reducing) to be measured at the measurement electrode. The counter electrode passes the current and allows it to flow across the sensor cell. Depending upon the nature of the target gas (Oxidizing/reducing), the atmospheric oxygen is either reduced or oxidized over the counter electrode and hence the derived current flowing through the sensor is calculated which is directly proportional to the concentration of target gas molecules. The major drawbacks of electrochemical sensors is the destabilization of sensor due to swollen electrolyte if humidity comes in vicinity of it.Further, sensor is limited towards certain applications due to its requirement of minimum concentration of oxygen required for reliable operation.

1.5.5 Surface Plasmon Resonance (SPR) Sensors

Surface Plasmon Resonance (SPR), as discussed by Paliwal, et al.,(2015) [33] , is a sensitive technique for gas/vapor and chemical sensing. Surface Plasmons (SPs) are the collective charge density oscillations that may possibly exist at the interface of two dielectric media with opposite charges.

The SPs are easily excited using prism coupling technique with Krestchmann configuration where a metal film of appropriate thickness is deposited over the face of the prism as represented by Figure 1.7 (a). Now, as a monochromatic beam of light is incident over the prism surface, SPs modes excites occurring a resonance at a particular combination of wavelength of light and the angle of incidence which is referred to as SPR. At resonance condition, the intensity of the light reflected is minimum represented in the Figure 1.7 (b).

Figure 1.7 (c) presents a schematic for SPR sensor where gas is allowed to interact with sensing (dielectric material) layer and the change in reflected intensity is measured as a function of change in gas concentration. The SPR mode gets changed at the interface which is a result of change in the dielectric properties due to the interacting target gas with sensing layer. Hence the change in SPR conditions of sensing layer is proportional to the gas concentrations allowing to determine the concentration of the target gas using the calibration curve.

Paliwal, et al.,(2015) [33] exploited the WO_3 sensing layer towards the detection of NOx gas using SPR technique and the developed sensor was found to be highly sensitive and selective [33].

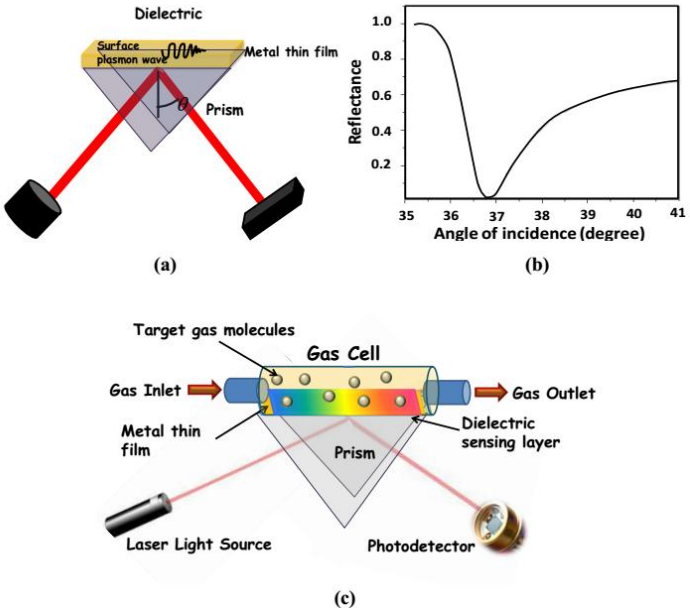

Figure 1.7: *(a) Kretschmann configuration for SPRtechnique, (b) Variation of reflected intensity at fixed wavelength, (c) SPR based gas sensor schematic [33].*

Another effort was also made by Paliwal, et al.,(2016) [34] towards the detection of NH_3 gas using sensing layer [34]. With an advantage of working of this sensor to be its capability to work at room temperature there are various drawbacks of the SPR based sensors, including a complicated and a bulky setup for the measurements. Also this technique is having another critical issue regarding the selectivity of the gases.

1.5.6 Surface Acoustic Wave (SAW) based Gas Sensors

Surface acoustic wave (SAW) sensors are based over the principle of mechanical vibrations propagating over the surface of a piezoelectric material deposited over a lower density medium. SAW waves are generated using a pair of metallic IDT's over the piezoelectric material surface. When the electric field is applied over these piezoelectric materials, it exhibits mechanical strain and vice versa [35]. The working of a SAW based sensor can be explained using the principle of changing propagation characteristics of SAW waves like velocity, in-order phase and attenuation of the signal on interacting with target gas molecules.

A SAW sensor basically comprises of a piezoelectric transmitter, a transmission line deposited over with sensing layer and a piezoelectric receiver with sensor architecture as shown in Figure 1.8. Here the input IDT, using the principle of inverse piezoelectric effect, converts an electrical signal into an acoustic wave signal which then propagates through the sensing layer medium between the pair of IDT's and then it is detected by the output IDT's on the other side by means of direct piezoelectric effect. The interaction of target gas molecules directly with sensing layer in between the two IDT's amend the mechanical and/or electrical properties for the sensing layer and hence causing the SAW properties to change.

Figure 1.8: *Schematic diagram for a working SAW sensor (Tyagi and Gupta,(2017) [32]*

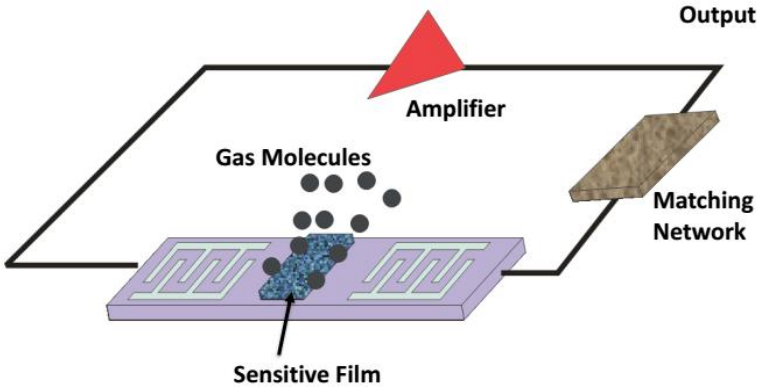

).

As shown in Figure 1.8, a SAW based gas sensor is based on a SAW resonator or delay line being put in the feedback loop of a high frequency amplifier along with a phase compensation network which results in a SAW oscillator. This SAW oscillator works at a characteristic frequency which is amended on interaction of the sensing layer with the gas molecules. SAW based sensors are having advantages of working at room temperatures, high sensitivity, and portability due to its smaller sizes over other types of sensors. But the

disadvantage of this technique is the complexity of its working which hinders the tuning capabilities for the sensor each time before installations.

1.5.7 Semiconducting Metal Oxide based Thin Film Gas Sensors

Semiconducting metal oxides based sensors have evoked a lot of interest of researchers for accurate monitoring of automobile exhausts, toxic, polluting and explosive gases for the past many decades. Sensors of this kind have a simple design that makes mass production feasible and is strongly linked to the availability of better sensing materials with improved functional properties. The phenomenon of change in the resistance of semiconducting sensing element in the presence of a reducing or an oxidizing gas while being operating at elevated temperatures is the basic principle of operation of semiconducting metal oxide gas sensors. Research in semiconducting metal oxide sensor started way back in 1962 with the discovery of this phenomenon in Zinc oxide (ZnO) by SUZUKI, et al.,(1962) [36] and focused on the development of sensors based on bulk materials [36]. Since then, there have been numerous reports on utilizing semiconducting metal oxides as gas sensors due to their low cost, small dimensions and high compatibility with microelectronics.

Later, demand for enhanced sensitivity and fast response speed prompted the development of efficient thin film based sensors that promise a high surface to volume ratio, reduced power consumption due to relatively low operating temperatures, fast response and recovery time and possibility of miniaturization. Currently, worldwide efforts are focused in both the basic as well as applied areas and there is continued interest in developing new sensing materials along with novel design structures for obtaining improved sensitivity.

A semiconductor based gas sensor performs two main functions: (1) Receiving and recognizing or identifying of the analyte, and (2) conversion of the analyte signal into a measurable output, like electrical signal. Figure 1.9 shows the whole function as discussed above, where the receptor function is felicitated by the surface of grains of semiconducting metal oxide, where gas to solid interaction phenomenon is occurring.

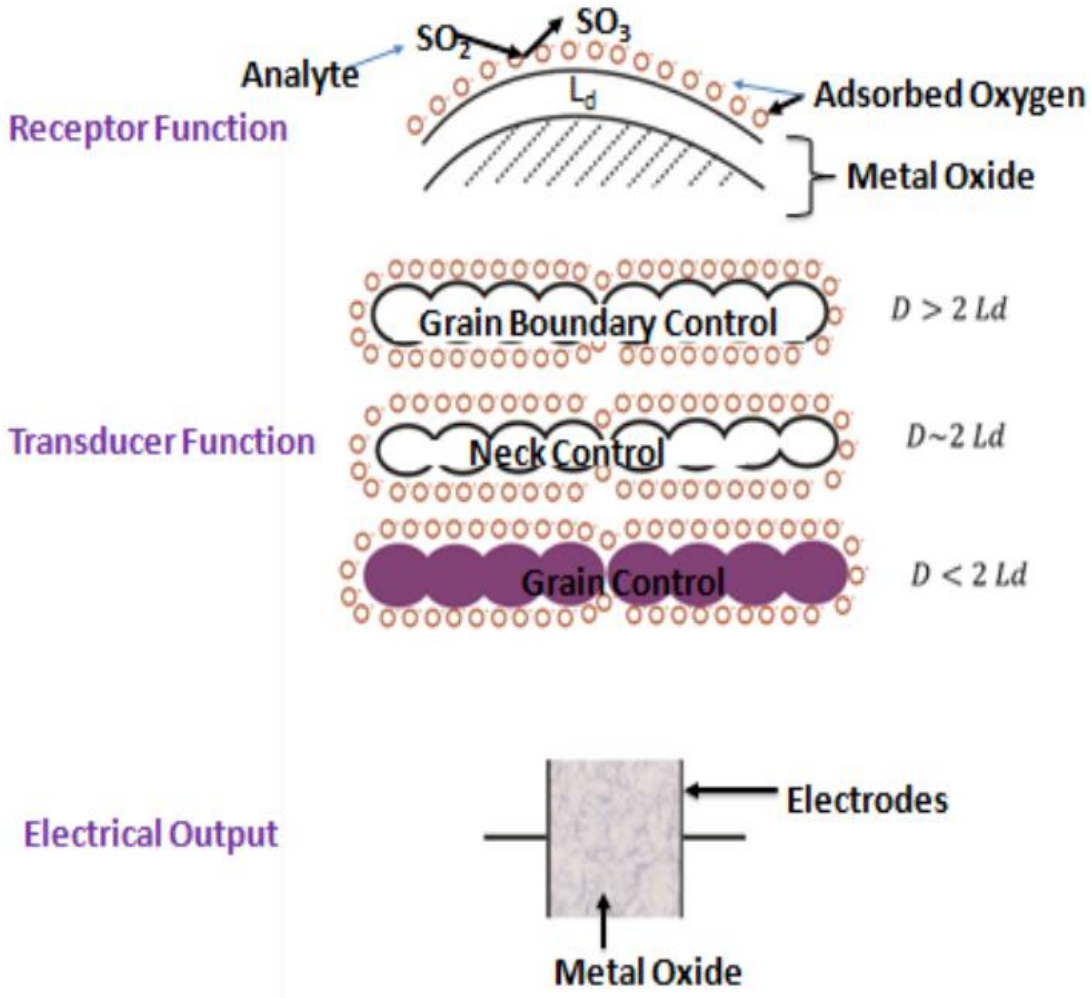

Figure 1.9: *The functional receptor and transducer elements of a semiconductor gas sensor.*

Such interactions includes the processes like oxidation and reduction of the sensing layer molecules over the semiconductor surface, adsorption of the gas molecules directly or due to reaction with the associated surfaces and vice versa. Hence, an interaction of an analyte with a metal oxide semiconducting surface is a surface dominating phenomena with all above mentioned phenomenon to be reversible processes. The main phenomena for gas sensing properties for a sensor are explained in the upcoming Chapters with explanation of working physics and other phenomenon with each sensor.

The oxidation/reduction of metal oxides results in the increase in the concentration of charge carriers within the conduction band and hence increasing the conductivity for a semiconductor which is a crucial fact for gas sensing applications. Figure 1.10 shows few of the most utilized semiconducting metal oxides by various researchers for gas sensing applications.

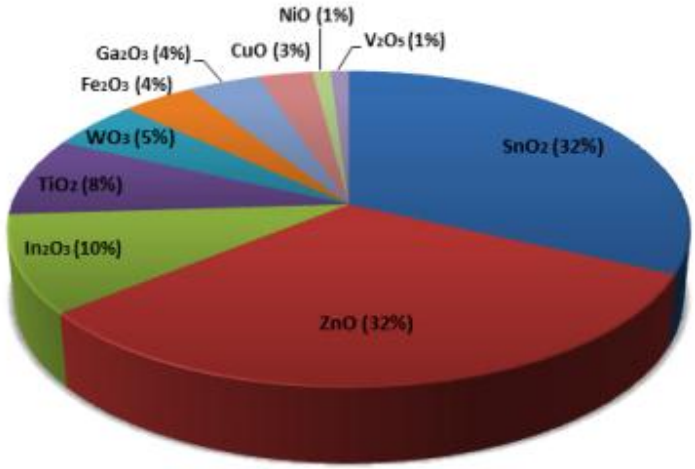

Figure 1.10: *Pie-chart of the most utilized semiconducting metal oxides used for gas sensor applications [37].*

It may be clearly seen from Figure 1.10 that amongst all oxide materials[37], SnO_2 and ZnO are widely used (32% each) for detection of various gases. ZnO is extensively used as thick/thin films or porous ceramic, because of several advantages it offers over other materials, including easy processing using a number of deposition techniques and good sensitivity towards different gas species. Oxides of tungsten, titanium, and indium besides other oxides like V_2O_5, NiO, CuO etc. have also drawn considerable attention for gas sensing. Other oxide materials are used for realization of semiconductor sensors for specific gases. Each oxide material has its own advantages and must be carefully selected according to their applicability for the sensing of specific target gas. Table 1.2 summarizes some important results reported on various oxide sensing materials for the detection of different harmful, flammable or toxic gases along with the deposition techniques used for the fabrication of sensing materials.

Table 1.2: *Summary of some important results on the conductometric gas sensors based on various semiconducting metal oxides for detection of different gases.*

Reference	Sensing material	Fabrication technique	Target gas	Gas Conc.(ppm)	Response	Topt (°C)
Cabot, et al.,(2000) [38]	SnO_2	Sol-Gel	CO, CH_4	500	22	350
Zhang, et al.,(2000) [39]	CuO-SnO_2	Sol-Gel	NO	1000	4.5	200
Rao,(2000) [40]	Pd-ZnO	Hydrolysis	Ethanol	1000	95%	175
Baik, et al.,(2000) [41]	SnO_2	Sol-Gel	CO	800	500	350
Ling, et al.,(2001) [42]	ZnO/$BaTiO_3$	Hydrothermal	NO_2, CO_2	5000	6	320
Solis, et al.,(2001) [43]	WO_3	Reactive gas evaporation	H_2S	10	10	250
Yu, et al.,(2001) [44]	ZnO/ SnO_2	Hydrothermal	CO	200	5	160
Solis, et al.,(2001) [45]	WO_3	Reactive gas evaporation	H_2S	10	10^3	RT
Savage, et al.,(2001) [46]	TiO_2	Hydrothermal	CO, CH_4	1000	2	600
Comini, et al.,(2002) [47]	SnO_2	Thermal Evaporation	Ethanol, NO_2	250, 0.5	41.6, 15.5	400
Roy, et al.,(2002) [48]	ZnO	CVD	DMA	1%	73.3%	300
Chang, et al.,(2002) [49]	ZnO:Al	RF Sputtering	CO	1000	60%	400
Moon, et al.,(2002) [50]	CuO-ZnO/SnO_2	Pellets	CO, H_2	200	15	300, 250
Tamaki, et al.,(2002) [51]	In_2O_3	E-beam evaporation	Cl_2	5	69	400
Neri, et al.,(2002) [52]	Au, Zn-Fe_2O_3	LPD	CO, NO_2	2.5	30	400
Lee, et al.,(2002) [53]	SnO_2	Silk Printing	VOC's	100%	3000	400
Barsan, et al.,(2003) [54]	SnO_2	Thick Film	CO	500		275
Nicolas-Debarnot, et al.,(2003) [55]	PANi	Hydrolysis	NO_2	4	$4.4*10^{-11}$	RT
Yamazoe, et al.,(2003) [56]	SnO_2	Spin Coat	H_2S	50	35	200
Li, et al.,(2003) [57]	CNT	Hydrolysis	NO_2	6	0.5	RT
Li, et al.,(2004) [58]	WO_3	Hydrolysis	VOC's	500	13.5	40
Villalpando-Paez, et al.,(2004)	CN_x NT's	Thermolyzing	Acetone	1000	4%	RT

[59]						
Niu, et al.,(2004) [60]	ZnM_2O_4 (M = Fe, Co, Cr)	Microemulsion	Cl_2	50	83.6	270
Zhu, et al.,(2004) [61]	TiO_2/ZnO	Sol-Gel	VOC's			370
Sahay,(2005) [62]	ZnO	Spray Pyrolysis	Acetone	2000	45%	325
Shishiyanu, et al.,(2005) [63]	Sn-ZnO	SILAR	NO_2	1.5	10%	150
Yoo, et al.,(2005) [64]	ITO	RF Sputtering	H_2	1000	0.008	300
Zhang, et al.,(2006) [65]	Cu_2O / CuO	Dip Coating	Alcohol	800	2	210
Zhang, et al.,(2006) [66]	$La_{1-x}Pb_xFeO_3$	Sol-Gel	Acetone	500	30	250
Liu, et al.,(2006) [67]	$LaFeO_3$	Polymerization	Acetone	80	204	400
Zhao, et al.,(2006) [68]	SnO_2	Dip Coating	Acetone	1000	29	RT
Rezlescu, et al.,(2006) [69]	$NiFe_2O_4$ + 1%CaO	Self- Combustion	Acetone, LPG	Saturated Vapours	4.5	215
Rella, et al.,(2007) [70]	TiO_2	PLD	Acetone, Ethanol	200	12.5	400
Zhang, et al.,(2007) [71]	$ZnFe_2O_4$	Pyrolysis	Ethanol, Acetone	500	12.27	200
Kim, et al.,(2007) [72]	SnO_2/ZnO	CSD	C_2H_5OH	200	20	400
Hsueh, et al.,(2007) [73]	ZnO NW's	Hydrothermal	Ethanol	1500	61%	300
Ge, et al.,(2007) [74]	CeO_2/ZnO	Dip Coating	VOC's	100	80	320
Chang, et al.,(2008) [75]	Au/ZnO	Au Adsorption	Acetone	200	82.5%	300
Qi, et al.,(2008) [76]	ZnO	Facile Solution	Acetone	50	16	300
Qin, et al.,(2008) [77]	SnO_2	Hydrothermal	Acetone	500	16	290
Ahn, et al.,(2009) [78]	ZnO NW's	Carbothermal	NO_2	20	90	225
Wisitsoraat, et al.,(2009) [79]	NiO_x/TiO_2	E-beam Evaporation	Acetone, Ethanol	100	50	300
Zhu, et al.,(2010) [80]	SnO2	Sonochemical	Acetone	50	15	350
Kakati, et al.,(2010) [81]	ZnO	Sol-Gel	Acetone	1000	15 sec	200
Pawar, et al.,(2010) [82]	ZnO	Dip Coating	Acetone	2000	90%	275
Wen, et al.,(2010) [83]	SnO_2–TiO_2	Sol-Gel	Ethanol	65	30 sec	276
Murade, et al.,(2011) [84]	$LaFeO_3$	Sol-Gel	Acetone	700	0.8	275
Liu, et al.,(2011) [85]	ZnO	Electrospinning	Acetone	1000	78	360

Ahn, et al.,(2011) [86]	ZnO	Electrochemical	Acetone		1.75	RT
Shi, et al.,(2011) [87]	WO_3	Sol-Gel	Acetone	0.05		300
Righettoni, et al.,(2012) [88]	WO_3	Flame spray pyrolysis	Acetone	20	10 sec	350
Gao, et al.,(2012) [89]	WO_3–Cr_2O_3	Sol-Gel	Acetone	20	8.91	320
Song, et al.,(2012) [90]	SnO_2	PS spheres	Acetone	100	12	250
Wang, et al.,(2012) [91]	ZnO	Sol-Gel	Acetone	100	5	270
Zhang, et al.,(2013) [92]	WO_3	Hydrothermal	Acetone	55		200
Do, et al.,(2013) [93]	Au/Al_2O_3	Chemical	Acetone	29	3-10 min.	
Shan, et al.,(2013) [94]	Fe_2O_3	Electrospinning	Acetone	50	10 sec	240
Shao, et al.,(2014) [95]	ZnO	CVD	Ethanol	320	212	RT
Liu, et al.,(2014) [96]	ZnO	In-situ production	NO_2	80	26	RT
Talwar, et al.,(2014) [97]	ZnO	Template Approach	Ammonia	100	2.5	27
Cheng, et al.,(2014) [98]	SnO_2	Elecro-Spinning	Acetone	100	65	340
Hosseini, et al.,(2015) [99]	ZnO	vapor phase transport	H_2S	5	300	250
Zhou, et al.,(2015) [100]	$ZnFe_2O_4$	Acetone	Acetone	100	3	200
Wang, et al.,(2015) [101]	NiO	hydrothermal reaction	Acetone	100	500	250

The selection of a material has to be performed by considering various desired parameters like electro-physical/chemical catalytic properties, adsorption abilities, electronic architectures, thermal stability and compatibility issues with other material or compounds with technologies to be used for fabrication etc. Gas sensing being primarily a surface phenomenon, it is becoming necessary to manipulate the sensor surface for enhanced interaction with target gas, by generating reactive species that sensitize the surface with appropriate catalytic additives or modifiers[102], [103]. To meet and tailor all these properties of sensing materials, growth kinetics plays an important role. Various deposition techniques have been exploited for the fabrication of different sensing materials with controlled surface morphology. Korotcenkov,(2013) [102] have used Successive Ionic Layer Deposition (SILD) technique for the fabrication of Ag doped SnO_2 thin film for the detection of trace level of H_2 gas. However, the reported operating temperature was relatively high (240°C) [104]. Singh, et al.,(2012) [105] were able to detect CO using ZnO-Graphene oxide composite at room temperature. Benkara, et al.,(2013) [106] and Chow, et al.,(2013) [107] detected H_2 at 160°C and 150°C using composites of ZnO with TiO_2 and Hjiri, et al.,(2014) [108] detected 80 ppm CO using Al doped ZnO at 300°C and Bai, et al.,(2017) [109] was able to detect 10 ppm NO_2 at 125°C using Fe doped ZnO. Li, et al.,(2015) [110] reported detection of NO_2 gas (10 ppm) at lower operating temperature of 70°C using SnO2 nanocrystal with graphene aerogel. Cardoza-Contreras, et al.,(2015) [111] detected H_2 gas at 100°C using ZnO nanowires. A number of physical and chemical deposition techniques have been reported in literature for the fabrication of metal oxide based conductometric gas sensors (Table 1.2). Currently, focus is on the low temperature detection of variety of toxic gases along with attaining efficient response characteristics. The literature suggests that the surface modification of sensing layer by varying growth kinetics or ion bombardment, and/or incorporation of suitable catalyst/modifiers including carbon based Nano-materials may result in enhanced sensing response characteristics towards a particular gas.

Since focus of the present thesis is the development of efficient conductometric gas sensor for acetone detection, a review was made on conductometric semiconducting metal oxide based acetone gas sensors. Various materials have been exploited for the detection of acetone gas and important reports are summarized in Table 1.3.

Table 1.3: *Summary of important results on semiconducting metal oxide based acetone gas sensors.*

Reference	Sensing material	Fabrication technique	Target gas	Gas Conc.(ppm)	Response	Topt (°C)
Rao,(2000) [40]	Pd-ZnO	Hydrolysis	Ethanol	1000	95%	175
Lee, et al.,(2002) [53]	SnO_2	Silk Printing	VOC's	100%	3000	400
Li, et al.,(2004) [58]	WO_3	Hydrolysis	VOC's	500	13.5	40
Villalpando-Paez, et al.,(2004) [59]	CN_x NT's	Thermolyzing	Acetone	1000	4%	RT
Zhu, et al.,(2004) [61]	TiO_2/ZnO	Sol-Gel	VOC's			370
Sahay,(2005) [62]	ZnO	Spray Pyrolysis	Acetone	2000	45%	325
Zhang, et al.,(2006) [66]	$La_{1-x}Pb_xFeO_3$	Sol-Gel	Acetone	500	30	250
Liu, et al.,(2006) [67]	$LaFeO_3$	Polymerization	Acetone	80	204	400
Zhao, et al.,(2006) [68]	SnO_2	Dip Coating	Acetone	1000	29	RT
Rezlescu, et al.,(2006) [69]	$NiFe_2O_4$ + 1%CaO	Self- Combustion	Acetone, LPG	Saturated Vapors	4.5	215
Rella, et al.,(2007) [70]	TiO_2	PLD	Acetone, Ethanol	200	12.5	400
Zhang, et al.,(2007) [71]	$ZnFe_2O_4$	Pyrolysis	Ethanol, Acetone	500	12.27	200
Kim, et al.,(2007) [72]	SnO_2/ZnO	CSD	C_2H_5OH	200	20	400
Ge, et al.,(2007) [74]	CeO_2/ZnO	Dip Coating	VOC's	100	80	320
Chang, et al.,(2008) [75]	Au/ZnO	Au Adsorption	Acetone	200	82.5%	300
Qi, et al.,(2008) [76]	ZnO	Facile Solution	Acetone	50	16	300
Qin, et al.,(2008) [77]	SnO_2	Hydrothermal	Acetone	500	16	290
Wisitsoraat, et al.,(2009) [79]	NiO_x/TiO_2	E-beam Evaporation	Acetone, Ethanol	100	50	300
Zhu, et al.,(2010) [80]	SnO2	Sonochemical	Acetone	50	15	350
Kakati, et al.,(2010) [81]	ZnO	Sol-Gel	Acetone	1000	15 sec	200
Pawar, et al.,(2010) [82]	ZnO	Dip Coating	Acetone	2000	90%	275
Murade, et al.,(2011) [84]	$LaFeO_3$	Sol-Gel	Acetone	700	0.8	275
Liu, et al.,(2011) [85]	ZnO	Electrospinning	Acetone	1000	78	360

Ahn, et al.,(2011) [86]	ZnO	Electrochemical	Acetone		1.75	RT
Shi, et al.,(2011) [87]	WO_3	Sol-Gel	Acetone	0.05		300
Righettoni, et al.,(2012) [88]	WO_3	Flame spray pyrolysis	Acetone	20	10 sec	350
Gao, et al.,(2012) [89]	WO_3–Cr_2O_3	Sol-Gel	Acetone	20	8.91	320
Song, et al.,(2012) [90]	SnO_2	PS spheres	Acetone	100	12	250
Wang, et al.,(2012) [91]	ZnO	Sol-Gel	Acetone	100	5	270
Zhang, et al.,(2013) [92]	WO_3	Hydrothermal	Acetone	55		200
Do and Wang,(2013) [93]	Au/Al_2O_3	Chemical	Acetone	29	3-10 min.	
Shan, et al.,(2013) [94]	Fe_2O_3	Electrospinning	Acetone	50	10 sec	240
Cheng, et al.,(2014) [98]	SnO_2	Elecro-Spinning	Acetone	100	65	340
Zhou, et al.,(2015) [100]	$ZnFe_2O_4$	Acetone	Acetone	100	3	200
Wang, et al.,(2015) [101]	NiO	hydrothermal reaction	Acetone	100	500	250

Research Gaps and Objectives

1.1 Research Gaps

In the work carried according to literature survey, it has been observed that

A. Uniform heating of the sensing layer will be a key parameter which indirectly influences the sensitivity and detection mechanism for gas sensor. ZnO based gas sensor is lacking in the efficiency due to non-uniform heating for microheaters. There are different geometries that are analyzed and compared to one another. But very less work is done to optimize geometry area and to achieve temperature uniformity in particular geometry. Hence, analyzing the efficient design of a microheater for uniform heating shall be of high interest. Further to study the geometries for uniform heating with In-Plane integrated IDT cum microheater, the form of sensitivity for the different gas sensors remains an open area of research. An analysis of different type of In-Plane integrated IDT cum microheater geometries & uniform microheating has been lacking in research literature.

B. Further the literature survey suggests for the improvement in gas sensing parameters which can be optimized separately for every sensor. The acetone sensors are now rapidly gaining the researcher's interest due to medical as well as environmental aspects. Hence there is a lot of work to be done towards enhanced and precise detection of acetone for parts per million (ppm) as well as parts per billion levels (ppb).

1.2 Research Objectives

The following research objectives are formulated:

A. Design and Fabrication of microheater and IDT.

B. Study of sensing properties of gas sensors.

2. Research Methodology Adopted

2.1 Literature review & workflow

The research is started by following the above said objectives, with a comprehensive literature review. Literature review radiance the parameters or the constraints that are affecting the sensitivity and detection mechanism of ZnO based gas sensors. To have a clear idea about the uniform heating, some microheater structures are studied with different geometries. Various microheater and IDT architectures are studied in continuation with most prominent geometries for the microheaters, so that an efficient

geometry can be designed by the help of simulation tool (COMSOL software). The best outcome results for the optimized geometry has been fabricated for gas sensing applications.

2.2 Performance study of gas sensing by optimizing the following parameters:

A. Annealing temperature variation
B. Thickness variation of sensing layer
C. Dopants for high selectivity for the sensor.

The above said studies are performed in continuation such that a high crystalline layer with optimum thickness of the sensing film shall be obtained in order to achieve high sensitivity and selectivity for the sensor.

After achieving the optimized parameters for the high sensitive and a selective acetone sensor, the research work has been published in reputed journals of the related area.

3. Organization of Thesis

The thesis is organized into six chapters. A brief outline for the thesis is as follows:

- Chapter 1: This chapter introduces to the basics of a gas sensor, motivation of the work, research methodology and survey of literature. Further, defining the research objectives that comes out from the literature survey.
- Chapter 2: This chapter deals with the various characterization techniques and equipment that have been used for the fabrication and characterization of the gas sensor.
- Chapter 3: The chapter presents a complete processes for the fabrication of gas sensor that has been followed for fabricating the presented sensor. The chapter includes various optimizations like annealing temperature variation, thickness variation of the sensing layer with molarity concentration variations.
- Chapter 4: This chapter deals with the various dopants used for the fabrication of the sensor to optimize the sensor performance for optimum sensing responses as well as high selectivity towards particular gases.
- Chapter 5: This chapter deals with a new proposed architecture for an In-plane or coplanar Microheater with inter digitated electrodes/transducer (IDE/IDT). The chapter includes a designing of the microheater for efficient heating of the sensing

layer with IDT in a coplanar fashion. The architecture with most efficient heating has been fabricated and studied for a hydrogen based gas sensor with pre-optimized parameters.

- Chapter 6: Conclusion and Future Scope

Chapter 2

Thin Film Deposition and Characterization Techniques

"This section presents a brief description about the various thin film deposition techniques and characterization tools employed for the research work presented in the thesis. Deposition techniques include chemical solution deposition method and RF sputtering which are used for the deposition of pure ZnO, metal doped ZnO thin films, metal nanolayer and nanodots and Pt/Ti inter-digital electrodes. Brief description of various characterization tools including thickness profiler, X-ray Diffractometry (XRD), Scanning Electron Microscopy (SEM), Atomic Force Microscopy (AFM), Transmission Electron Microscopy (TEM), UV-visible, Photoluminiscence (PL) and Raman Spectroscopy used for the structural, surface morphology, optical band gap and modes studies of the thin films is presented in this section. The basic working principle of these deposition technique and characterization tools have also been highlighted".

2.1 Introduction

In today's era, the field of nanotechnology is progressively conceiving the novel materials with such combinations of chemical, physical as well as electronics and mechanical properties that leads the development towards the safety concerns and other luxuriating resources for the society. The requirement of sub-micron miniaturization leads towards the development of thin film technology imperative which could lead to the fabrication of cost-effective, reproducible, controllable, reliable and small electronic devices. This has stimulated a new expanding and interesting branch of material science known as thin film semiconductors[106]. A thin film may be defined as a submicron dimensional materials that are fabricated by depositing one by one condensed atomic/ionic/molecular species of matter. Thus thin films posses different properties from the bulk material due to which these can be used for semiconductor device fabrication and optical coatings. It is a layer of material ranging in thickness from fractions of a nanometer (monolayer) to several micrometers. Availability of variety of thin film materials, techniques for their deposition, spectral and optical characterization have increased the utility in the manufacturing of devices for different applications.

Fabrication of a thin film of a material via any deposition method begins with the arbitrary deposition atom by atom, molecular/ionic nucleation of the species over the substrate surface and consequently filling the network to form a continuous layer of material. There are several properties that can affect the deposition conditions, such as, temperature, atmospheric conditions surrounding ambience and the growth rate on which nucleation and the growth stage depends. In particular, controlling grain size, surface morphology, crystallographic structure, preferred orientation and reproducibility are primary concerns of all thin film deposition techniques. There exists broadly two main approaches to grow nano-materials in thin film forms, namely physical deposition and chemical deposition [106].

Physical deposition produces thin films at nanoscale by exploiting large and externally-controlled targets by thermodynamic or mechanical means. The material is placed in an energetic and entropic atmosphere, so that particles of material can escape from its surface. The substrate surface acts as a platform for the formation of solid layer by redistributing the energies of particles of material. The complete assembly is kept in the deposition chamber having a low pressure vapor environment, which enables the maximum free movement of particles. Thin films produced from physical method approach are directional as particles are

likely to follow a straight path. In contrast, thin film deposition via chemical deposition involves molecular species which are usually precursors. These precursors when dissolved in a required solvent reacts chemically and results in the formation of more complex molecular structures at a solid surface in the form of thin film.

The major advantages of employing chemical deposition methods for thin film fabrication are cost effectiveness, good control over stoichiometry, ease in the synthesis of self-organized thin films with complex chemical compositions. Different techniques used for thin film deposition using physical and chemical route are broadly classified in Figure 2.1.

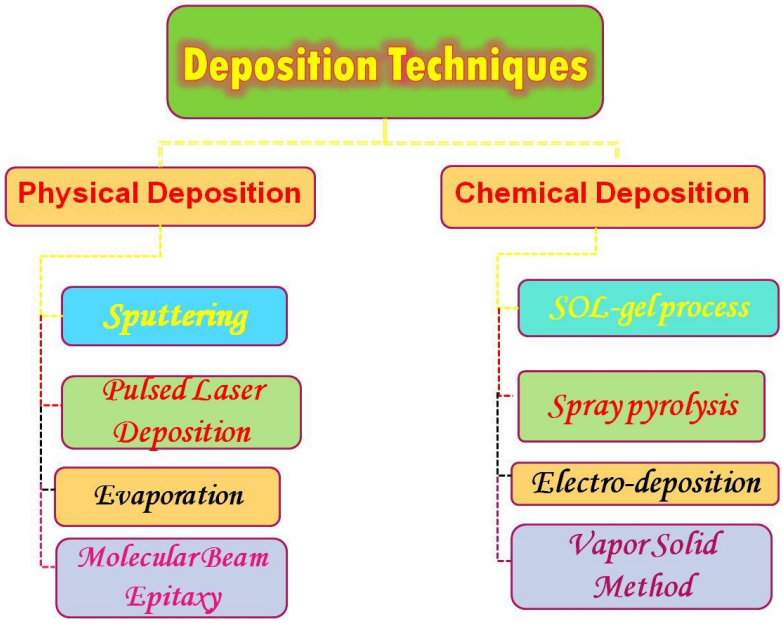

Figure 2.1: *Classification of thin film deposition[107].*

Nevertheless, most of the above mentioned physical deposition methods can be used for the fabrication of high quality ZnO thin films, but these cannot be used for mass production due to limitations like temperature requirements, high vacuum, expensive production equipment etc. However, the sol-gel process is the chemical deposition technique which need relatively simple instruments, resulting in reduced bulkfabrication costs and ability for deposition with complex shapes.Besides this, many advantages can be drawn from sol–gel such as fabrication ease in making large-area films, quick composition adjustment, and ability in carrying out doping at molecular level. Especially, this method provides suitability for the fabrication of multi-component metal oxide thin films[108]. In the present work, thin films of ZnO and metal doped ZnO are fabricated using sol-gel route due to so many advantages over any physical method. However, the nanodots, nanolayers of metal and inter digital electrodes for electrical and UV sensing are deposited using RF sputtering and thermal evaporation

techniques. The present section describes the theoretical background of the Sol-gel process, RF sputtering and thermal evaporation with their advantages and disadvantages respectively.

2.2 Sol-gel Processing or Chemical Solution Deposition (chemical method)

Sol-gel process or Chemical Solution Deposition (CSD) is a route followed for producing solid materials using tiny molecules. Fabrication of semiconductor thin films in several forms like powders, fibers, thin film coatings, micro-porous inorganic membranes, monoliths and porous aerogel materials can be done very easily by employing CSD technique as shown in Figure 2.2[109].

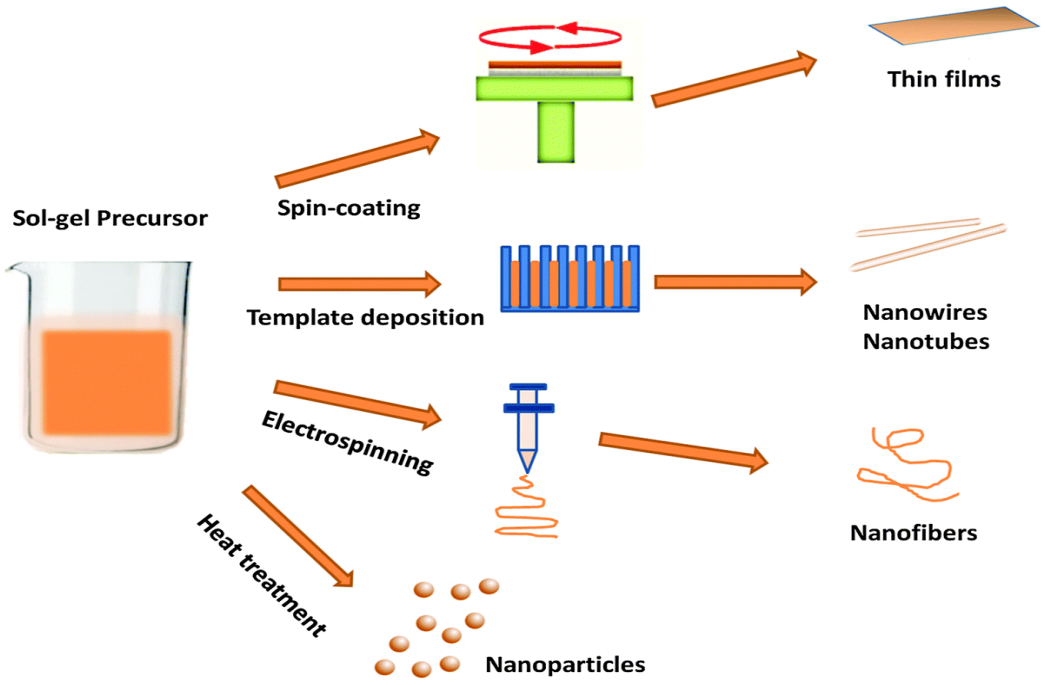

***Figure 2.2**: Sol-Gel Fabrication Techniques.*

The basic principle of sol-gel method is conversion of monomers into a stable suspension of colloidal solid particles or polymers in a liquid (*sol*) which acts as the precursor for a porous, three-dimensional, continuous solid network surrounding a continuous liquid phase (or *gel*) of either discrete particles or network polymers. In the term of physical chemistry it can be inferred that chemical solution deposition (CSD) or sol gel method involves the formation of homogeneous solution of desired compounds by dissolving metal-organic (or inorganic) salts in a required polar or non-polar solvents. In this processing, chemicals with which the process begins are usually complex compounds of the significant metal ions, acting as solutes and are

called precursors. The solution prepared is treated with appropriate stabilizers for reducing aging effects and act as capping agent to obtain the desired controlled shape.

For thin film fabrication, various combinations of precursor solvents and stabilizers have been employed. The reaction between precursor, solute and stabilizers and their unique properties affects the preparation process and establish the final product. High metal content, high solubility in common solvent, chemical compatibility, cost effectiveness and thermal decomposition without evaporation are some of the essential features of a compound to be a precursor. On the other hand, the solvent should possess high vaporization rate and should be chosen carefully in order to get a solution with high concentration of necessary components, proper viscosity, and surface tension. Nature of the precursor decides the preparation technique out of many CSD synthesis techniques available. The two major techniques have been discussed in the subsequent section.

2.2.1 All Alkoxide method

In this method, alkoxide of each metal with required composition are dissolved in an alcohol solvent. Thereafter, hydrolysis is done by adding water to alkoxide solution followed by condensation and network formation. This leads to the eventual formation of polymeric gel/sol. The advanced ceramics which are used at large scale are multicomponent materials having two or more types of metal cations in the same lattice[110]. Solutions which are formed using this method are expected to be highly homogeneous as alkoxide precursors are mixed at the molecular level in the solution.

However, unequal hydrolysis and condensation rates of the used metal alkoxides are the major problems in the synthesis of homogeneous multicomponent solutions. This results in separation of phases leading to higher crystallization temperatures or undesired crystalline phases. These problems in the formation of multicomponent- alkoxides thus force to choose an alternative method for its synthesis[111].

2.2.2 Modified Alkoxide-Salt Method

The alkoxide-salt approach deals effectively with the problems which are coming with the formation of multicomponent materials using allalkoxide method. The term salt in the alkoxide-salt method basically refers to carboxylates, nitrates, sulfates, carbonates, chlorides, and hydroxides. The alkoxides and the carboxylates are organic derivatives of metals with

metal-oxygen-carbon bonds while nitrates, sulfates, carbonates and chlorides are inorganic derivative of metals. Carboxylate anions $(RCOO)^-$ and nitrates $(NO_3)^-$ are versatile ligands capable of binding the metals in chelating or bridging modes. The metal carboxylates have the important feature of forming metal-metal bond[112].

Acetate or nitrates of metals works for most metals and are active source of metal oxide. The solvents used in alkoxide-salt approach should be chosen carefully as it can modify the reaction by stabilizing the intermediates. In modified alkoxide-salt approach, comparatively nonreactive side products are formed in comparison to all alkoxide approach which makes this method superior than all alkoxide method. In all acetate-alkoxides sol, either choice of carboxylate salts (solutes) or alkoxide alcohol (solvents) holds bridging position and binds different metals together [112]. Stabilizers are further added to control these reactions by reacting with metal precursors at a molecular level, giving rise to new molecular precursors of different structure, reactivity and functionality. To obtain the layered inorganic oxide thin film structures, the homogeneous solution which is prepared in above mentioned methods is coated on a substrate using the spin coating or dip coating techniques.

The thin films which are coated on the substrates are amorphous in nature so the post-deposition thermal treatment is required for the crystallization of as deposited films [26]. In the dip coating technique, the uniformity and thickness of the film is controlled by the optimizing various parameters like rate at which the film is pulled out of the gel, time for which the substrate was kept in the solution and the viscosity of the solution. While in the case of spin coating technique, the uniformity and thickness of the film are controlled by the spinning rate, spinning time and the viscosity of the sol. Figure 2.3 depicts the schematic of deposition of thin films via chemical route technique.

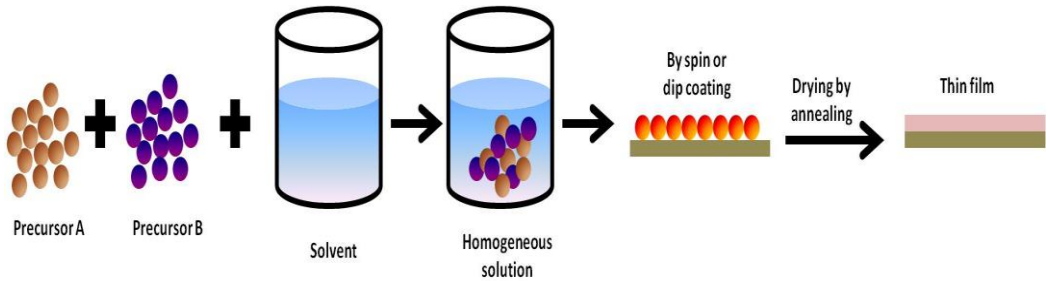

Figure 2.3: *Schematic of chemical route technique.*

2.2.3 Spin Coating

Spin coating is a process in which solution is spread evenly over a surface using centripetal force, producing highly cross-linked and relatively uniform thin film of specific thickness. The photograph of a spin coater used in the present thesis work is shown in Figure 2.4. Fabrication of thin films using a spin coater is done by putting the substrate on the chuck table and holding it by vacuum of the order of 10^{-2} mTorr in order to keep it stable position during revolutions[113]. Once, the substrate is placed properly on the chuck the required drops of precursor solution are casted on the substrate using the pipette and allowed to spin at a particular optimized value of rpm (Figure 2.4). Spinning speed applied to the substrate for thin film fabrication depends on the properties of fluid and the substrate and is typically ranging from 500 to 6000 rpm. Various combinations of spin speed and time are tried and the optimized combination is selected to achieve a required thickness of film along with uniformity.

Figure 2.4: *Photograph of spin coater used in the present thesis work.*

The precursor solution in the spin up stage flows radially in the outward direction by the means of centrifugal force acting outwardly resulting in the formation of uniform thin film. In order to fabricate thinner films, generally higher spin speeds and longer spin times are applied. There is large number of factors and variables involved in spin coating which cancel and average out during the spin coating process. As represented by Figure 2.4, a multi stage. After high-speed spin step, a separate drying step is sometimes required to further dry the film.

For thick film fabrication, it comes out to be advantageous, since long drying times are sometime required to increase the physical stability of the film before handling. In order to remove the residual organic solvents and organic groups, the deposited film should undergo a firing or pyrolization process. The firing of the deposited film converts organic precursor film into an inorganic film. Large volume shrinkage along with the densification process occurring at firing stages, results in the cracking of the films. In order to prevent this serious problem of cracking, a multistage deposition process is adopted.

The spin on layers is pyrolyzed one by one in air at 280 °C for two to three minutes on a preheated hot plate. Thick film fabrication is done by repeating the deposition and pyrolyzation cycle. In order to achieve required thickness, multiple coatings are required. Finally, a post deposition heat treatment at 650°C is provided in oxygen atmosphere for further densification, grain growth and to obtain highly crystalline structure of thin films.

Sol-gel method or CSD technique for thin film fabrication has many advantages and disadvantages as well[113]. Excellent adhesion of the coating on substrate, less deterioration of substrate surface, formation of desired shapes of materials into complex geometries, fabrication of highly pure film by employing precursors of high purity, deposition at low operating temperatures, cost-effectiveness etc. are some of important advantages of CSD the technique over other deposition techniques towards the formation of high quality thin films. On the other hand, there are certain problems which appear during CSD like weak bonding, low wear-resistance, high permeability, difficulty in controlling the porosity of materials, cracking due to high thickness of the film[114].

2.3 Sputtering technique (physical deposition method)

Sputtering is a widely exploited physical deposition method which is used for the deposition of diverse range of coating materials atom by atom. The sputtering phenomena of surface atoms has been discovered in 1852 by W. R. Groove, who then recognized the effect while performing hi studies on plasma discharges. Sputtering process is to be performed under high vacuum conditions, typically ~10^{-6}Torr, which has to be created by accurate vaccum pump or series of pumps (rotary pump backed by either diffusion pump or turbo molecular pump) [115, 116].

Now, the sputtering process can be performed in an inert gas environment, preferably argon (Ar), by maintaining an optimized constant pressure inside the chamber. Then plasma is

created inside the chamber in the presence of the gas molecules by application of high electric field between the two electrodes. The power source which is used to generate plasma and the manipulation of the plasma within the deposition chamber are two main factors which categorizes the type of sputtering. Direct current (DC), alternating current (AC), and radio frequency (RF) sources with utilizing the effective magnetic fields and the bias voltage applied to the target are certain modifications done in sputtering technique for the enhancement of the plasma properties to improve the desired properties for the growth of thin films.

Generally, **"*DC sputtering*"** process has been used from several years for the growth of metal thin films. An insulating target cannot be used for dc-sputtering due to the formation of positive space charge layer on the target surface which prevents further bombardment of the ionized Ar gas molecules thereby halting the sputtering process. Rf sputtering has been employed to successfully overcome this problem as explained below[115].

2.3.1 RF sputtering

The RF Sputtering, as discussed byKern [117], techniques uses an alternating current fieldhaving frequency in the RF region is applied between the electrodes. Electrons oscillate to and fro in an alternating current (AC) electric field and they collide with the processing gas atoms present in deposition chamber during the motion. The motion of electrons becomes highly random due to higher rates of collision with other electrons. This increases the energy of electrons sufficiently which results in ionization collision leading to increase in the number of electrons in the chamber. The processing gas atoms are ionized directly by the electrons present in the plasma as they have sufficient energy. Hence saving the dependency over the secondary generation of electrons at cathode for sustaining the plasma.

Now, these highly charged electrons after creating plasma which is a cluster of very highly charged particles strikes at the target in a to and fro motion causing a release to the atoms of target material. These atoms are deposited over the substrate placed in front of the target at the other end.

2.3.2 DC/Magnetron Sputtering

According to Kern [117], in DC/ magnetron sputtering the strong electric field as well as the magnetic fields are utilized for trapping of the electrons close to the target surface. Secondary

electrons, the electrons of interest, these are ejected from the surface of cathode followed by an ionic collisions with the cathode surface. In dc-diode sputtering, the secondary electrons maintain the discharge. By arranging magnets behind the cathode, magnetic fields can be set up above the cathode surface in magnetron sputtering. The probability of ion collision is enhanced by prolonging the electron residence time in the plasma by magnetic field. This result in large discharge current and increase in sputtering deposition rates.

In the present work the RF sputtering system is used in magnetron and non-magnetron mode. The Pt/Ti inter-digital electrodes (IDEs) are fabricated by depositing the Pt/Ti thin film on glass substrates using RF sputtering in diode configuration (non-magnetron). The nanodots and nanolayers of gold of different thickness are deposited using RF sputtering in magnetron mode.

For electrode fabrication, glass substrates are placed on 3 inch and 4 inch diameter electrodes whereas for deposition of dots and layers of gold, substrates are placed on 2 inch diameter electrode. The photographs of the sputtering unit with 3 inch, 4 inch and sputtering unit with 2 inch diameter electrodes have been shown in Figure 2.5 (a&b). The chamber in both the system is attached with turbo molecular pumps (Pfeiffer make(TC 400)), frequency 833 Hz) backed by a rotary pump (Pfeiffer (DUO 10 MC)) to evacuate the chamber to an ultimate vacuum of 10^{-6} Torr. The vacuum measurements are carried out by using Pfeiffer make full range gauge (PKR-251).

Figure 2.5: *Photograph for (a) RF Sputtering, (b) Magnetron Sputtering.*

2.4 Characterization of thin films

2.4.1 Surface profiler

Thickness profile of a thin film is studied by surface profiler. It also helps in studying the surface roughness of the thin film. The stylus is moved in the vertical direction at a specific contact force in order to obtain a contact with the sample surface. Subsequently the stylus is moved in lateral direction across the sample surface for a particular distance.

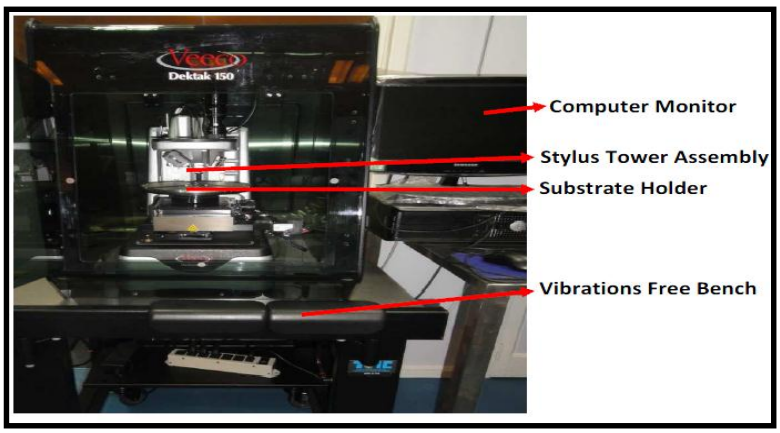

Figure 2.6: *Surface profiler Dektat 150.*

The profilometer is designed to measure very small variations present on the surface following the vertical displacement as a function of the stylus position. An analog signal is generated by the position of the stylus which is then converted to the digitized signal and then it is stored, analyzed and displayed. The average thickness and roughness of thin films fabricated using different deposition methods can be obtained easily using a surface profiler[26]. In the present study, the thickness measurement are carried out using Dektat 150 (M/s Veeco, USA) (as shown in Figure 2.6) with vertical resolution of the system of about 2 nm.

2.4.2. X-Ray Diffraction (XRD)

Crystallographic structure of the fabricated thin films was studied using X-ray diffraction analysis. The phase, crystallite size and stress of the deposited films can easily be determined by this technique. For impurity detection and material identification it is the most commonly and widely used technique[118]. When beam of X-ray incident on a material, it get scattered by the atoms which are arranged in a 3D regular pattern in a lattice. Since, the order of X-ray wavelength matches with inter-Planar spacing of the crystallographic arrangement this leads

to the diffraction of X- ray beam from the surface of material. The rays which got scattered by the atoms combine together constructively at a particular angle following the Bragg's conditions for diffraction.

$$2d\,Sin\theta = n\lambda \quad \ldots\ldots\ldots\ldots\ldots\ldots\ldots\ldots\ldots\ldots\ldots\ldots\ldots\ldots 2.1$$

Where, 'n' and 'λ' is the order of diffraction and the wavelength of X-rays (λ = 1.5406 Å for Cu KS1 radiation), 'θ' is the angle of diffraction and 'd' is the inter-planar spacing. θ is the Bragg's angle for which Bragg's law (Equation 2.1) is satisfied [118].
The crystallite size is calculated using Scherrer's relation for the thin films as:

$$d = \frac{0.94\lambda}{\beta cos\theta} \quad \ldots\ldots\ldots\ldots\ldots\ldots\ldots\ldots\ldots\ldots\ldots\ldots\ldots\ldots 2.2$$

Where, d is the particle size, λ = 1.5406 Å for CuKα$_1$ radiation β= $(\beta_m - \beta_i)^{1/2}$where, β is the FWHM of the dominating XRD peak in radian, β_m and β_i are the measured FWHM and the instrumental broadening respectively, and θ is Bragg's angle.

The image of the XRD sytem used for the present work, Bruker Discover D8 (Central facility, University of Delhi) X-ray diffractometer, is shown in Figure 2.7. It has been used to study the crystallographic structures of prepared thin films and nanostructures.

Bragg's reflections corresponding to the crystal planes (hkl) are observed in the XRD spectra which are indexed and matched with the standard available data. 2θ was recorded at the accuracy of 0.01^o .

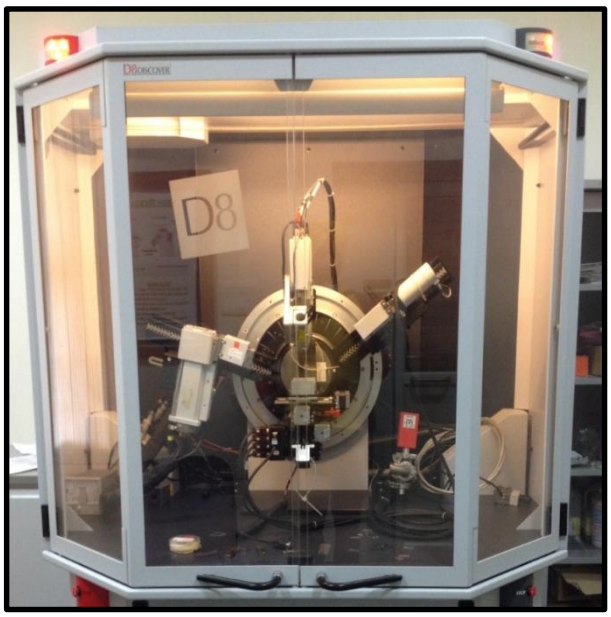

Figure 2.7: *A photograph of XRD system used for present work.*

2.4.3. Atomic Force Microscopy (AFM)

In order to understand morphological changes of the thin film surface, a technique known as Atomic Force Microscopy (AFM) is employed. A sharp probe is utilized which moves above the complete surface of a thin film sample in a raster scan. The tip of the probe is made up of Si or Silicon Nitride on the end of a cantilever which bends in response to the force between the tip and the sample surface. The system operates by measuring repulsive or attractive forces between the tip and the sample [119]. The tip at the end of a leaf spring or cantilever touches the sample very lightly in repulsive "contact" mode. The light coming from laser is reflected onto the split photo-diode when the cantilever flexes. The local height of sample surface is indicated by measuring the vertical deflection of the cantilever measured by detection system by dragging the tip over the sample in a raster scan. Contact mode, Non-contact mode and Trapping mode are the three commonly used modes in AFM imaging. In non-contact mode, the tip does not touch the sample and the topographic images are obtained from measurements of attractive forces.

In tapping mode, the key advances in AFM in order to overcome the problems associated with adhesion, friction, electrostatic forces and other difficulties faced during contact and non-contact modes. In this process, high resolution is provided by making the tip in contact with the surface and then tip is lifted off the surface to avoid dragging the tip across the surface alternately. For small displacements, cantilever obeys Hook's law and due to which the interaction force between the tip and the sample can be estimated. A precise positioning device made up of piezo-electric ceramic material mostly in the form of a tube scanner is used for the tip movement on the sample. Sub-angstrom resolution in X-,Y-,Z- directions is provided by the scanner. The resolution depends on the shape of the tip and it will be limited since the tip may not be able to profile the sides of the surface i.e. rough surface steeper than the sidewall of the tip available[119]. The setup used for AFM studies in the present studies is shown in Figure 2.8. Veeco DICP2 instrument was used for carrying out AFM measurements available at the Department Central Facility and images were analyzed by SPM Lab analysis software.

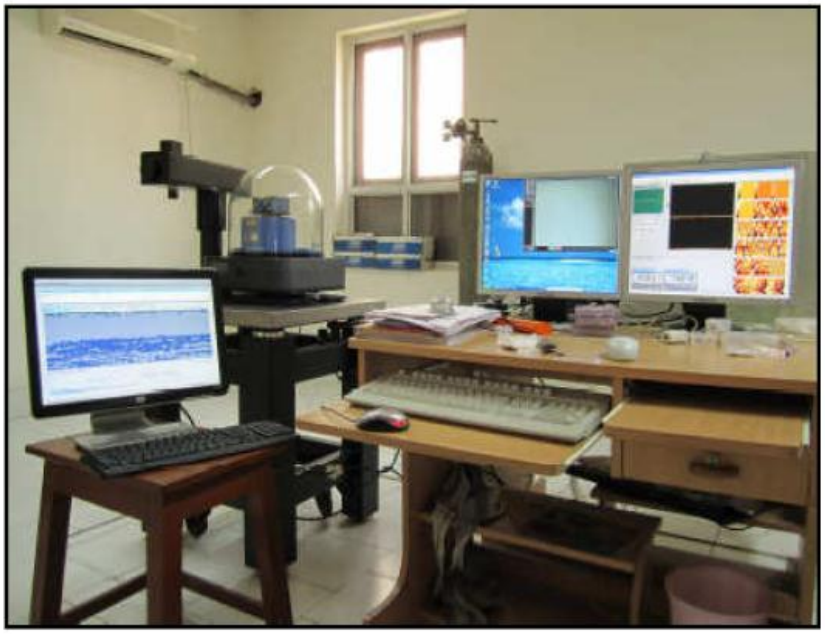

Figure 2.8: *A photograph of AFM system used for present work.*

2.4.4 Scanning Electron Microscopy (SEM)

Scanning electron microscopy (SEM), as stated by Suvarna, et al. [120], is considered to be a relatively fast, cost effective and basically a non-destructive approach for surface analysis. A highly- focused primary scanning electron beam is used for obtaining high resolution images of surface topography with excellent depth of field. Three types of electrons namely primary or backscattered, secondary and Auger electrons are ejected when incident electron beam interacts with specimen.

On the basis of type of electrons used, imaging using SEM can be grouped into two parts: (a) Primary electron imaging and (b) Secondary electron imaging.

In the case of backscattered (primary) electron imaging, electrons emerge from the incident surface of the sample and are collected for SEM imaging. At a given detector position, the primary electrons arrives and can be used to yield images containing both topological and compositional information since the scattering angle is strongly dependent on the atomic number of the nucleus involved.

For elemental analysis of a material, analytical technique known as energy dispersive X-ray spectroscopy (EDX) is used along with SEM. It relies on the investigation of a sample through interaction between the electromagnetic radiation and matter.

2.4.5. Transmission electron microscope (TEM)

The calculation of size, shape and positioning of the nanoparticles over atomic scale levels has been performed by transmission electron microscopy (TEM). It is very helpful technique in producing high resolution two-dimensional images. Because of its maximum potential magnification of 1 nanometer, TEM is one of the best techniques over other microscopes. As discussed by Tyagi and Gupta [26], *"Electrons with high energy nearly upto 300 kV accelerating voltage are used in TEM which are nearly accelerated to the speed of light. In TEM, the beam of electrons acts like a wave-front having wavelength about a million times shorter than light waves. When a beam of electrons passes through a thin section of a material, electrons are scattered and a sophisticated system of electromagnetic lenses focuses the scattered electrons into an image or a diffraction pattern, or a nano-analytical spectrum, depending on the mode of operation. A different insight about the specimen is offered by each of these modes. A highly magnified view of the micro and nanostructure is provided by the imaging mode and finally in the high resolution imaging mode a direct map of atomic arrangements can be obtained (high resolution TEM = HRTEM). The diffraction mode (electron diffraction) displays accurate information about the local crystal structure. The nano-analytical modes (x-ray diffraction and electron microscopy) provide the information about the elements present in the tiny volume of material*". The present studies have been facilitated by University Science Instrumentation Centre (USIC), University of Delhi where FEI TECNAI G230-U-TWIN TEM is used to study the nanoparticles.

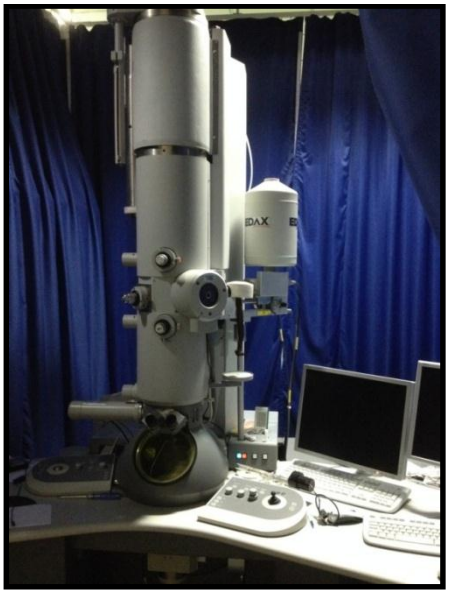

Figure 2.9: *A photograph of TEM system used for present work.*

2.4.6 Optical Studies

Ultravoilet-Visible (UV-Vis) Spectrophotometer

The optical constants like band gap and refractive index of the thin film samples prepared on transparent substrate can be calculated by extracting data from UV-Vis spectra. It involves the measurement of the light absorbed by the sample as a function of wavelength in the far ultraviolet, near ultraviolet and visible region. Electronic structure of solids and thin film can be easily determined by optical absorption studies. In the present studies, the optical transmittance and absorbance spectrums for pure and doped ZnO thin films deposited on the quartz substrate are measured using Perkin Elmer UV-Vis spectrophotometer (Lambda 35) in the wavelength rage of 190 nm to 1100 nm. The instrument used is as shown in Figure 2.10 [121].

As stated by Tyagi and Gupta [26], "*Optical bandgap or the minimum photon energy required to transfer electron from valence band to conduction band of the deposited thin films is calculated from the values of the absorption coefficient (α) given by*

$$\alpha = [\ ln\ 1/T)\ ]\ /\ t \quad \ldots\ldots 2.6$$

Where, t is the film thickness and T is the transmittance. Accuracy of the absorbance values in the wavelength region of strong absorption is better than 2%. Values of the absorption coefficient are determined near the fundamental absorption edge".

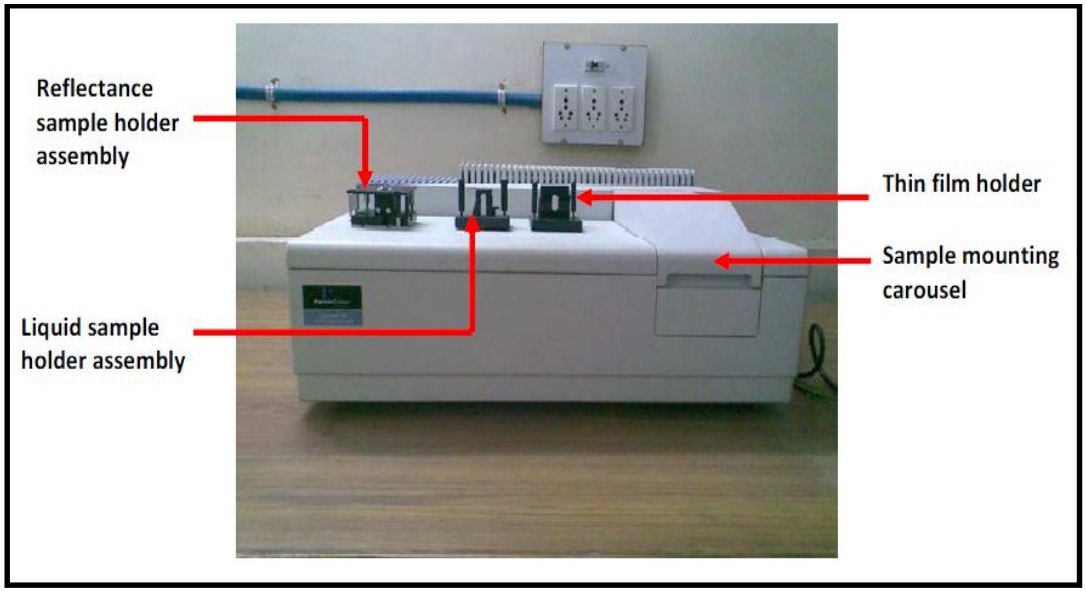

Figure 2.10: *A photograph of UV-VIS spectrophotometer used for present work.*

"For a direct bandgap material the transition probability near the fundamental edge is approximately constant, therefore the dependence of absorption coefficient on the incident photon energy is given by

$$\alpha h\nu = const\ (h\nu - E_g)^{1/2} \quad \ldots\ldots 2.7$$

where, hν is the incident photon energy and $E_g$is the direct optical bandgap of the sample. Value of the bandgap (E_g) was obtained by extrapolating the linear part of the $(\alpha h\nu)^2$versus hν plot to the energy axis".

2.5 Lithography and Etching

In the present study, the fabrication of a gas sensor is to be started with preparation of Inter-digitated electrodes/transducers (IDE/IDTs) over the silicon substrate. The fabrication of these standard 1cm X 1cm IDE/IDTs has been done by a pre-metallization (platinum) of silicon substrate by RF Sputtering process and then using the UV lithography and wet etching procedures[122] as explained below.

The main steps included in the fabrication of IDE/IDTs are as follows:

1. Cleaning of Substrate
2. Deposition of titanium/platinum thin films
3. Deposition of photoresist
4. Preparation of a photomask
5. UV Photo-Lithography
6. Chemical/ Wet etching

The full process from cleaning of the wafer substrate to development and preparation of the photomask will be discussed in the upcoming chapters. Here, the standard process of lithography and the wet chemical etching has been discussed that are used in the present work.

2.5.1 UV Lithography

Lithography is a printing technique which is used for transfer of a pattern over the designated surface using a mask. There are various types of lithography techniques which are differentiated by their printing techniques. There are mainly three types of printing techniques[122]:

1. Contact printing (UV Lithography),
2. Proximity printing (X-Ray Lithography), and
3. Projection printing (e-beam evaporation/lithography)

These printing techniques are identified by the holding position of the mask used for transfer of pattern. The various lithography techniques are specified by the means of the mask positioning and hence their printing techniques. In the present study, UV Lithography technique has been used which is widely exploited for the pattern transfer in the industries as well. The UV lithography technique is done using a photoresist (PR) layered pre-metallized substrate which is then placed over with the photomask patterned over a thin ploy-acrylate sheets which are placed over in contact with the surface of the PR layered substrate. Then the substrate is placed inside the UV exposure chamber. The substrate is exposed in the UV light for an optimized time such that the PR becomes soluble in developers solution (generally 30% KOH (potassium hydroxide)). Now, the pattern of the poly-acrylate sheets is transferred to the surface of the substrate in the form of PR layer. The UV exposure unit used in the present study is shown in Figure 2.11. After this process, the remaining metal not covered by the PR layer is etched using wet/plasma etching processes.

Figure 2.11: *UV Exposure unit.*

In the present study the wet chemical etching has been used for removal of the residual platinum layer over the surface of the substrate using the *Aqua Regia* solution (3 parts HCl + 1 Part HNO_3) at a temperature of about 80°C.

The detailed process for the fabrication is also explained in the upcoming chapters for the Inter-digitated electrodes/transducers (IDE/IDT's).

Chapter 3

Growth Parameter Optimization and Fabrication of Gas Sensor

"This chapter presents the fabrication process of a gas sensor and the results for different parameters optimization by variation in annealing temperature, thickness of thin film and the molarity concentrations of the solution. The results presents a comprehensive study about the thickness of the thin film optimized for an oxidizing gas/vapors followed by the optimum annealing temperature for the thin film fabrication with optimum sol-molarity for the thin film preparation. "

3.1 Introduction

From the past few decades, increasing attention towards environment, human and industrial safety has led to a great improvement in the performance of gas sensing devices. Nano-structured materials have emerged as promising materials towards the development of high performance gas sensors [123]. Although, thin film technology is well established and is playing an important role in semiconductor industry for developing micro- and nano-electronic devices, decorative parts, optical and hard coatings etc. for the last 50 years[106]. Still there is a scope of improvement to fulfill the current requirements in electronics and sensing devices. High surface to volume ratio and possibility to tune the structural and electrical properties as per requirement make thin film advantageous for gas sensor applications in comparison to their bulk counterparts. Thin film with high crystallinity, controlled grain size, and larger availability of active surface sites for interaction of target gas requires reproducible growth conditions and advanced deposition techniques[124]. Gas sensitivity is seen to be drastically enhanced with the reduction of grain size, particularly when the grain size is smaller than twice the space-charge layer thickness[75]. By choosing appropriate deposition technique and growth parameters, various physical properties like crystallite size, porosity and crystallinity of thin film can be easily tailored. Thin film deposition technique like sol-gel offers a great advantage of controlling the particle size and homogeneity at nanometer level[27, 125]. However, nanostructured thin films fabricated using this technique suffer problems of stability and reproducibility. Therefore, a much precise control over the growth process is desirable for realization of commercial devices[126]. Physical deposition techniques offer advantages over the chemical solution deposition technique for obtaining highly stable and reproducible thin films having precise control over the stoichiometry and electrical properties.

It is evident from the literature presented earlier in chapter 1 (Table 1.2) that due to the naturally existing non-stoichiometry and pronounced adsorption of atmospheric oxygen molecules on its surface, ZnO is the most appropriate semiconducting metal oxide sensing material for the detection of several toxic and harmful gases. However, poor selectivity and most of the times high operating temperature (> 300 °C) are some issues that need to be worked upon [127].There are some reports in literature showing good sensing response towards acetone and other volatile organic compounds (VOC's) gas but most of them are working at higher operating temperatures (> 300 °C) (Table 1.3).There are also a few reports

on the lowered or room temperature sensing of acetone gas but they all observed a poor sensing response along with higher response time and recovery time even at relatively higher concentration of target gas, which limits their practical application (Table 1.3). The operating temperature and sensing response of a gas sensor can be tailored by varying the surface morphology and the quality of ZnO thin film [126, 127]. This chapter presents the optimization of growth parameters of ZnO thin films using cost effective sol-gel technique towards efficient sensing of acetone and other VOC's vapors/gas.

3.2 Fabrication of a Sensor Device

3.2.1 Sensor Structure

Figure 3.1 (a) shows the fabricated sensor structure employed in the present study. The sensor structure consists of Platinum (Pt) inter digital electrodes (IDE's) designed over oxidized silicon substrates (IDE's/Si). IDE's were patterned by conventional UV photo-lithography (PLG) technique using a photo mask as discussed in chapter 2. After patterning Pt IDE's over Si, ZnO thin film (sensing layer) was deposited using sol-gel technique (ZnO/IDE's/Si) after protecting the contact pads.

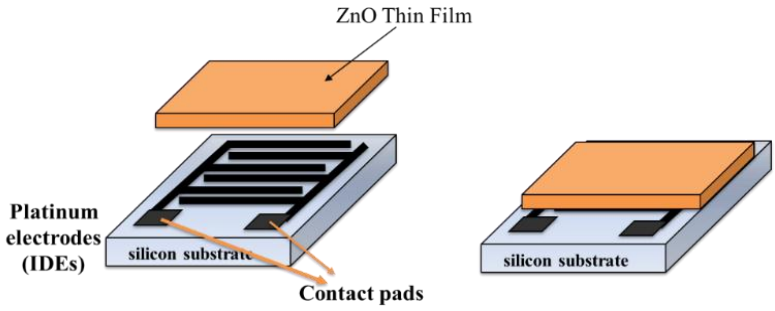

(a) (b)

Figure 3.1: *(a) Prefabricated IDE, (b) Thin film over IDE.*

Following are the process steps utilized for the fabrication of complete sensor device structure (ZnO/IDE's/Si):

1. Wet cleaning of the Si substrate followed by dry cleaning using plasma.
2. Deposition of Pt/Ti bi-layer films using rf sputtering technique.
3. Patterning of IDE's of Pt/Ti using UV photolithography technique.
4. Deposition of ZnO thin film over IDE/Si substrate by sol-gel technique.

The detailed description of above process steps has been given in the following subsections.

A. Substrate Cleaning

The oxidized silicon (SiO_2/Si) is used as substrate with a thickness of 500 nm of SiO_2 layer over the silicon surface. The substrate is cleaned thoroughly through standard RCA 2 procedure. Prior to deposition, Si wafers are cleaned in piranha solution (25 % H_2O_2 and 75 % H_2SO_4) followed by RCA-2 cleaning (heating the Si wafer at 80 °C in a ratio 5:3:2 of de-ionized water, H_2O_2 and HCl solution for 20 minutes respectively). The Si wafer substrates are exposed to reactive oxygen plasma in plasma cleaning system to remove all the microscopic organic impurities attached to the surface of substrate.

The parameters followed for plasma cleaning process of the substrates are given in Table 3.1.

Table 3.1: *Parameters for Plasma Cleaning*

Processing Gas	O_2
Processing Pressure	50 mTorr
RF Power	80 Watts
RF Frequency	13.56 Mhz
Exposure time	15 minutes

B. Pt-IDEs Pattern Fabrication

Design and position of metal electrodes are known to play a significant role in obtainingan enhanced sensor response. The two major factors crucial for obtaining a highsensingresponse are: (i) the amount of active surface area available on the sensing layer forrapid interaction with the atmospheric oxygen or target gas molecules, and (ii) efficientcollection of charge carriers generated on the surface of sensing layer during adsorption/desorption of target gas molecules. The cross-comb like structure (Inter Digital Electrodes, IDEs) of metal with very small spacing between the two nearby fingers (Figure 3.1 (a)) facilitate an efficient collection of charge carriers [128]. Furthermore, fabrication of electrodes (IDEs) underneath the sensing layer offers a large surface area of thesensor to interact with the gas molecules. Pt metal was chosen for the fabrication of IDEs because Pt remains unaffected under high temperature conditions and harsh environment of various toxic gases including highly oxidizing acetone vapors.

The structure has been fabricated over the surface of the oxidized silicon wafer [129] followed by wet/chemical etching method [130]. Figure 3.2 presents a flowchart for the processes involved in the fabrication of the reported architecture in the present work. As shown in the flowchart (Figure 3.2), the fabrication process sequence initializes with the

deposition of platinum over pre-cleaned oxidized silicon wafers. An ultrathin buffer layer of 10 nm thin titanium was grown before depositing Pt on the substrate to enhance the adhesion of Pt thin film. The cleaning process of the wafer is followed as discussed in the previous section. Then the wafers are placed inside the RF sputtering chamber with a distance of ~13 cm from the platinum target. These films were deposited at a pressure of 18 mTorr using 99.99% pure platinum and titanium metal targets in 100% argon ambient with RF power of 100 W and 150 W respectively.

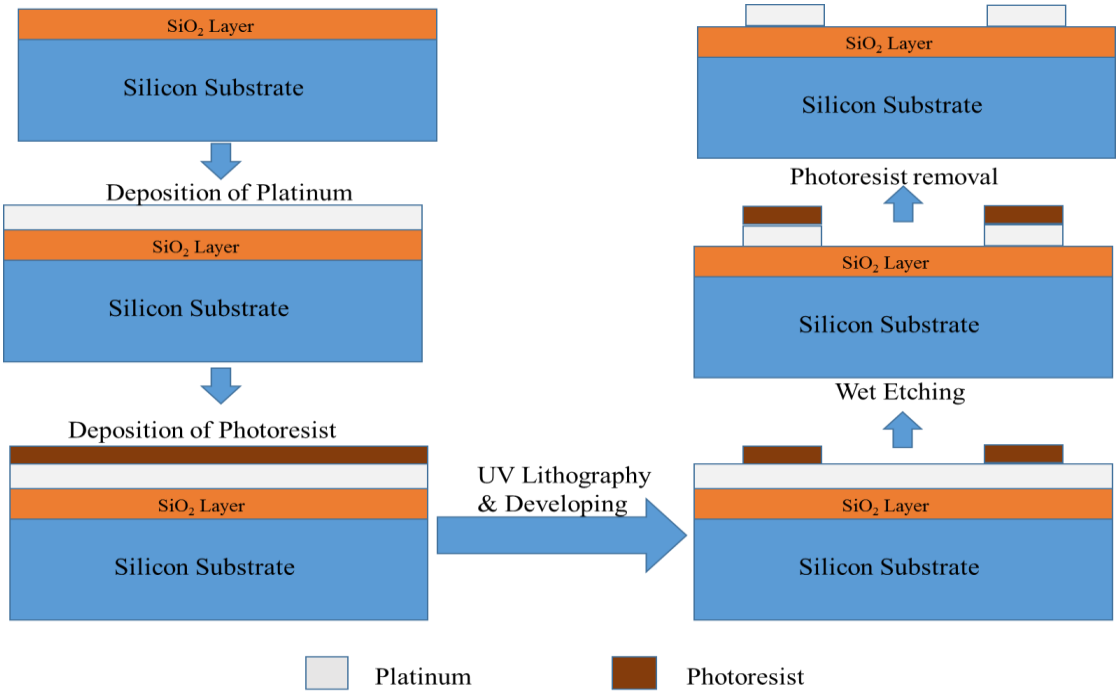

Figure 3.2: *Flowchart of fabrication process.*

After the sputtering process the deposited platinum is over-layered with a positive photoresist. The photoresist is then covered with a mask of shape as that of IDE's and then the sample is exposed to the ultra violet (UV) radiation for 15- 20 seconds. Now, the sample is placed in the developer solution (30% KOH) where the exposed part of the photoresist in UV radiations is removed. The whole process of photoresist layering and removal of the undesired part, are done in dark room having only mild yellow lights. Now the uncovered platinum part over the wafer is etched through wet/chemical etching process. Finally, the remaining photoresist is stripped away by washing the substrate with acetone.

C. Growth of ZnO thin Film

After preparation of the desired architecture over the oxidized silicon or SiO_2/Si substrate, the ZnO thin films are deposited through sol-gel method with pre-optimized 0.1 M concentration of solution (also discussed in upcoming sections) [131]. Analytical grade chemicals provided by Sigma Aldrich are used for the fabrication. The solution is prepared using zinc acetate dihydrate and ethanol as starting materials in a 0.1 M concentration followed by addition of monoethanolamine (MEA) as a stabilizing agent. The solution is refluxed for 30 minutes in open air at a temperature of 80°C [125, 132-134]. Thereafter, the solution is left for 24 hours for ageing process in closed environment. The sol-gel technique is deployed for the growth of the thin films layer by layer. The layers of the ZnO are deposited using an 8-stage programmable spin coater. Each coat is deposited at 3500 rpm for 20 seconds. After each coat the sample is kept for baking at 300°C for 20 minutes. The thickness and the surface roughness of the thin film is estimated and monitored using a stylus based surface profiler (DEKTAT 150). Initially the film thickness is maintained at 410 nm (discussed in upcoming section) by depositing the required number of layers over the substrate. Now, the deposited films are found to be amorphous in nature. Hence, to improve the crystallinity of the deposited thin film, the thin film had been annealed at a temperature of 650°C. The study related to the optimized annealing temperature of 650°C has been discussed in the upcoming sections.

A number of characterization techniques have been utilized to optimize the growth condition for ZnO thin films including Atomic Force Microscopy (AFM), X-ray diffraction (XRD), Scanning Electron Microscopy (SEM), and UV-Visible spectroscopy. Results obtained using these characterization tools are presented in the following sections.

3.3 Structural Property

3.3.1 X-Ray Diffraction Pattern (XRD Pattern)

The sol-gel deposited thin films baked at the temperature of 300°C are found to be amorphous. Therefore the as-grown thin films were annealed at a temperature of 650°C under heated conditions for 5 hours. The Figure 3.3 depicts the XRD graph for the annealed ZnO thin film sample and the inset depicts the XRD graph for the amorphous thin film of ZnO. Well defined peaks of diffraction in the XRD pattern (Figure 3.3) for ZnO thin films after annealing were observed at 2Θ = 31.72°, 34.48°, 36.32° corresponding to the hkl planes

(100), (002), (101) respectively suggesting for the hexagonal wurtzite structure for ZnO. The XRD graph agrees with the literature reported as well as with JCPDS file (JCPDS No. 36-1451) for ZnO confirming for the polycrystallinity for the ZnO thin films on annealing at 650°C under atmospheric conditions but in closed environment.

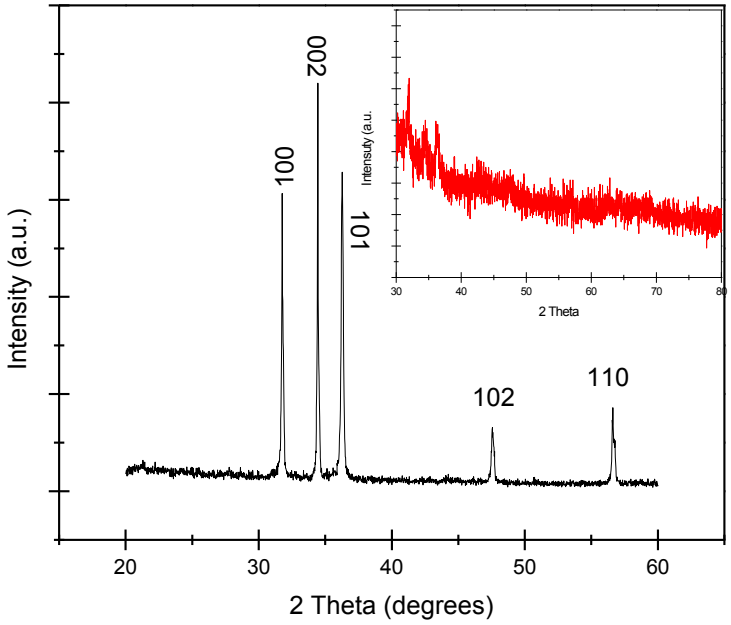

Figure 3.3: *XRD Graph for ZnO.*

This may also be observed from the XRD graph, as presented in Figure 3.3, the full width half maxima (FWHM) of the peaks increased significantly for the sample after annealing at high temperatures. The significance of the higher annealing temperature is discussed in the following sections also. So, this may be concluded that with high annealing temperature the FWHM increases attributing towards a decreasing crystallite size. The detailed XRD graphs for the other studies have been discussed with respective optimizations.

3.4 Optical Properties

3.4.1 UV transmittance Studies

The optical transmittance spectra of ZnO thin film prepared after annealing were measure over the wavelength range of 190 to 1100 nm and are presented in Figure 3.4. Transparency of the thin film was found to be more than 80% in the visible region (Figure 3.4) attributing for good optical quality and low absorption losses. The optical bandgap of the prepared thin film requires the extrapolation of linear portion of the plot of $(\alpha h\upsilon)^2$ versus photon energy ($h\upsilon$); where α is the absorption coefficient, h is planck's constant and υ is the optical frequency. This is basically tauc plot as previously explained in chapter 2. The observed

values of the band gap in the present study are found to be within the range as reported in the literature.

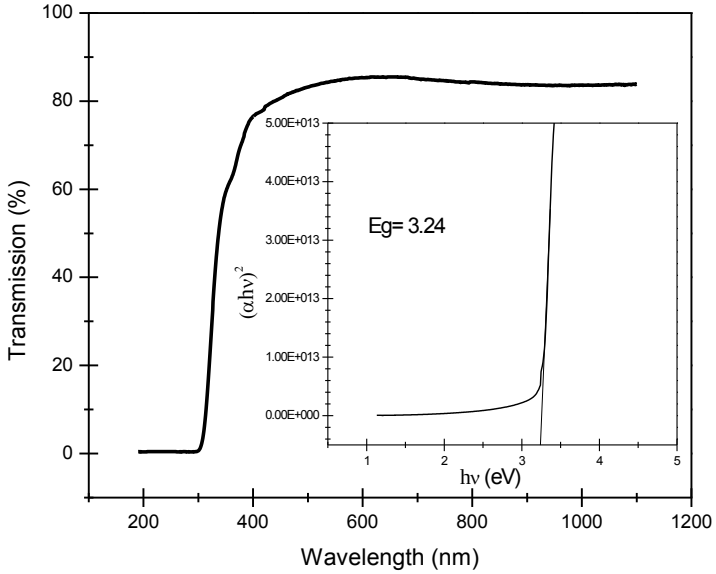

Figure 3.4: *UV-Vis Transmittance spectra of annealed ZnO thin film, Inset shows tauc plot with Eg = 3.24eV.*

3.5 Surface Morphology

3.5.1 Atomic Force Microscopy (AFM) Study

AFM was used to examine the morphology of annealed ZnO thin films grown on silicon substrate.The surface characteristics were examined in the non-contact mode over an area of 5μm x 5μm. As shown in Figure 3.5, it can be established using the AFM images of ZnO thin film for its nano-crystallinity with uniformly distributed grains.

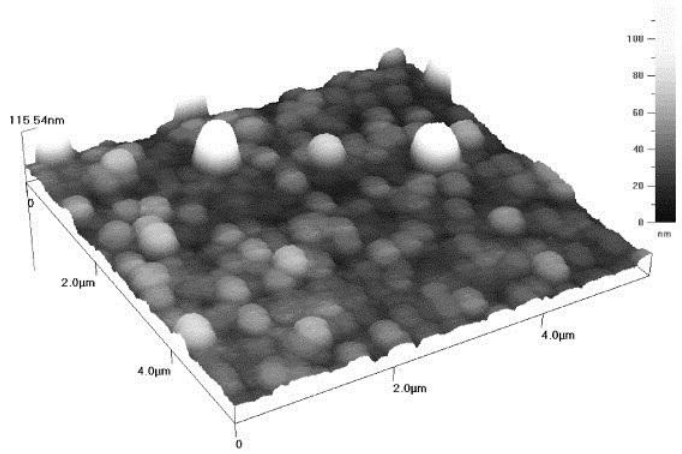

Figure 3.5: *AFM micrograph for ZnO sample.*

The AFM micrograph represents the surface grain structures for the annealed ZnO thin film. The grown structure mainly consists of some tower like homogeneous columnar grains.

3.5.2 Scanning Electron Microscope (SEM) Study

SEM micrographs were recorded for the investigation of the surface characteristics of ZnO thin film. Figure 3.6 represents the SEM micrograph for the prepared sample. The prepared sample needs to be gold coated before taking SEM images, to make the layer of the ZnO conductive. The SEM images may be explained for the high micro-structured porosity with smaller grain sizes attributes for the larger grain boundaries and high surface to volume ratio.

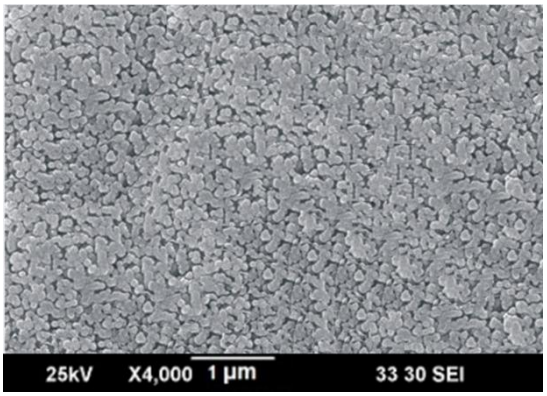

Figure 3.6: *SEM image for the surface of ZnO thin film.*

3.6 ZnO Based Thin Film Sensor

3.6.1 Effect of Molarity Concentrations over thin films of a sensor

The research about the fabrication of ZnO thin films started with the study of molarity concentration variations of the solution prepared using zinc acetate dehydrate with ethanol. The other parameters as shown in the table 3.2 are kept constant. The molarity concentration is varied from 0.05 M to 0.6 M. The study has been performed for the uniformity of the thin film, number of layers deposited (while keeping the thickness constant), surface roughness as well as the porosity of the thin film. As the present study is concerned about the gas sensing of various gases, the layer is characterized and optimized for larger surface to volume ratio with high porosity and ease of fabrication.

Table 3.2: *Constant parameters for the study of molarity concentration variation*

RPM of spin coater & time	3000 RPM & 20 seconds
Baking temperature & time	300°C & 20 mins.
Thickness of sensing layer	400-450 nm
Annealing temperature & time	650°C & 5 hours

The spin coater used is an eight step programmable spin coater maintaining at 3000 rpm for 20 seconds. The samples have been placed in an oven for 20 minutes maintaining 300°C temperature. The thickness of the thin films were monitored using DEKTAT 150 stylus based surface profiler. Then the samples are placed inside a closed air oven at 650°C for 5 hours. The variation in the molarity concentrations with varying number of coats per sample to keep thickness approximately constant is as follows:

Table 3.3: *Variation in molarity concentration with varying number of coats*

Molarity Concentration	**Number of coats**	**Thickness**
0.05 M	15	455 nm
0.08 M	12	440 nm
0.1 M	8	430 nm
0.2 M	5	410 nm
0.3 M	2	415 nm
0.5 M	1	410 nm
0.6 M	1	520 nm

As shown in the table 3.3, with the variation in the molarity concentration, the thickness of the thin film also varies. Hence to keep the thickness approximately constant the number of coats has to be optimized. So, after getting the correct number of coats such that the thickness remains in the range of 400 – 450 nm which is the range optimized for sensing of the oxidizing gases as reported in the literature. The layers with molarity concentration play a vital role for the porosity and the surface roughness issues for the thin film. As the number of layers to be deposited decreases the SEM images shows that the single layered deposited or 2- 3 layers deposited thin films shows a coagulated architecture instead of uniform depositions as shown in Figure 3.7 (a). Hence to optimize the thickness with molarity concentration variations the number of coatings have to be increased and hence the surface uniformity and the betterment of surface porosity and roughness factors, represented by the Figure 3.7 (b).

As the number of coatings increased, the first two to three layers deposited acts as seed layer for further deposition of the thin films. Now, the deposited coatings over previous layers provided increased uniformity with porosity and crystal growth, uniformly over the substrate surface resulting in the increased effective area for sensing over IDT's.

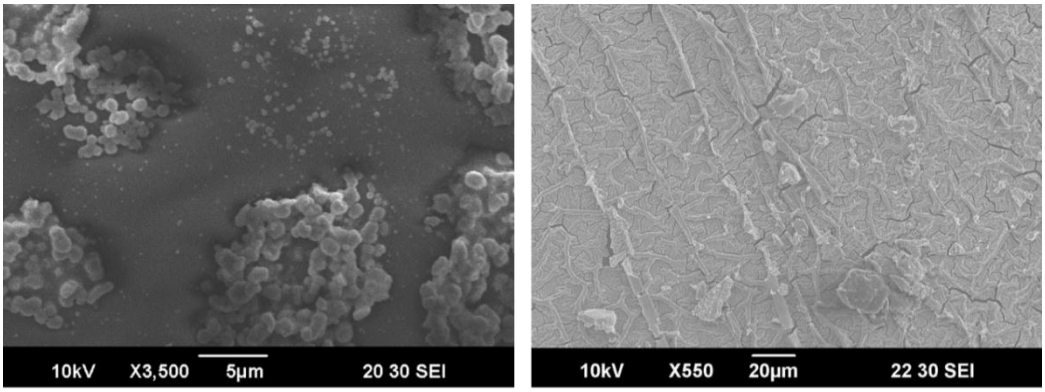

a. Single-coat layer deposition b. 10 coats layer deposition

Figure 3.7: *Different number of coatings for layer deposition.*

3.6.2 Effect of Annealing Temperature Variations

ZnO thin films were synthesized using analytical grade reagents by Sigma-Aldrich. The precursor solution was prepared by dissolving zinc acetate dehydrate powder in ethanol maintaining 0.1 M molarity. Then monoethanolamine (MEA) was added as the stabilizing agent. The solution was stirred at 70°C for 20 minutes in closed environment. The solution was left overnight for ageing. The pre-fabricated IDE patterned silicon wafers (as shown in Figure 3.1) were used for the growth of ZnO thin films using spin coater at 3500 rpm for 15 seconds subsequently heating the prepared films at 300°C for 20 minutes (Figure 3.1).

The spin coating was performed recurrently to achieve the desired thickness of 410 nm. Then the prepared films for the sensors were annealed at various temperatures ranging from 450°C to 750°C individually for 6 hours. The characterization processes were carried out for the films deposited on the plane silicon wafer with IDE patterns with same parameters. The samples annealed at different temperatures 450°C, 550°C, 650°C and 750 °C are encoded as S1, S2, S3 and S4 respectively. The characteristic studies for optical, structural and surface morphologies for the samples were carried out using UV-visible spectrophotometer, XRD and FESEM. An indigenously developed Gas Calibrator and Test System (GCTS) consisting a glass bell jar, thermocouple, heating element, temperature controller and the contact pins

connected to Digital Multimeter (DMM) Keithley 2002 is used for the data acquisition.

Thermal volatization of liquid VOC's is used for preparation of VOC's vapours which are inserted in the chamber through calibrated inlets with desired concentration. The sensing response (S) is given by[12]:

$$S = \frac{R_g - R_a}{R_a} \quad \text{..... (3.1)}$$

Where R_a and R_g represents the resistances of the sensor in air and gas respectively. The time taken to achieve 90% for the total resistance change for adsorption is termed as response time and for desorption, is termed as recovery time.

A. Results and discussions

XRD Analysis

Figure 3.8 represents the XRD patterns for the prepared ZnO thin films at distinctly annealed temperatures. The XRD graphs show the increasing profile of poly-crystallinity patterns for the samples viz. S1, S2, S3, S4.

As can be seen from Figure 3.8, all of the 4 samples indicates preferential orientation along c-axis. The peaks are identified to (100), (002), (101), (102), and (110) plane of reflections for a single phase wurtzite ZnO structure. The diffraction peaks in the XRD spectrum are matched with a pure hexagonal wurtzite structure (JCPDS No. 36-1451) for ZnO. For investigating the effects of annealing temperature variation over crystallinity patterns for the samples, the diffraction peaks (100), (002) and (101) are monitored. This can be concluded from the results that relative intensity for the monitored diffraction peaks increases with the decreasing pattern for full width at half maxima (FWHM) of the ZnO thin films with annealing temperature variation from 450°C to 750°C, which clearly indicates the refined crystallite sizes with increase in annealing temperature.

The results verified that the degree of crystallinity with the crystallite sizes for the samples with increasing annealing temperatures are improved significantly over the temperature ranges.

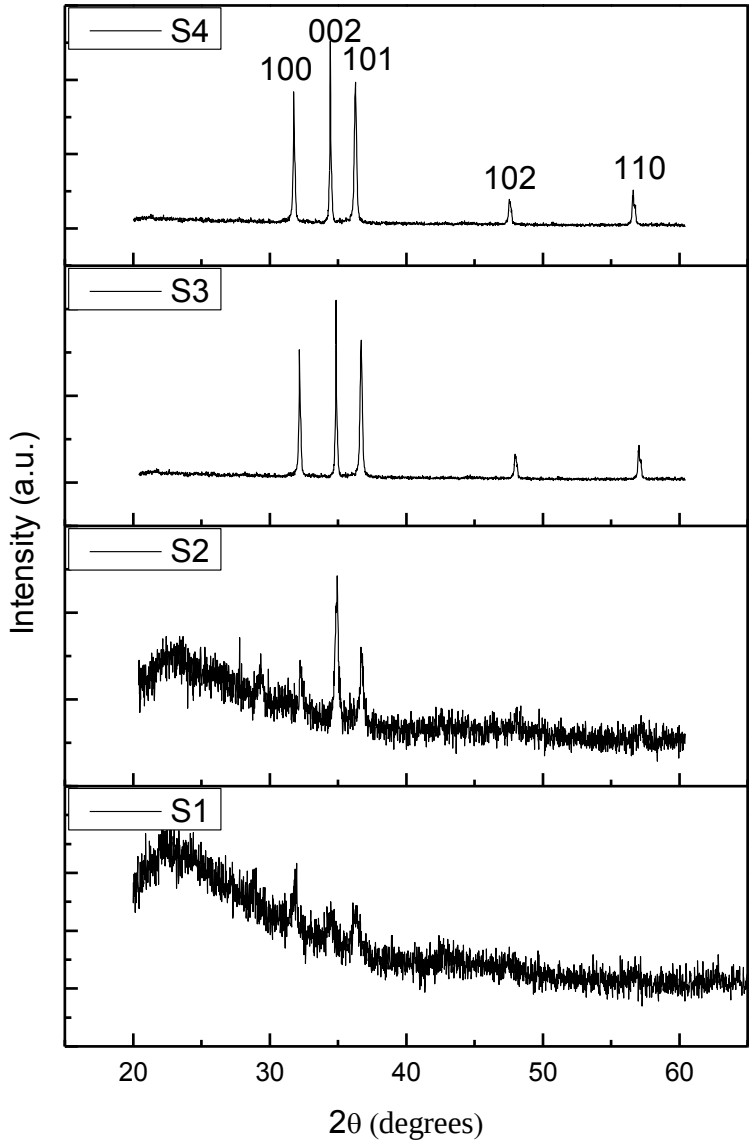

Figure 3.8: *XRD micrograph for all the four samples.*

Surface morphology

The structural characterizations are performed for the structural analysis of the prepared samples. Figure 3.9 shows the FESEM images of the ZnO thin film based sensor architecture.

As shown in Figure 3.9.a, S1 structure where the coagulated nanoparticles of ZnO over the sensor surface results in poor structural forms probably due to non-crystallinity or insufficient annealing temperature. Figure 3.9.b presents the structure of S2, here it may be concluded that the sample S2 exhibits a better architecture but still a non-uniform less coagulated structures formed with much less surface to react with gas particles. Figure 3.9.c and Figure 3.9.d shows the samples S3 and S4 respectively, which represents the ZnO nano-threads like structures are prepared with very high surface area to react with the gas molecules. Figure

3.9.e also represents a thickness of the sample of 410 nm. The FESEM images presents clearly the changing crystallinity phases for all the four samples.

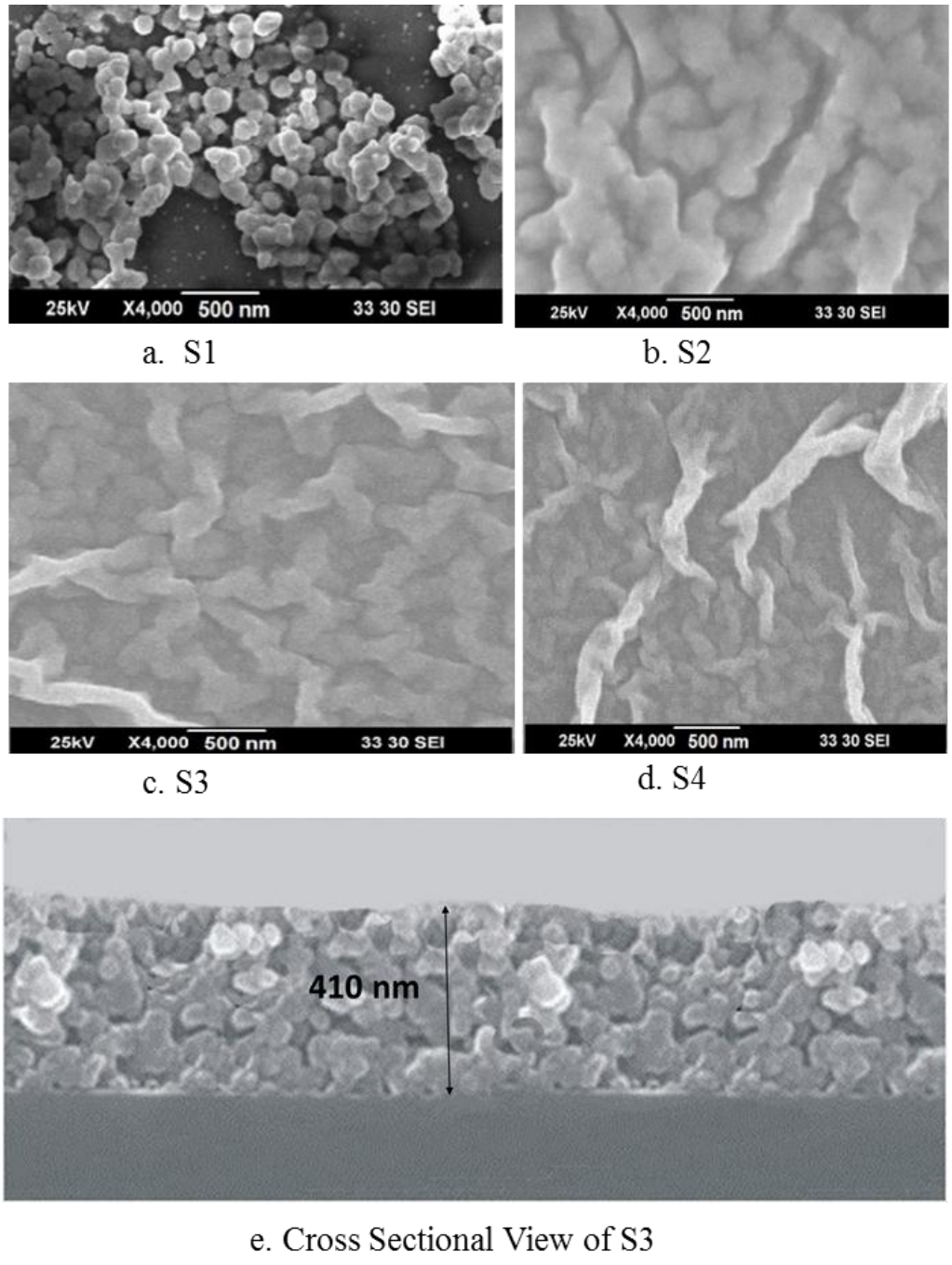

Figure 3.9: *SEM Images for all four samples.*

Optical properties

Figure 3.10 shows the UV-visible transmittance spectra of ZnO thin films deposited on quartz substrates under similar deposition parameters. ZnO thin films are found to be highly transparent (~80%) in the visible region with adsorption edge at around 375 nm.

The energy band gap (Eg) is calculated using Tauc plot (insets of Figure 3.10) and is estimated to be in range for 4.3eV to 3.7 eV. The energy band gap of ZnO decreases from 4.3 eV to 3.7 eV with the increase in annealing temperature. The change in the values of transmittance as well as the band gaps clearly indicates the improving optical properties with increasing annealing temperature of the samples.

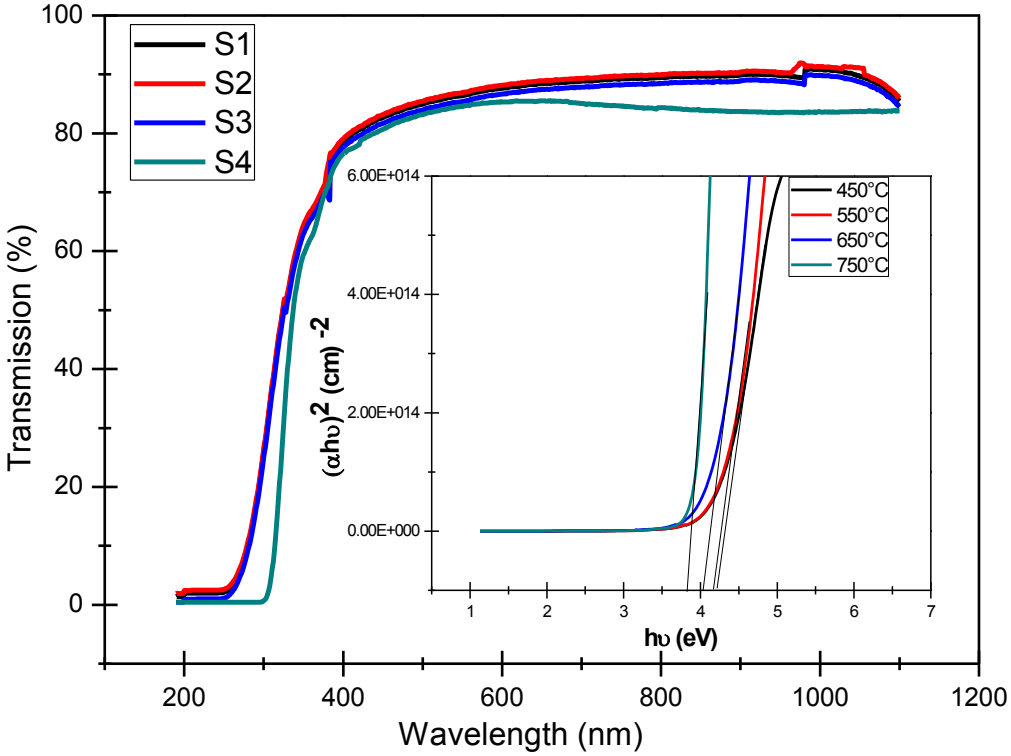

Figure 3.10: *UV transmittance.*

B. Gas Sensing Response

Before gas sensing, all the prepared sensors are annealed at 250°C for 1 hour for desorbing the surface of the samples for any gas contamination. It has also been observed with increasing annealing temperature that the effect of humidity and also other environmental interferences are also reduced with crystallinity of the samples. As the crystallinity of the samples betters the stable resistances in air are achieved more efficiently even at some lower operating temperatures of about 180°C. Figure 3.11 shows the sensors responses for all the samples with temperature ranging from 180°C to 360°C for the four different VOC's. Figure 3.11 also represents the sensor's optimum operating temperatures in a closed environment with concentration at 500 ppm of VOC's vapors. The sensing response values for S1, S2, S3, and S4 increases evidently till maximum values at optimum operating temperatures, then the

sensing responses degrades with increasing operating temperatures [30]. These results may be explained by kinetics and the gas sensing mechanisms over the ZnO thin film surfaces [23].

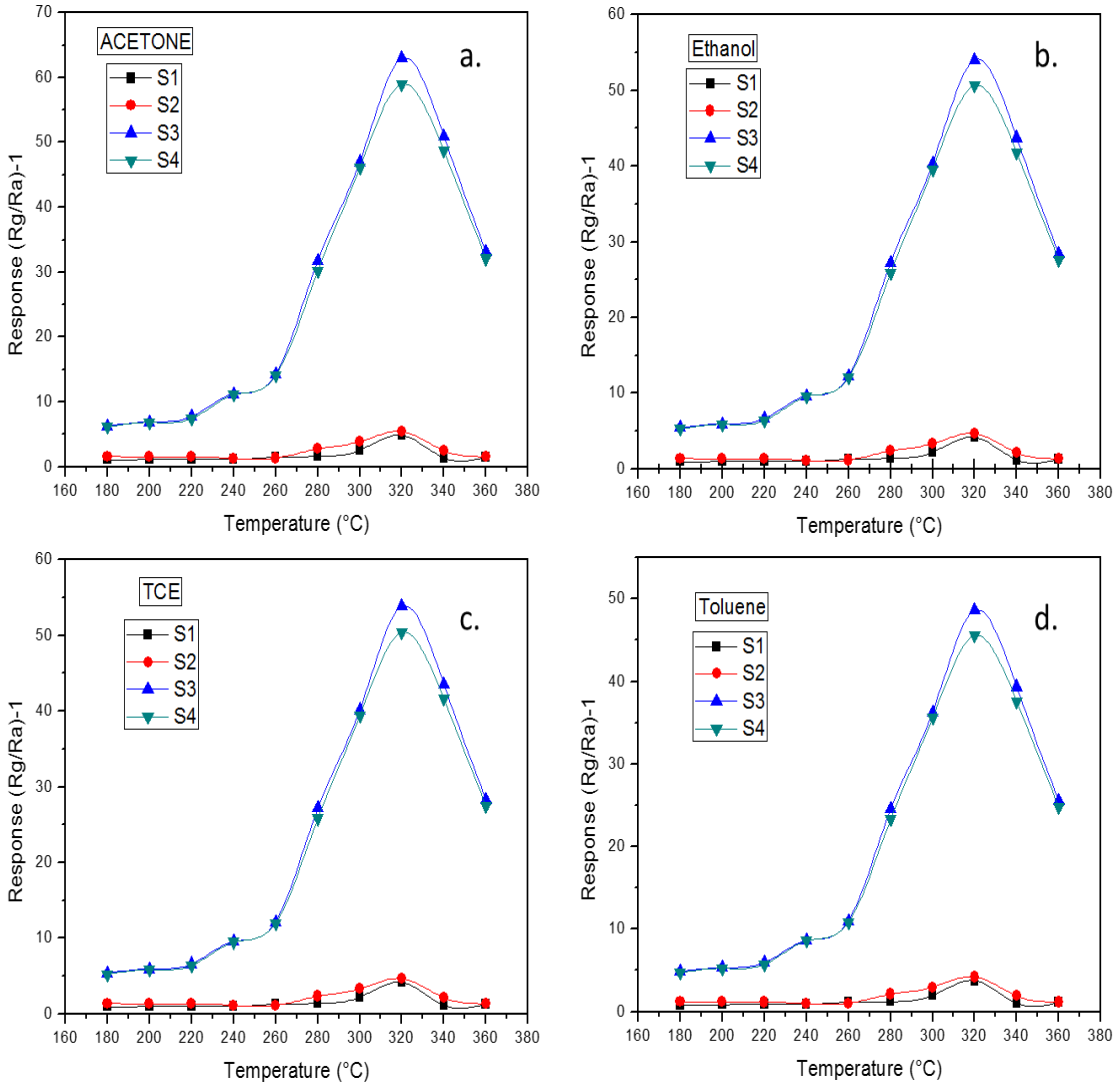

Figure 3.11: *Sensor responses for sample S1, S2, S3 and S4, (a) For acetone, (b) For ethanol, (c) For TCE, (d) For toluene.*

At lower operating temperatures, the gas molecules kinetics is low which results in lower sensing responses. Also, at operating temperatures higher than the optimal operating temperature, the kinetics of gas molecules is that much large that molecules may escape from the active centers of the surface before reactions and will affect the quantity of the gas to be adsorbed. Hence resulting in lowered sensor response. As clearly seen from the Figure 3.11, for all the VOC's vapors S3 and S4 exhibits the highest and somehow equal responses that may be due to the large surface interactions, oxygen vacancies and open network architectures. Analyzing the results we may conclude that this sample is performing best for acetone as it is showing highest response for the acetone vapors. So, further studies are

regarding acetone vapors only. Figure 3.12 shows the sensing response of the sample S3 (with the highest sensitivity) with concentrations ranging from 50 ppm to 500 ppm at 320°C optimal operating temperature.

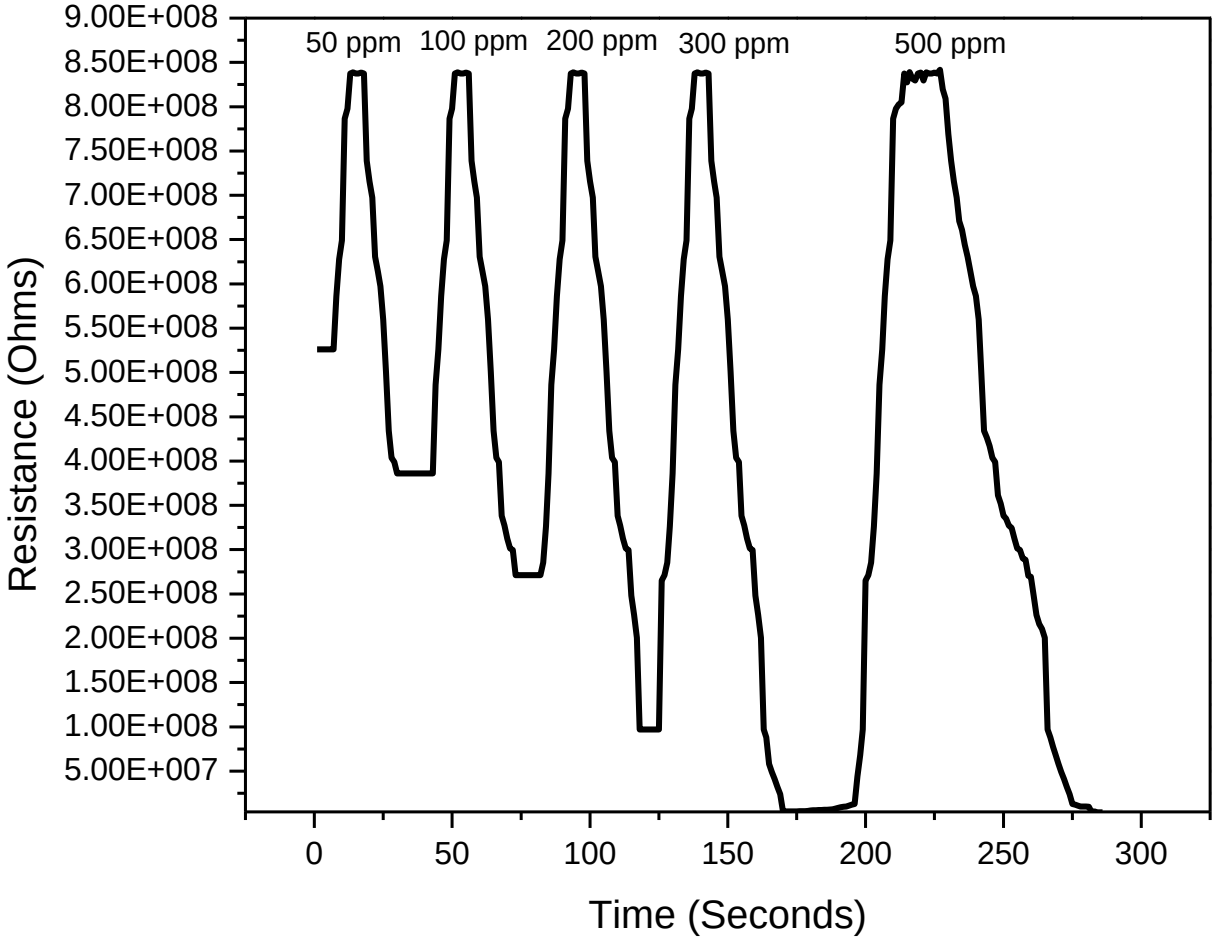

Figure 3.12: *Response at various concentrations.*

Now, it may be concluded that the samples with higher annealing temperatures which in turn, makes the sample highly crystalline exhibits higher and stable responses with nearly equal optimal operating temperatures. Figure 3.13 and Figure 3.14 shows the response and recovery times, respectively, for all the four samples giving another important relation between the samples which depicts the decrease in response times and recovery times of the samples which are annealed at higher temperatures. Also with the increasing operating temperatures, the response times and recovery times decrease for all the four sensors which relate to the higher rates of adsorption and desorption at high operating temperatures as discussed earlier.

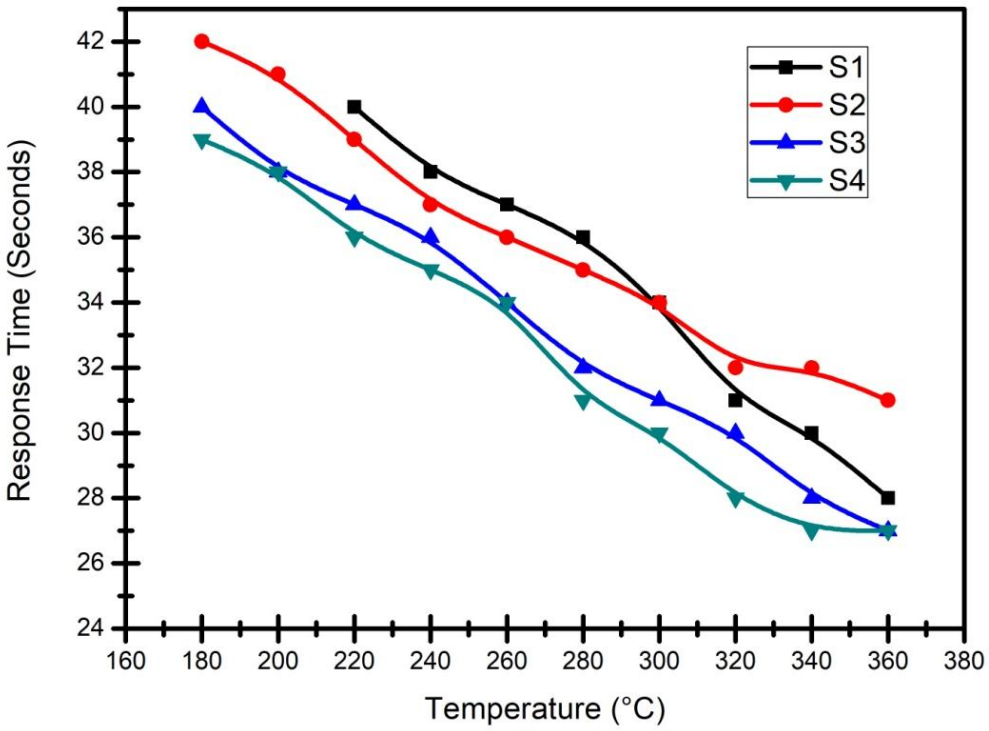

Figure 3.13: *Response Time vs Temperature.*

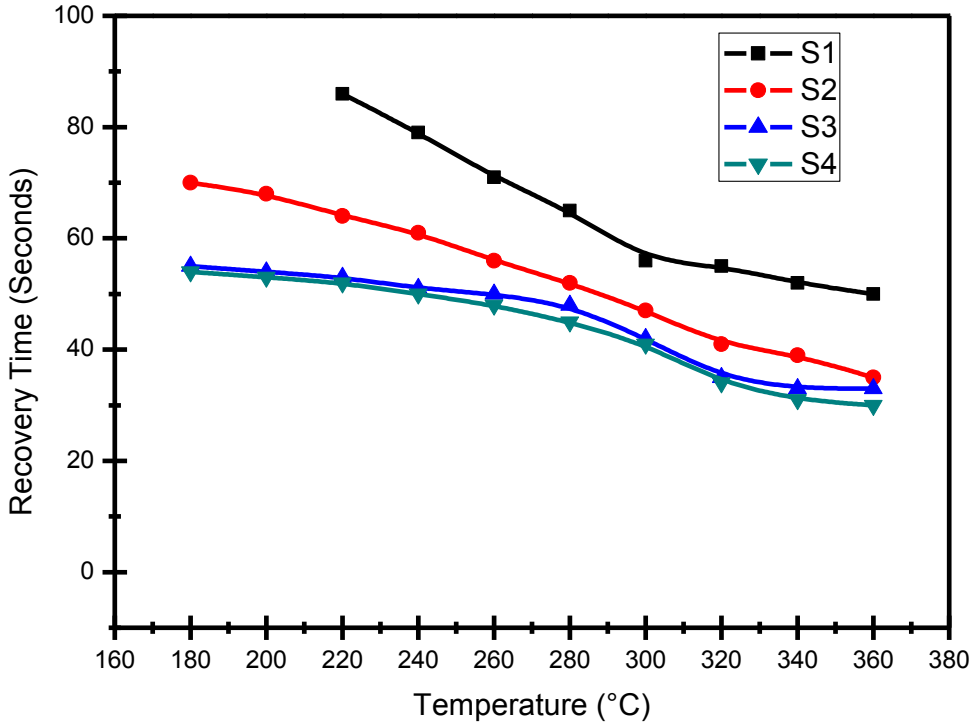

Figure 3.14: *Recovery time vs temperature.*

3.6.3 Effect of Variation in Sensing Layer Thickness

In the present work, ZnO thin films have been studied for various thicknesses of 160 nm, 280 nm, 410 nm and 540 nm to find the optimum thickness such that the sensor exhibits high sensitivity, quick response and recovery times. The optimized thickness comes out to be 410 nm which shows the highest sensing response of 63. The present study proposes for the optimum thickness for an acetone sensor which is further related with high degree of crystallization and larger surface areas.

A. Experimental

The chemical reagents used in this experiment are of analytical grade and the distilled water is having resistivity of 18.2 $M\Omega cm^{-1}$. The Zinc acetate dihydrate $Zn(CH_3COO)_2 \cdot {}_2H_2O$) is dissolved with ethanol to prepeare 0.1 M sol. Subsequently, monoethanolamine (MEA) is added drop wise in distinct amount as stabilizing agent followed by refluxing of solution at 80°C for 20 minutes. The prefabricated inter digitated electrodes (IDE) over SiO_2/Si substrates are ultrasonically cleaned in acetone for 30 minutes followed by desiccation in hot air oven. ZnO thin films has been coated using spin coating technique over the prefabricated IDE's at 2500 rpm for 20 seconds and repeated till the desired thickness is achieved with subsequent baking at 300°C for 5 minutes after each coat. The thin films are annealed at 650°C for 5 hours in a closed and controlled environment for decomposition and oxidation of the precursors of the solution. The samples with thicknesses 160 nm, 280 nm, 410 nm and 540 nm are prepared with repetition of spin coats and termed as samples S1, S2, S3 and S4 respectively. The optical, structural and surface morphological characteristics for the samples have been carried out using UV-visible spectrophotometer, X-ray diffraction (XRD) and field emission scanning electron microscope (FESEM) respectively. For UV-visible spectrophotometer the samples are prepared over quartz substrates with same conditions. For gas sensing characterization processes, the films are deposited on the IDE patterned silicon substrate with same parameters. An indigenously developed Gas Calibrator and Test System (GCTS) consisting of a glass bell jar, thermocouple, heating element, temperature controller and the contact pins connected to Digital Multimeter (Keithley 2002) is used for the data acquisition as shown in Figure 3.15. Thermal volatization of liquid acetone is used for preparation of vapours which were inserted in the chamber through calibrated leaks with desired concentration of 500 ppm in atmospheric conditions. The gas is injected through the inlet nozzle and suctioned using a rotary pump from the other side. The measurement for the

gas sensing response is started at the moment when the gas is introduced in the chamber. The sensing responseis given by equation 3.1.

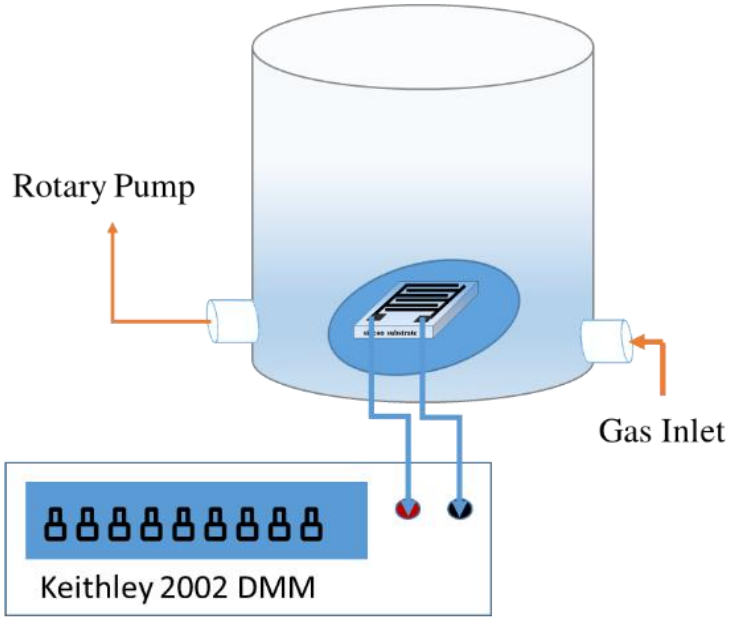

Figure 3.15: *GCTS system.*

B. Results and Discussions

Optical properties

As shown in Figure 3.16, all the four samples have been studied for UV-visible transmittance spectra. The ZnO thin films were found to be highly transparent (~80%) in the visible region with adsorption edge at around 375 nm. The energy band gap (Eg = 3.7 eV) is calculated using Tauc plot (inset of Figure 3.16) and comes out to be almost equal for all the four samples S1, S2, S3 and S4. The same band gap for all the four samples clearly shows the negligible effect of thickness variation over the band gap while the changes in the transmittance with the thickness of thin films may be attributed to the strain changes due to which the interatomic spacing of semiconductors and hence the energy gap is affected. As the thickness is decreased, tensile strain may have decreased and compressive strain along c-axis may have increased which resulted in lower transmittance in the visible region[135].

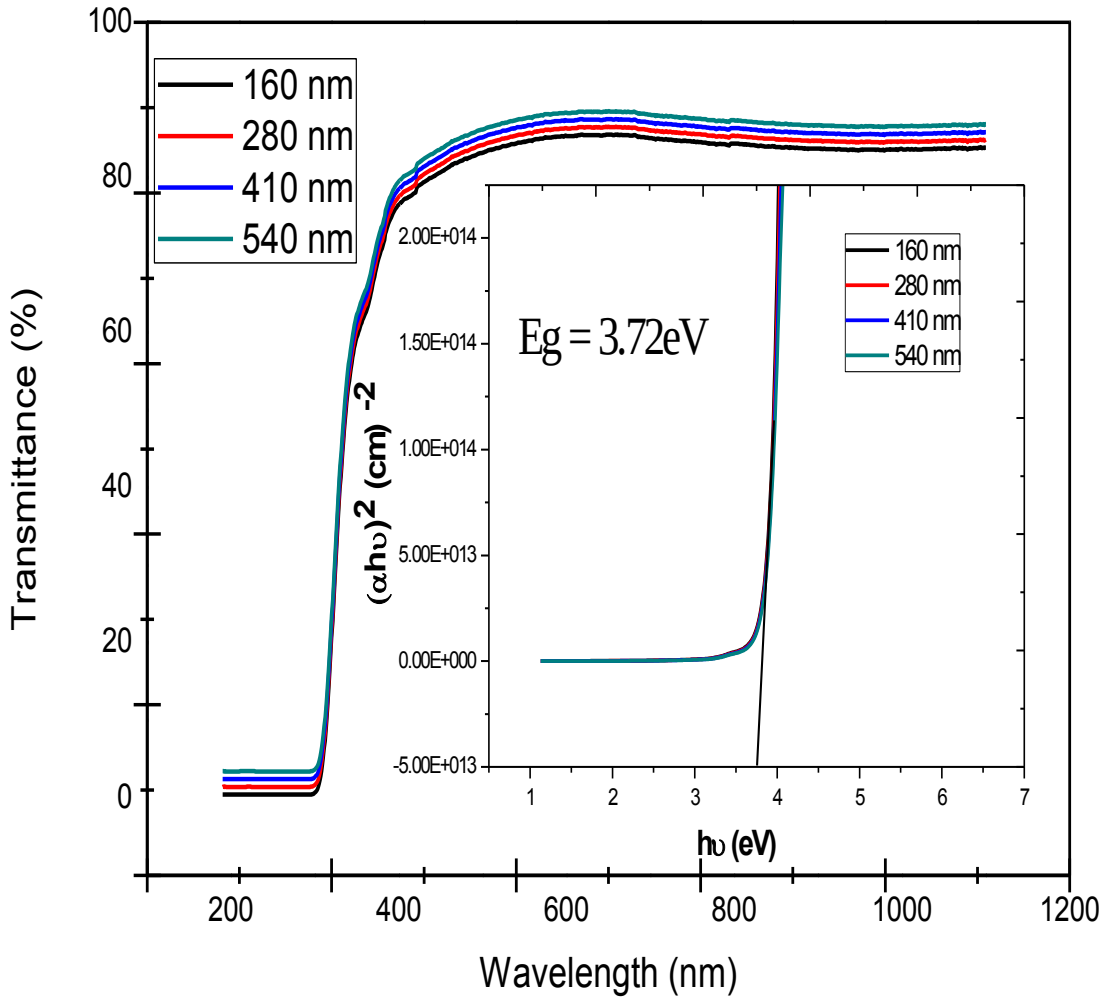

Figure 3.16: *UV Transmittance.*

XRD Analysis

Figure 3.17 depicts the XRD graph for all the four samples. The XRD pattern is analysed from 20 to 60 degrees as presented in Figure 3.17. As can be seen from Figure 3.17, all of the 4 samples indicates preferential orientation along c-axis[136]. The peaks are identified to (100), (002), (101), (102), and (110) plane of reflections for a single phase wurtzite ZnO structure. The diffraction peaks in the XRD spectrum are matched with a pure hexagonal wurtzite structure (JCPDS No. 36-1451) for ZnO[137]. The calculations performed using XRD graph is clearly indicating the increase in the crystallite size with the increase in thickness of the ZnO layer as shown in Table 3.4. According to this calculation the minimum grain size comes out to be 55.6 nm for the sample S1 and maximum grain size of 84.312 nm for the S4. It is clear from the results that there is an increase in the crystallite size with the increase in the thickness. Hence the sensitivity also increase as there is an increase in porosity but after a certain level the crystallite size becomes that much large that it starts hindering the

electron movements[138]. Hence the sensitivity starts degrading after a certain thickness of the sensing layer of the sample.

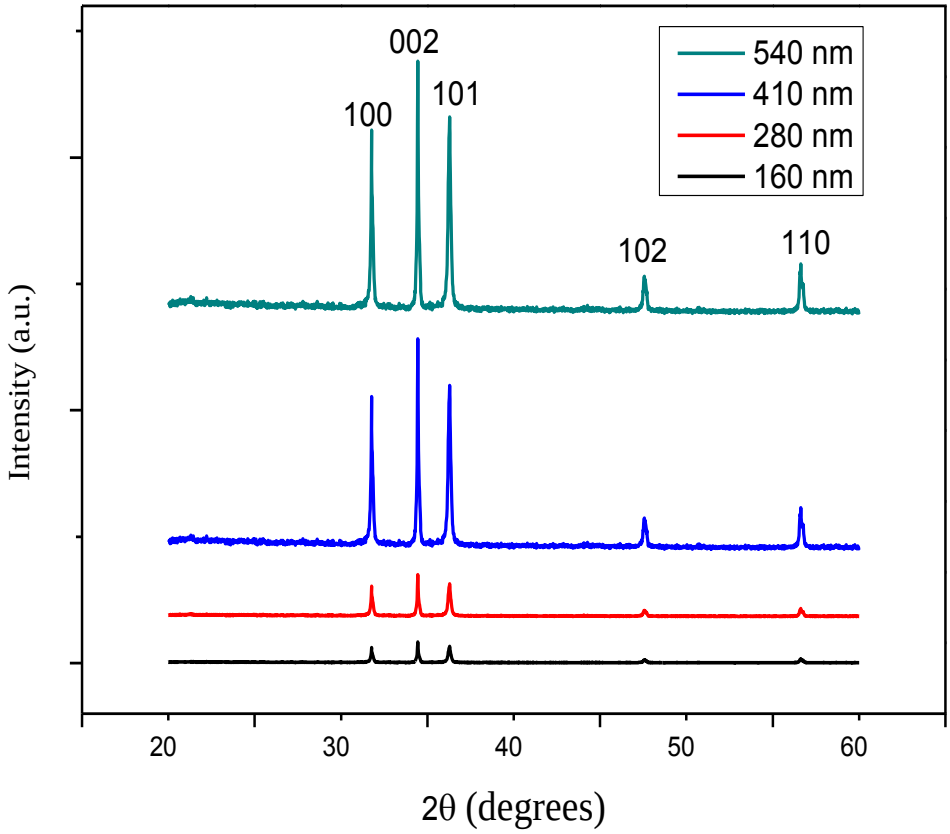

***Figure 3.17**: XRD Patterns.*

***Table 3.4**: Crystallite size calculations using Scherrer's formula*

Sample Coding	Peak position 2θ (°)	FWHM Bsize (°)	Dp (nm)	Sensing Response
S1	34.4442	0.1563	55.606395	24.17
S2	34.4441	0.1498	58.014693	29.45
S3	34.4437	0.1093	79.479723	63.1
S4	34.4433	0.1031	84.312707	47.2

Surface morphology

The FESEM micrographs have been shown in the Figure 3.18. These SEM graphs depict the variations in the structures of all the four samples with their respective cross sectional views showing the thickness measurements for the four samples. The results may be elaborated for the increasing surface roughness of each sample in the increasing order of their thicknesses which suggests for the increased surface to volume ratio and hence the porosity. As reported in the previous studies the porosity and the surface to volume ratio plays an important role in enhancing the gas sensing behavior for a sensor [139]. The FESEM micrographs shows the

increasing porosity with increasing thickness and also it supports the results calculated using Scherrer's relation earlier which shows the increasing crystallite size with the increase in thickness of the sensing layer.

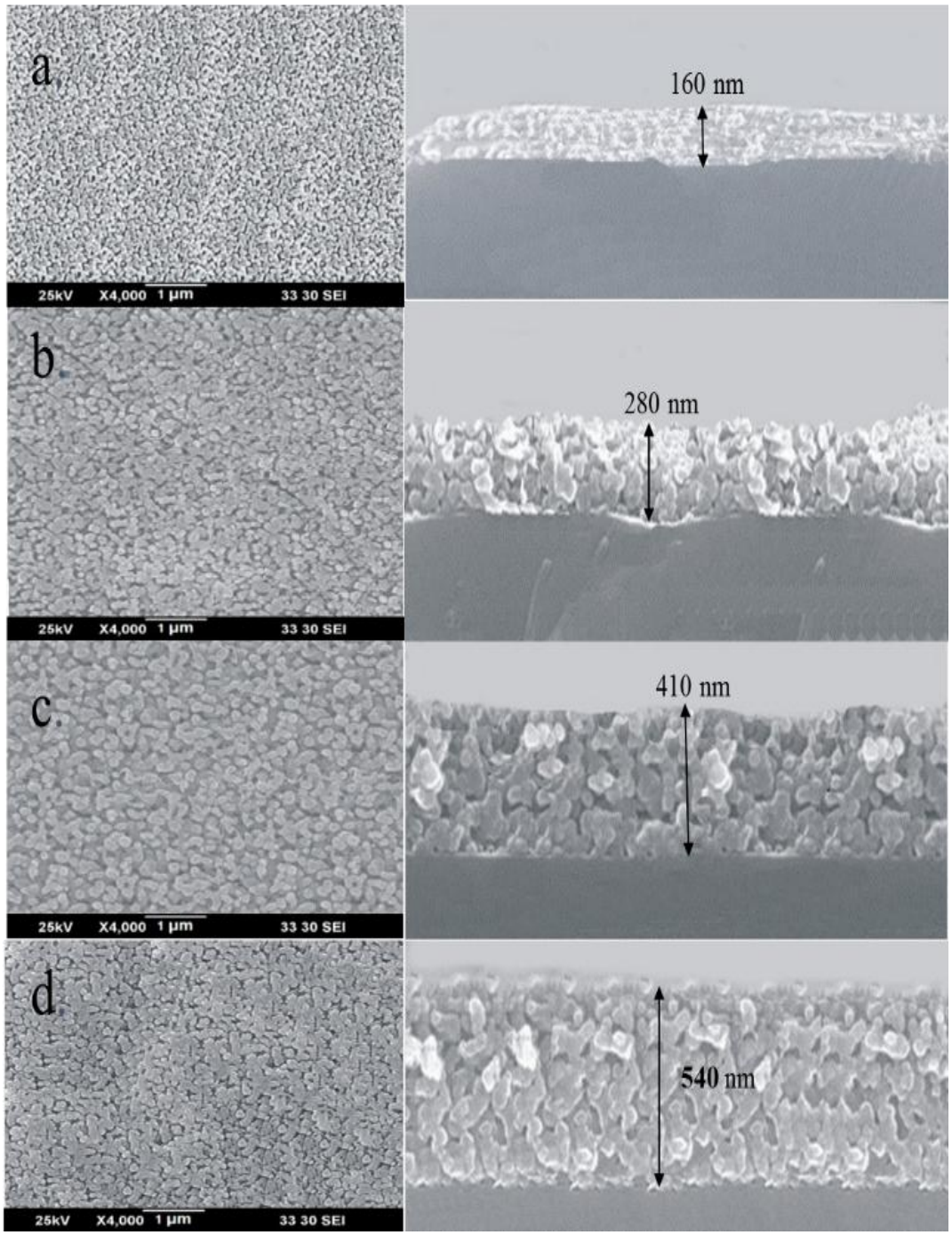

***Figure 3.18**: Top and cross sectional FESEM.*

C. Gas sensing properties

The gas sensing experiments for all the four samples have been performed with prior annealing at 200°C for 1 hour in a controlled environment so that, if any, gas particles are adsorbed over the surface of the sensor shall be desorbed before performing gas sensing. Figure 3.19 presents the sensing response of all the four samples wherein the sample S3 (410nm) shows highest sensitivity of 63 towards the 500 ppm of acetone vapors at an operating temperature of 320°C [70, 75, 140]. This shows that the optimum thickness for the sensing layer comes out to be 410 nm according to the present study. The samples S1, S2 and S4 also show high responses of 24.2 (at 300°C), 29.5 (at 320°C) and 47.2 (at 320°C) respectively. Hence, it can be stated that the optimum sensing response for the sensor S3 is due to the perfect defect states created and the increased surface roughness which is directly linked to the surface to volume ratio. The results clearly show that the sensing responses firstly increases but after a certain thickness, it starts decreasing.

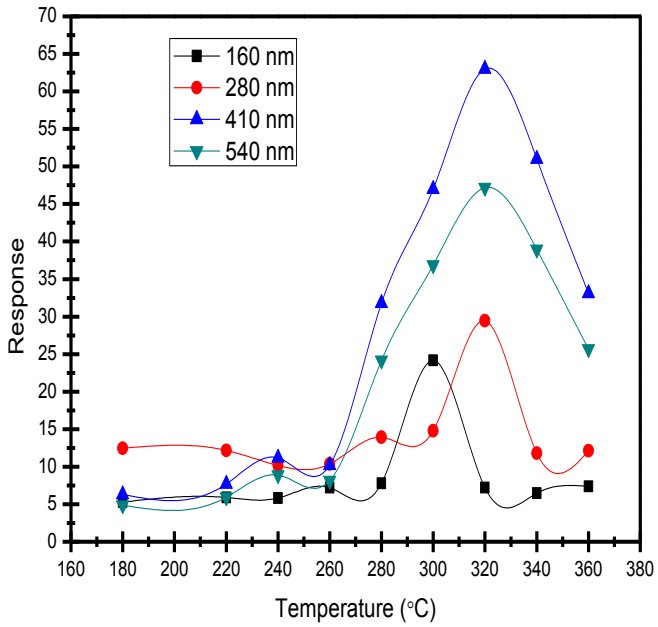

***Figure 3.19**: Sensing Responses of sensors.*

This phenomenon may be explained using the kinetics of molecules [124, 141, 142]. At low operating temperatures, kinetics of the gas molecules will be lowered which decreases the rate of adsorption resulting in low sensing responses. Also, when the operating temperature rises above a certain limit, the kinetics of the gas molecules also increases in such a way that the molecules will escape before reacting with the active centres of the sensing layer again resulting in lowered desorption of gas molecules at the surface of the sensing layer[143].

Hence, resulting in the decreasing adsorption quantity of the gas molecules over the surface of the sensing layer. This will cause lowering down of the sensing responses of all the sensors below and above the optimum operating temperatures. Figure 3.20 (a) and (b) present the response and the recovery times for all the four samples at fixed concentration of 500 ppm acetone gas. It shows the variations in the response and recovery times for all the sensors at the temperature ranges from 180°C to 360°C. It is evident from the graphs that there is a continuous decrease in the response as well as the recovery times with few humps representing almost equal times for the adjacent operating temperatures. This decrease in both response as well as recovery times are again due to the kinetics of the gas molecules at particular operating temperatures[143]. Figure 3.21 and Figure 3.22 represent the transient response curve and the stability and repeatability of the sensor S3 at optimum operating temperature T_{opt} = 320°C towards 500 ppm acetone vapours in the air respectively. The sensor S3 shows a stable resistance in air (R_a) of 3.67 MΩ initially. Now, as the target gas acetone (500 ppm) is inserted in the chamber, its resistance (in gas R_g) gradually increases to 2.32 GΩ in about 30 seconds (response time). When the acetone gas is suctioned out from the GCTS, the sensor resistance starts decreasing and reached to its stable initial value in approximately 35 seconds (recovery time).

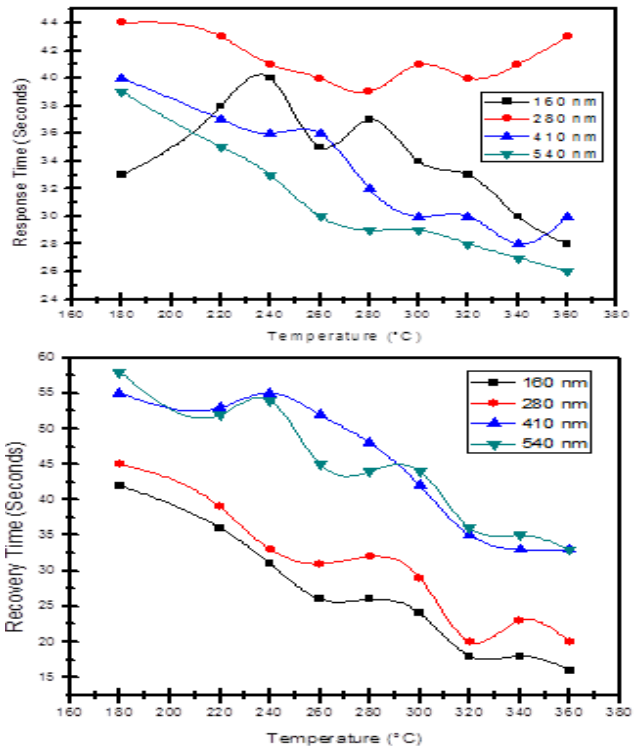

***Figure 3.20**: (a) Response time, (b). Recovery time.*

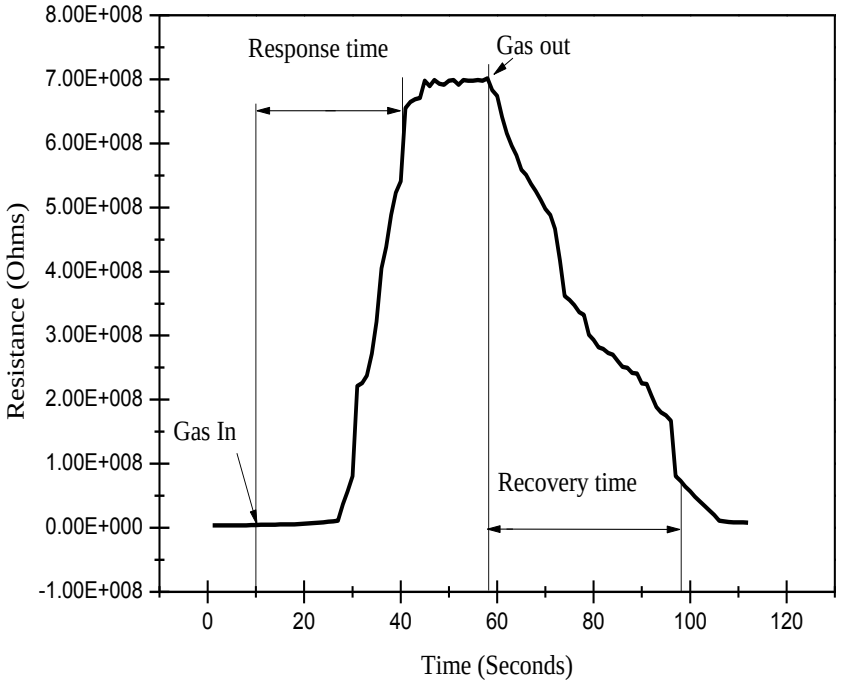

Figure 3.21: *Transient response curve.*

Figure 3.22 presents the reproducibility of the sensing results for at least six consecutive cycles (taken at an interval of 5 days each) without any degradation in the sensing response and the drift in the baseline.

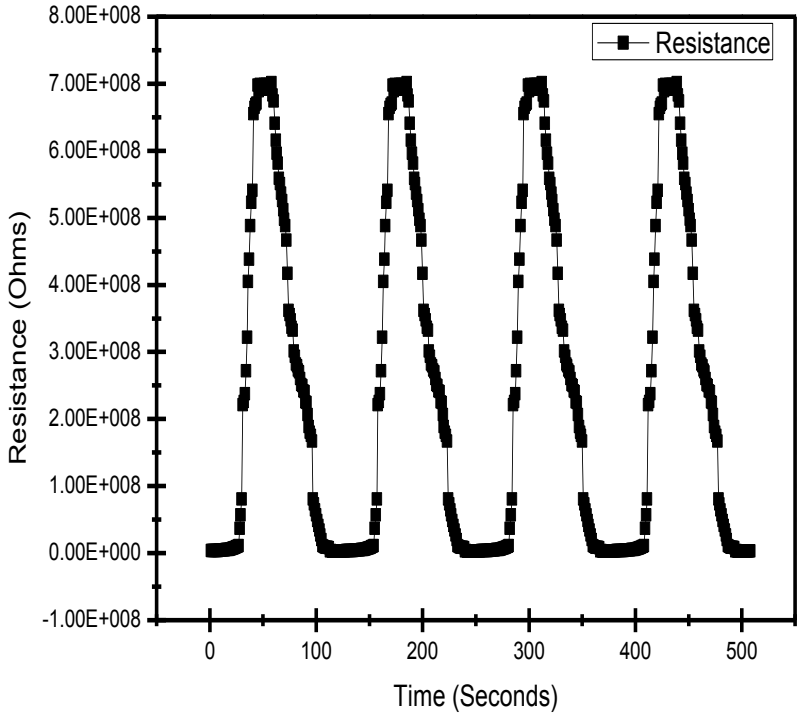

Figure 3.22*: Repeatability and stability of sensor.*

Further, the results clearly shows that the porosity and hence grain size with surface to volume ratio increases with the increase in thickness of ZnO sensing layer upto an extent (at particular annealing temperature of 650°C and thickness of 410 nm) beyond which the porosity of the film degrades causing the reduced oxygen vacancy sites over the sensing layer. This causes the degradation of sensing responses in the samples with thickness higher than 410 nm. Also as illustrated in Figure 3.23, the adsorption and desorption phenomenon of the acetone gas over the ZnO sensing layers affected by the porosity of thin films.

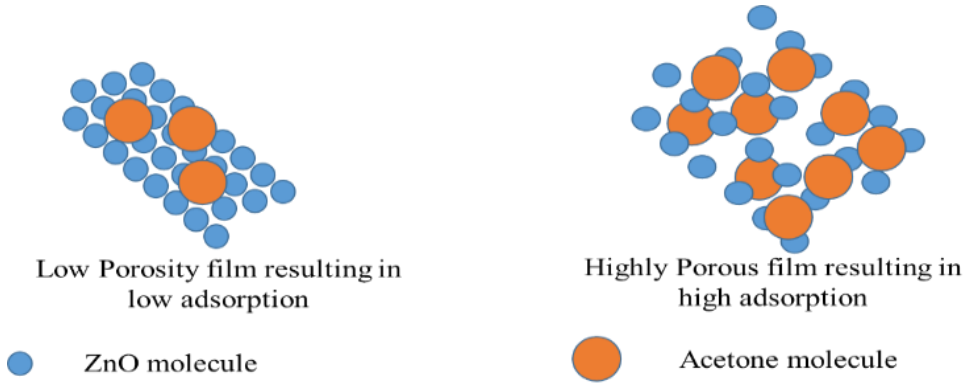

***Figure 3.23**: Gas Sensing Mechanism.*

According to previous studies [75], these results can also be explained using the activation energy concept, where the sensing mechanism of a sensor depends upon the chemical reactions over the surface of the sensing layer depends on activation energy. The higher activation energy results in the lowered electronic conduction in case of ZnO based acetone gas sensor. The previously reported literature, the ZnO thin film of thickness about 450 nm is having lowest activation energy as compared to other lower and higher order thick films[75].

Conclusion

ZnO thin films as sensing layers with varying thickness have been studied. Sol-gel spin coating technique is used for the fabrication of the sensing layers. The optical, surface morphological and structural properties has been studied and it was found that the porosity of the thin films increases with increase in the thickness of the sensing layer including an increase in surface roughness and the grain sizes. Further, the sensor results conclude that the optimised thickness of 410 nm for a ZnO sensing layer at an operating temperature of 320°C shows a high response of 63.3.

Chapter 4

Study of Gas Sensor with various Dopants and Doping Parameters

"The chapter 4 presents the studies related to the effects of various dopants incorporated with the ZnO thin film. The dopants have been incorporated through different techniques like chemical route and RF sputtering with either nano-dots like architectures or incorporated with the thin films."

4.1 Introduction

As discussed in Chapter 3, the thin films of ZnO has been deposited with variations of various parameters i.e. annealing temperature variation, molarity variations, and thickness variation, through chemical route. After achieving the three optimized parameters we got a sensing response for the sensor to be very low as compared to the present sensors reported in the literature. Hence, in order to modify the sensing properties for the sensor towards acetone, the literature suggests for incorporation of some catalysts/modifiers/ additives at very low concentrations either over its surface or within the interior of bulk. The addition of such materials significantly improves the sensing parameters like selectivity, sensitivity, response and recovery times etc. The improvement in the sensing characteristics may be attributed to the selective promotion of desired molecular level reactions at various sites. Also, the effect of the quantity and distribution of the modifier within the sensing layers are also accredited for the improvement of response characteristics.

There is very less literature reported towards the efficient development of acetone sensor and other VOC's. Further, the choice of selective modifiers/catalysts in the reported literature are also random and lacks for the crucial information about the systematic comparison for different catalysts. Therefore, in the present study, different modifiers/catalysts have been dispersed over the sensing ZnO thin films surface. The dispersed catalysts may be present in the form of nanoclusters or may occupy defect states and other lattice spaces with thicknesses of the order of nanometers. The catalysts are introduced to the sensing layer using different techniques like RF Sputtering and chemical sol-gel process.

4.2 Fabrication of Selective Gas Sensors

4.2.1 Doping of Platinum

A chemoresistive sensor for VOC's (enhanced sensitivity towards ethanol) with Pt-microdots doped zinc oxide (ZnO) thin film as sensing layer has been studied with a coplanar microheater architecture with inter-digitated electrodes (IDE's). ZnO thin films are fabricated using the sol-gel method. The doping with platinum is performed by RF Sputtering method. The present study suggests the use of a coplanar microheater with IDE's fabricated for the ethanol sensor. Further, the effect of doping on sensing properties of the sensor has been studied. The sensing response of the sensor with the film thickness of 430 nm at an operating

temperature of 180°C comes out to be 110. The prime aim of the study is to present a highly sensitive ethanol sensor having a coplanar architecture of microheater with IDE's in a ZnO based sensor.

A. Introduction

In recent times, the technology is reaching towards nanoscales for the fabrication in electronics with reliable miniaturization of a device. As a gas sensor is an essential for the modern industry for regulating environmental safety and other hazards, the miniaturization of its packaging is also necessary [1-3]. The gas sensor is required to operate at temperatures higher than room temperature, hence the use of the heater is its necessity [4-6]. Presently, various gas sensors have been fabricated but the mechanism of heating its sensing layer is external or with additional layers [7-10]. To minimize the layers deposited and an extra circuitry for heating of the layer, the presented architecture may be helpful in minimizing the number of layers to be fabricated for the sensor [1, 11]. As shown in Figure 4. 1, fabricated coplanar architecture in a single layer with sensing layer over the integrated pattern.

B. Experimental

Fabrication of Coplanar Microheater and IDE's

The coplanar architecture has been fabricated over a single oxidized silicon wafer with dimensions as 1 cm X 1 cm. The platinum is used as the material for both the heater and IDE's. The platinum is deposited over the silicon surface using RF sputtering or e-beam deposition technique in 1 m Torr Argon environment for the desired thickness of 400 nm. Figure 4. 2 represents the mask used for the photolithography. The structure has been fabricated over the surface of the silicon wafer using UV photolithography [12] followed by wet etching method [13]. In Figure 4.2 the contact pads have been numbered in series as 1, 2, 3, 4 where 1 and 4 contact pads represent the IDE/IDT's contact pads for the sensor and contact pads 2 and 4 represents the contact pads for the microheater.

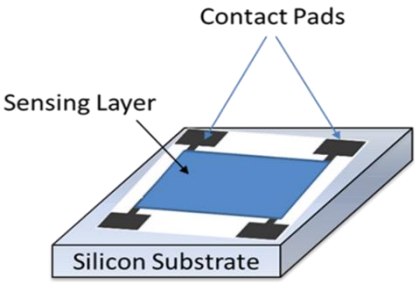

***Figure 4.1**: Fabricated coplanar architecture of sensor.*

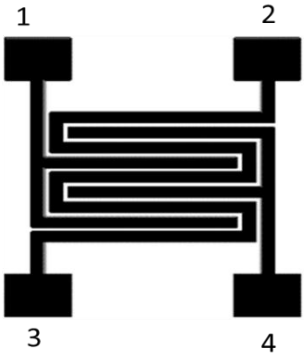

***Figure 4.2**: Mask pattern of coplanar microheater and IDE.*

Deposition of Sensing Layer for Gas Sensor

ZnO thin films are deposited over the substrate surface using the Sol-gel method with 0.1 M concentration of solution [14]. All the chemicals used are of analytical grade provided by Sigma Aldrich. The solution is prepared using Zinc Acetate Dihydrate and ethanol as starting materials in the desired concentration followed by addition of Monoethanolamine (MEA) as the stabilizing agent. The solution is refluxed for 20 minutes in open air at a temperature of 70°C [15]. Thereafter, the solution is left for 12 hours for aging process in a closed environment. The substrates are cleaned ultrasonically in acetone for 6 hours before the deposition of the ZnO layers. After the cleaning process, the substrates are deposited with ZnO layers using spin coating method followed by baking of the substrate at 250°C after each coat. After obtaining the desired thickness, the samples are annealed at 600°C for 6 hours. The platinum microdots (Pt-microdots) of radius 200 microns are deposited using the RF sputtering technique in 1 mTorr Argon environment and 120 Watts power. The indigenously developed Gas Calibrator and Testing Apparatus (GCTA), has been used for calibration of the gas and measuring the sensing response of the sensor as discussed in the section 3.6.3.

C. Results and discussions

XRD analysis and structural morphology

As shown in Figure 4. 3, the XRD patterns for the prepared ZnO thin film as the sensing layer. The diffraction peaks in the XRD spectrum are matched with a pure hexagonal wurtzite structure (JCPDS No. 36-1451). The peaks at 32.14°, 34.2° and 36.15° are matched with the

standard results verifying for the the ZnO standard peaks. The results verified with a high degree of crystallinity for the ZnO thin films [17].

Figure 4. 4 depicts the FESEM image for the prepared thin film of the sensor. The image shows the ZnO nano-fibred structure fabricated as the sensing layer over the substrate surface. The fabricated nano-fibred structures possess a very high surface area for adsorption of gas molecules which makes the sensor highly sensitive [18].

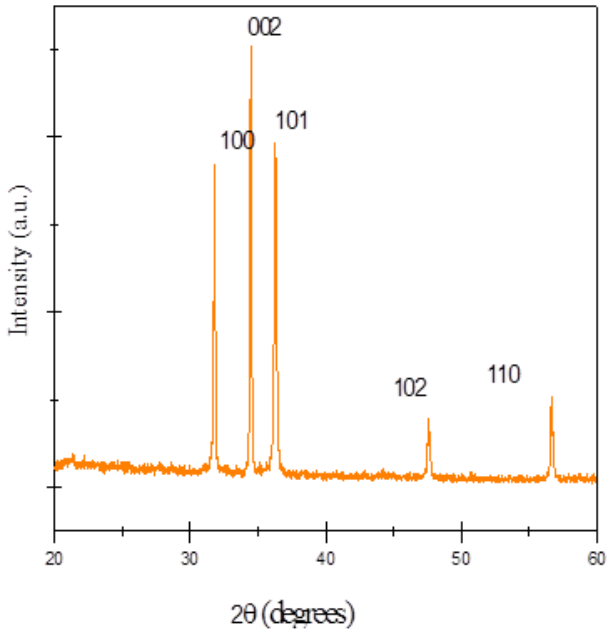

***Figure 4. 3**: XRD pattern.*

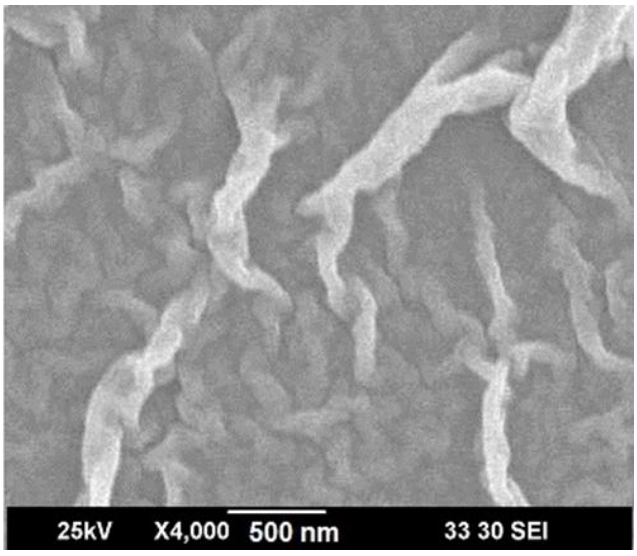

***Figure 4. 4**: FESEM Image.*

D. Gas sensing property

Figure 4. 5 presents the sensing response for the sensor to be 110 (response calculated using equation 3.1) at an optimized operating temperature of 180°C. The gas sensing response is enhanced as compared to the sensor presented by Mondal, et al. [19] and with a lowered operating temperature. This may be due to more uniform heating of the active sensing layer over the substrate as the microheater structure is covering a larger area over the substrate as compared to the existing sensor structures. Also, a high sensing response as compared with other sensors may be due to the high affinity of the ethanol molecules towards the platinum microdots. Hence this may be concluded that due to more uniform heating area with Pt-microdots acting as a catalyst contributes towards a very high response for the fabricated sensor.

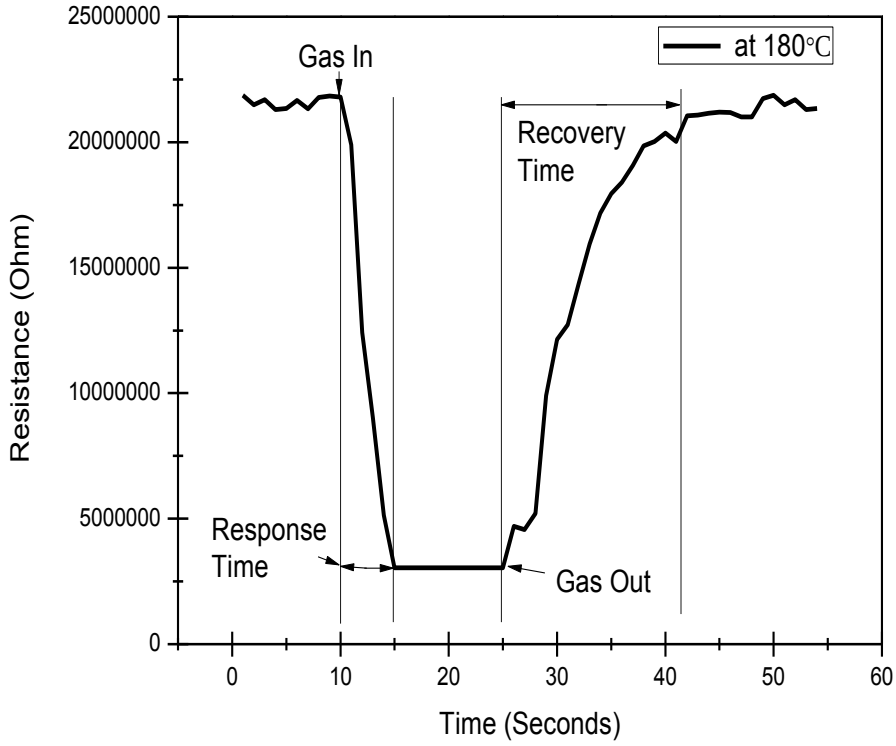

***Figure 4. 5**: Gas Sensing Response.*

Conclusion

The fabricated sensor for ethanol presents a coplanar microheater and the IDE's assembled in a comb-like structure providing a higher uniformity in the heating area for the sensor. Also with the presence of Pt-microdots as a catalyst also supports the high affinity of the particular gas molecules towards the sensing layer. These both parameters helps significantly in the increasing sensing response of the sensor.

Now, in continuation with the study of effect of dopants, the deposited ZnO layer is studied and characterized for gold doping.

4.2.2 Doping of Gold (Au)

In continuation with the study of effects of dopants, the layer is characterized for gold doping and studied for the sensing response of acetone vapors. Zinc acetate dihydrate ($Zn(CH_3COO)_2 \cdot 2H_2O$) was taken as starting material and a stable and homogeneous solution was prepared in ethanol by deliquescing the zinc acetate and distinct amount of monoethanolamine (MEA) as a stabilizing agent. The prepared solution was then coated on silicon substrates by spin coating method at 3000 rpm and then annealed at 650°C for preparing ZnO thin films. The thickness of the film was maintained at 410 nm. The structural, morphological and optical studies were done for the synthesized ZnO thin films.

The operating temperature and sensor response is considered to be an important parameter for the gas sensing behavior of any material. Therefore, the present study examined the effect of sensing behavior of 3% gold (Au) doped ZnO thin films as a VOC based sensor (with high sensitivity towards acetone). The response characteristics of 410 nm ZnO thin film for temperature ranging from 180°C to 360°C were determined for the acetone vapors. In comparison to the bare ZnO thin films giving a response of 63 at an operating temperature of 320°C, a much better response of 132.3 was observed for the Au doped ZnO thin films at an optimized operating temperature of 280°C.

A. Introduction

As a chemoresistive sensor, ZnO has been distinguishably proven as a highly sensitive material for reducing as well as oxidizing gases detection[144, 145]. Various efforts have been made for improving the response time and reaction time as well as its stability and selectivity [55, 146, 147]. One-Dimensional nanostructured ZnO provides a high surface to volume ratio as a higher surface area possesses extra sites for the adsorption of analyte molecules [148]. Till date, 1-Dimensional ZnO nanostructures having different morphologies have been fabricated which includes nanorods, nanotubes, nanowires, nanobelts and nanofibers [149-153]. In the present work, ZnO based gas sensor has been studied for high sensitivity and quick response/ recovery times to acetone using Au as a dopant. The high responses at lower operating temperatures for a gas sensor has been

observed in the present study. The results are related with the degree of crystallization, gas atoms affinity and larger grain sizes.

B. Experimental

The synthesis method used for ZnO thin films starts with the preparation of the precursor solution by dissolving zinc acetate dihydrate in ethanol with the 0.1 M molarity and then adding monoethanolamine (MEA) as the stabilizing agent in distinct amount. The solution is stirred at 60°C for one hour in closed environment. Then the solution is kept aside for 4 hours to cool down and ageing. As shown in Figure 4. 6, the pre-fabricated IDE patterned silicon wafers are used for the growth of ZnO thin films using spin coater at 2500 rpm for 20 seconds subsequently heating the prepared films at 300°C for 20 minutes. The desired thickness of ZnO thin films is obtained by spinning the solution over the substrate a number of times. Once the desired thickness is achieved, the prepared films are annealed at a temperature of 650°C for 6 hours.

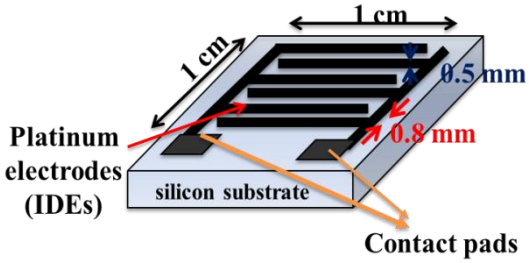

***Figure 4. 6**: IDE Pattern.*

For Au doping, 0.03 M solution of $HAuCl_4 \cdot 4H_2O$ with ethanol is prepared. Further the solution is mixed in the ratio of 1:10 with the earlier prepared solution of zinc acetate dihydrate in ethanol so that the 3% doping [154-156] would be achieved. The samples prepared for bare ZnO is designated as S1 and the 3% Au doped ZnO is designated as S2. For gas sensing characterization processes the same films are deposited on the plane silicon wafer with IDE patterns with same parameters. The characteristic studies for optical, structural and surface morphologies of the samples has been carried out using UV-visible spectrophotometer, XRD and SEM respectively. As discussed in previous sections, an indigenously developed Gas Calibrator and Test System (GCTS) consisting a glass bell jar, thermocouple, heating element, temperature controller and the contact pins connected to Digital Multimeter (DMM) Keithley 2002 is used for the data acquisition. Thermal volatization of liquid acetone is used for preparation of acetone vapors which are inserted in

the chamber through calibrated leaks with desired concentration. The sensing response (S) is calculated using equation 3.1 as discussed earlier.

C. Results and discussions

XRD Analysis

Figure 4. 7 represents the XRD patterns for the prepared samples S1 and S2. The XRD shows the poly-crystallinity patterns of the samples S1 and S2. The diffraction peaks in the XRD spectrum are matched with a pure hexagonal wurtzite structure (JCPDS No. 36-1451) for ZnO. The XRD graph for the ZnO films are established to be highly polycrystalline in nature. The S2 sample is also having a small peak of (111) plane for gold at 38.17 degrees. Hence the result verifies the presence of gold nanoparticles in the sample S2.

Surface morphology

Figure 4. 8 presents the FESEM image and TEM micrograph of the ZnO thin film based sensors architectural properties. The Figure 4. 8.a shows S2 sensor with Au doped ZnO nano threads like structures possessing very high surface area to react with the gas molecules [157]. Figure 4.8.b depicts the TEM micrograph for Au doped ZnO nanoparticles. As clearly seen from the results, the micrograph suggests for the doping of Au nanoparticles in ZnO. The micrographs results can be directly correlated with the XRD graph (Figure 4. 7) which also concludes for having Au doped ZnO nano-architectures. Figure 4. 8.c shows cross sectional view for sample S2 which validates the thickness uniformity and also provides a detailed cross sectional structure for the sensor.

Optical properties

Figure 4. 9 shows the UV-visible transmittance spectra of ZnO thin films deposited on quartz substrates under similar deposition parameters. ZnO thin films are found to be highly transparent (~80%) in the visible region with adsorption edge at around 375 nm. The energy band gap (Eg) is calculated using Tauc plot (inset of Figure 4. 9) and is estimated to be 4.01eV and 3.7 eV for samples S1 and S2 respectively. Further theTauc plot clearly indicates the decreasing band gap for the doped sample S2 as compared to the sample S1. The energy band gap of ZnO blueshifted from 4.01 to 3.7 eV with the doping of the bare ZnO sample with gold nanoparticles which may be attributed to the increased conductivity and higher mobility for electrons through the thin film after introducing the dopant atoms [158]. The change in the values of transmittance and the band gap clearly indicates the changing optical

properties due to doping in the samples. As clearly seen from the graph (Figure 4. 9) the Au doped ZnO exhibits lowered band gap as compared to the bare ZnO sample which reflects that the Au doped sample is more electrically active which is reflected in the sensing results where the optimized operating temperature is lowered for the sample S2 (Figure 4. 10).

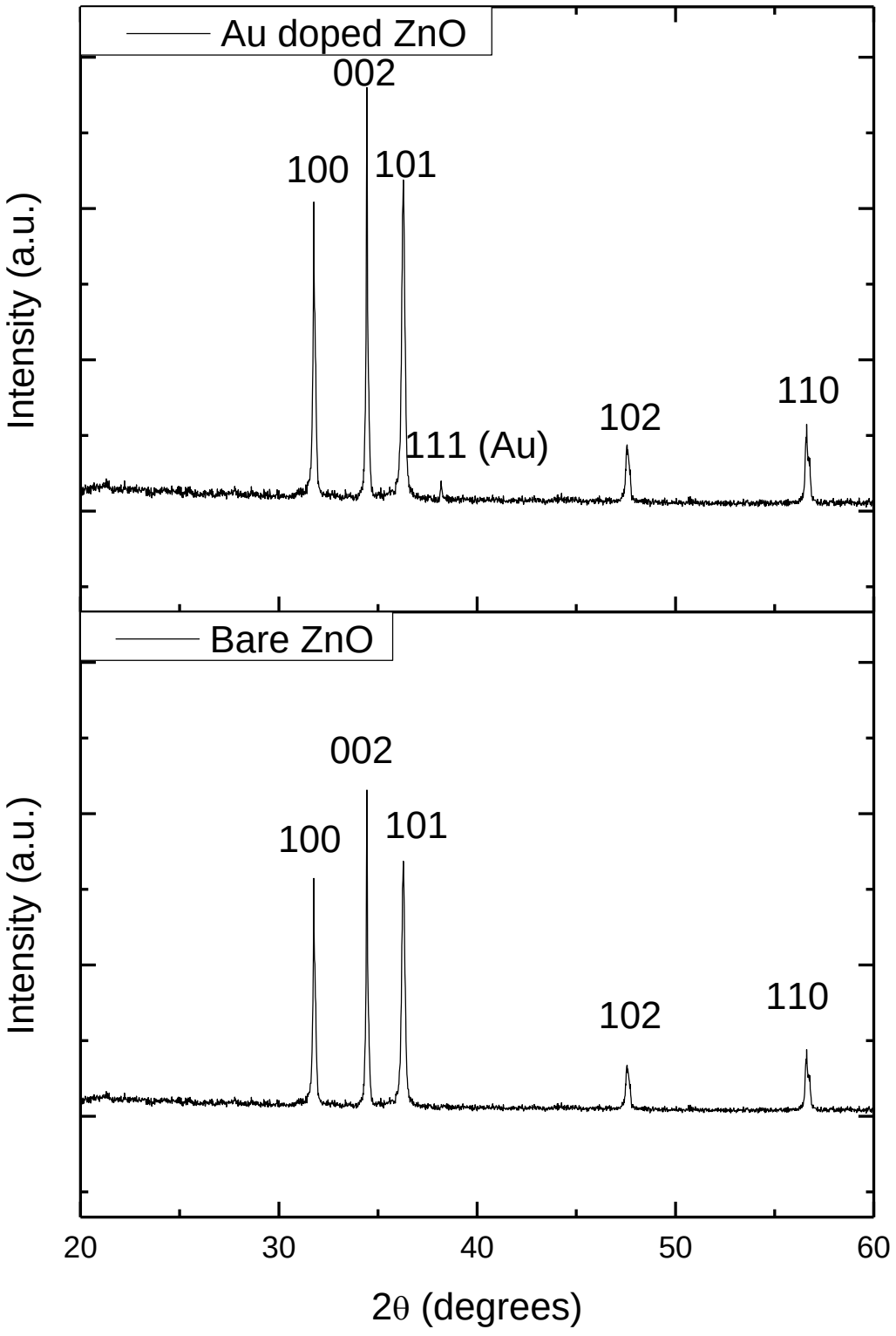

Figure 4. 7*: XRD Patterns of S1 and S2.*

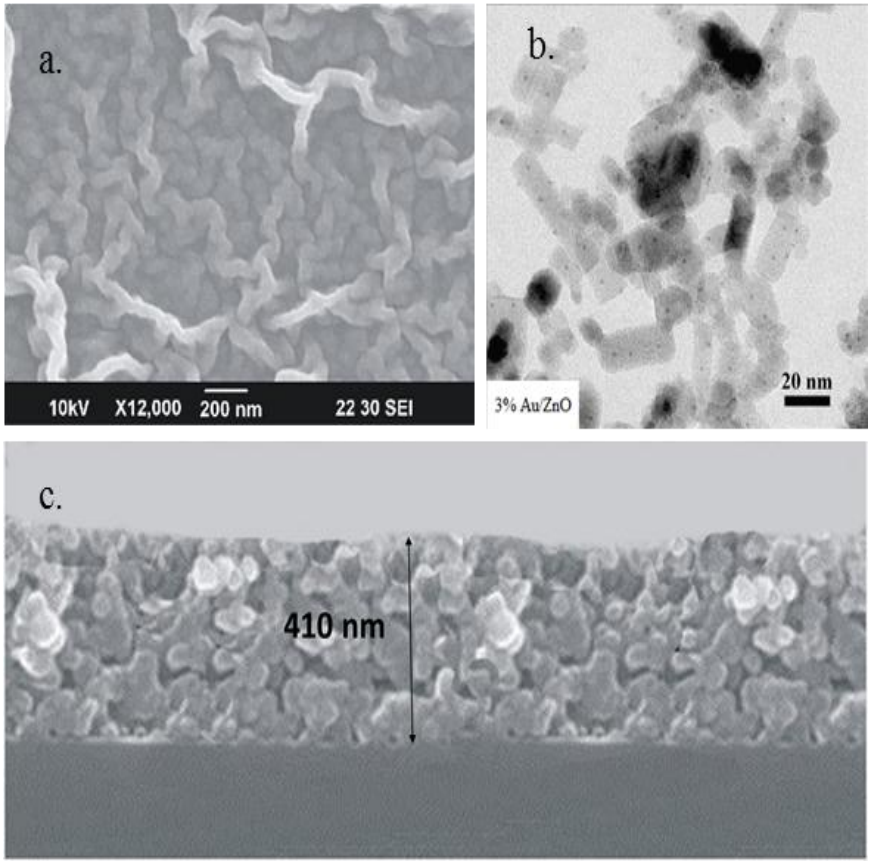

***Figure 4. 8**: (a) FESEM of S2, (b) TEM micrograph of Au doped ZnO nanoparticles, (c) Cross Sectional FESEM image of Au Doped ZnO.*

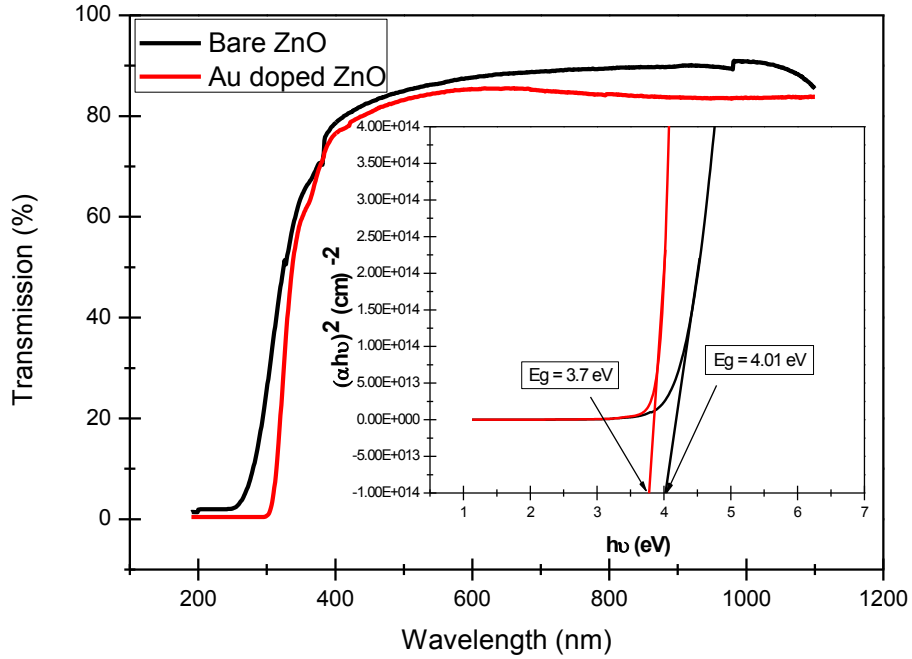

***Figure 4. 9**: UV-Vis Transmittance of S1 and S2.*

D. Gas Sensing Response

Both the prepared sensors are annealed at 250°C for 1 hour in order to desorb the surface of the samples for any gas contamination. Figure 4. 10 shows the sensors responses for the samples S1 and S2 with temperature varying from 180°C to 360°C. The optimal operating temperature for both the sensors is observed in the closed environment at 500 ppm of acetone vapors. This may be seen from the results that there is a decreased optimal operating temperature for the sample S2 [57]. The sensing responses for the sensors S1 and S2 increases distinctly initially till attaining the highest sensing responses at an optimal temperature, following with decreasing sensing responses with increasing operating temperatures. Kumar, et al. [143], illustrated this phenomenon by the kinetics and mechanics of gas reaction on the surface of ZnO. At lower operating temperatures the gas molecules kinetics is low resulting in lower sensing responses. Also, at operating temperatures higher than optimal operating temperature the kinetics of gas molecules is large in such a way that molecules may escape from the active centers of surface before reactions and will affect the quantity of the gas to be adsorbed resulting in lower sensor responses. The sensor response with optimal operating temperature for each sample is shown in Figure 4. 10, where, S1 exhibits high response that may be due to the large surface interactions, oxygen vacancies and open network architectures but when the S1 is 3% doped with gold (sample S2), the response of the sample increases by more than two fold. Further, it can be observed that the optimum temperature, response time as well as the recovery time are also reduced significantly. This may be observed that there is a dramatic enhancement of the response which is caused by the enlarged depletion layer, the extremely loosened and small structure, and the additional free electrons and catalysis of Au nanoparticles [159]. Also, this may be due to the high affinity of molecules of the gas towards gold nanoparticles present on the sensor layer surface. It is also clear from the results that the overall sensor response, response time, recovery time and the optimal operating temperature improved significantly. So, the difference can be observed clearly in the responses of sensors S1 and S2, when both the samples were annealed at 650°C with the thickness of layer to be 410 nm. The thickness of the ZnO layer has previously been optimized for the oxidizing nature of acetone vapors [75]. Figure 4. 11 represents the response taken at regular interval of 48 hours several times with previous standard procedure followed at optimum operating temperature. The graph shown in Figure 4. 11 proves the stability and repeatability of the sensing response of the sample S2 with 500 ppm concentration of acetone vapors at optimum operating temperature of 280°C.

Figure 4. 12 shows the response times and recovery times for both the samples giving another important relation between the samples which depicts the decrease in response times and recovery times for the sample which is 3% doped with Au nanoparticles. Figure 4. 13 represents the sensor response at various concentrations. The concentrations when varied from 100 ppm to 1000 ppm provides the valuable information regarding the sensitivity nature of the sensors towards higher and lower side of the concentrations. This can clearly be seen that the sensor shows linearly increasing sensitivity towards higher concentrations of acetone. Figure 4. 14 provides the detailed information for the selectivity of the sensor which proves that the doped sensor shows very high sensitivity towards acetone as compared to the other volatile organic compounds and other gases. A ZnO host matrix with incorporated Au exhibits improved performance, such as high adsorption, superior electro-catalytic activity for direct electrochemistry. Hence with the increase in operating temperature the response times and recovery times decreases for both the sensors which relates to the higher rates of adsorption and desorption as the range of temperature rises.

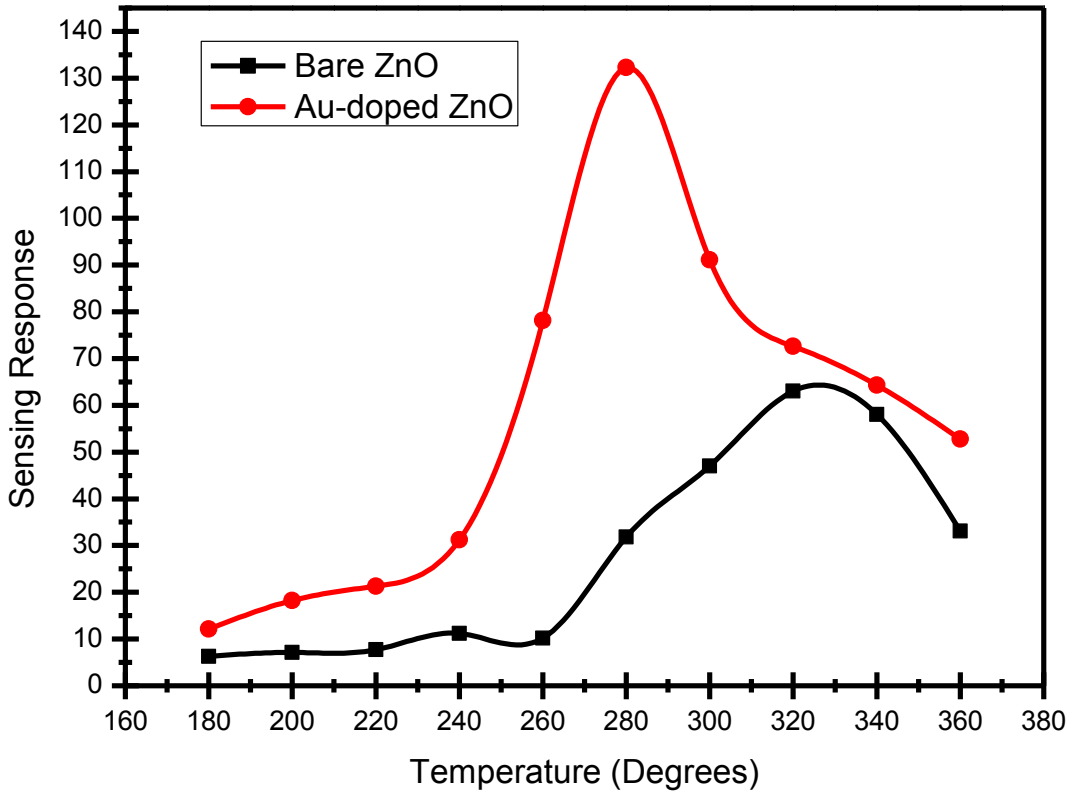

***Figure 4. 10**: Sensor Responses of Samples S1 and S2.*

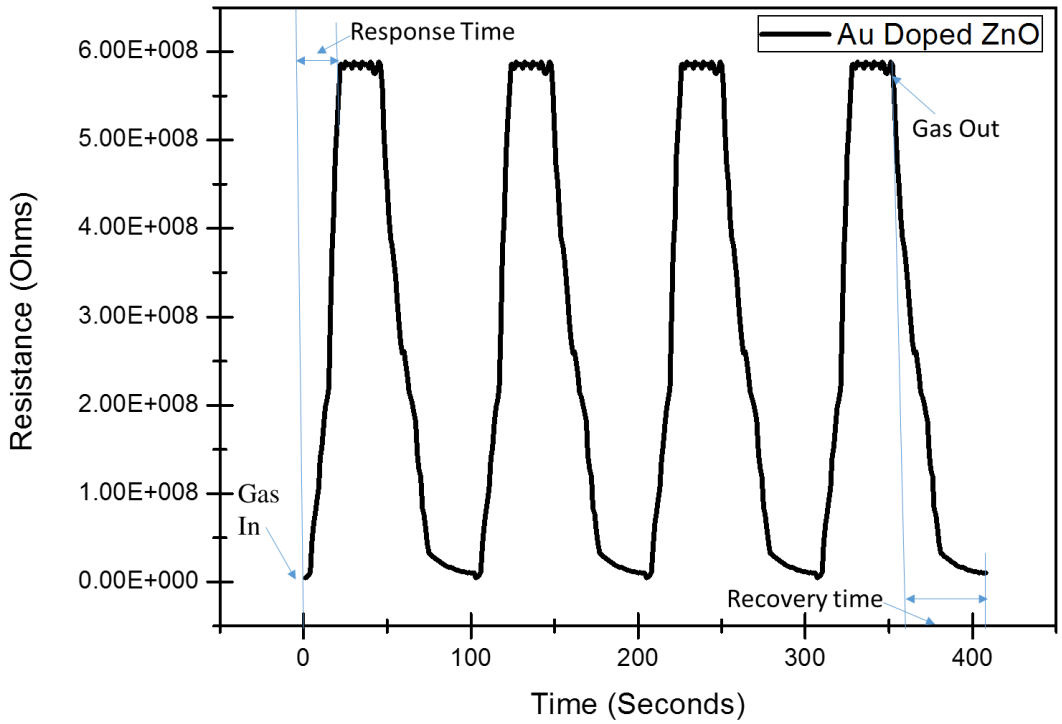

***Figure 4. 11**: Stability and Repeatability for Au doped ZnO.*

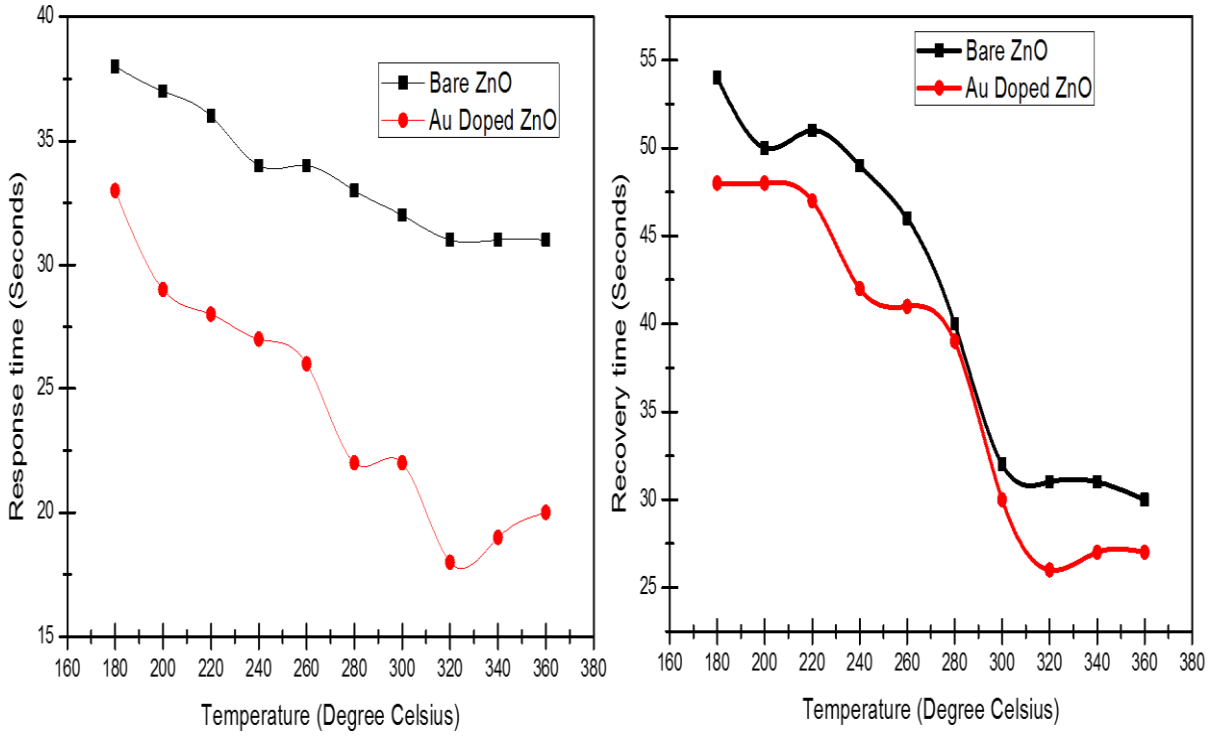

***Figure 4. 12**: Response and Recovery times for S1 and S2.*

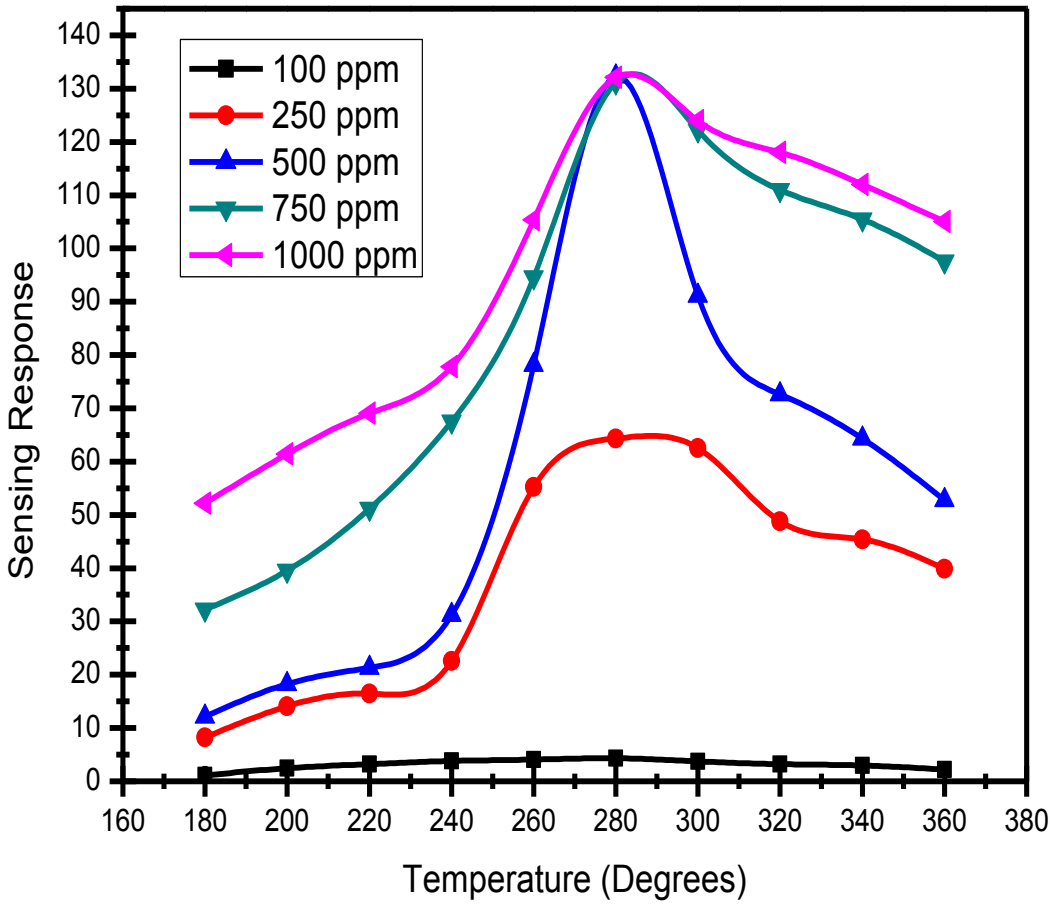

***Figure 4. 13**: Sensing Response at various concentrations.*

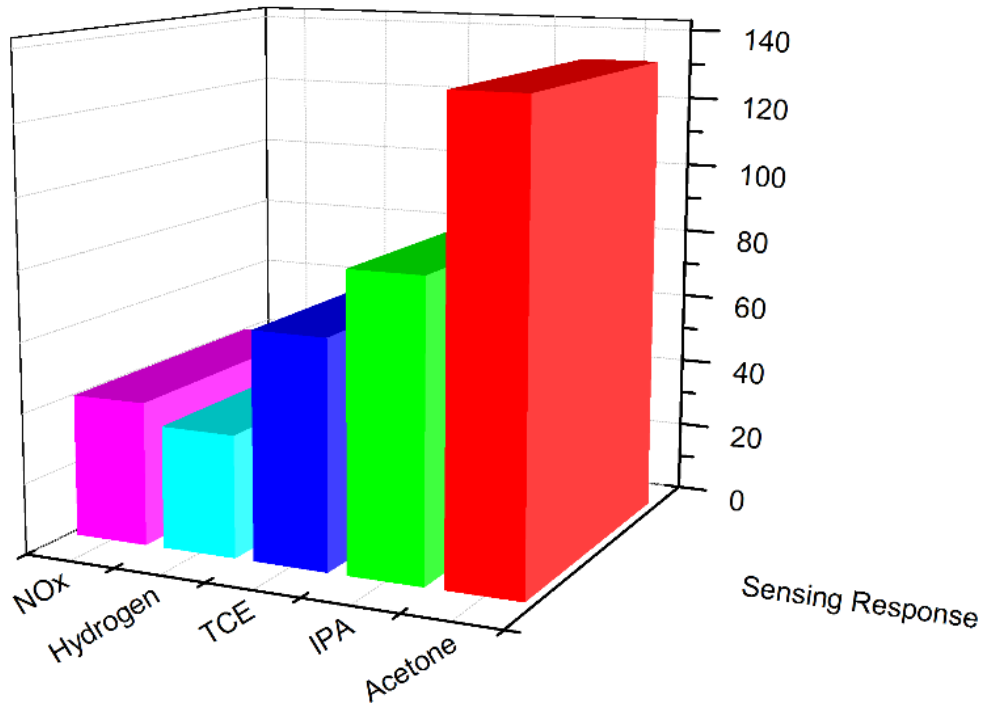

***Figure 4. 14**: Selectivity of Sensor.*

E. Gas Sensing Mechanism

The phenomenon of adsorption and desorption of gas molecules causing the resistance change over the surface of thin film is used to explain the gas sensing mechanism for ZnO based gas sensor [160-162]. As the thin layer of ZnO is exposed in ambient atmosphere, the oxygen molecules present in the atmosphere will be adsorbed over the surface of the ZnO layer forming O_2^-, O^- or O^{2-} Ions due to induced electrons for conduction band, which results in the reduction of free carrier density.

This results in the formulation of e^- depletion region at the surface causing the increase of resistance for ZnO thin films [163]. The stated process may be represented by the following equations:

$$O_{2\,(g)} \rightarrow O_{2\,(a)} \quad \text{.....(2)}$$

$$O_{2\,(a)} + e^- \rightarrow O^-_{2(a)} \quad \text{.....(3)}$$

$$O^-_{2(a)} + e^- \rightarrow 2O^-_{(a)} \quad \text{.....(4)}$$

$$O^-_{(a)} + e^- \rightarrow O^{2-}_{(a)} \quad \text{.....(5)}$$

$$O^-_{(a)} + e^- \rightarrow O^{2-}_{(l)} \quad \text{.....(6)}$$

$$V_0 \rightarrow V_0^{\cdot} + e^- \quad \text{.....(7)}$$

$$V_0^{\cdot} \rightarrow V_0^{\cdot\cdot} + e^- \quad \text{.....(8)}$$

The conduction band of ZnO thin films will be accepting the electrons donated by the surface donor defects (V_0) represented by the equations (7) - (8) [164]. Further as the thin film based sensor is exposed in acetone ambience, the acetone molecules get adsorbed and starts reacting with chemisorbed oxygen ($O^-$and O^{2-}) anions on ZnO surface. The following equations describe the reactions:

$$CH_3COCH_3(gas) \rightarrow CH_3COCH_3(ads) \quad \text{.....(9)}$$

$$CH_3COCH_3(a) + 8O^{2-} \rightarrow 3CO_2(g) + 3H_2O(g) + 16e^- \quad \text{.....(10)}$$

$$CH_3COCH_3(a) + 8O^- \rightarrow 3CO_2(g) + 3H_2O(g) + 8e^- \quad \text{.....(11)}$$

$$CH_3COCH_3(a) + 4O_2^- \rightarrow 3CO_2(g) + 3H_2O(g) + 4e^- \quad \text{.....(12)}$$

As suggested by the equations (9) – (12), the decrease in the resistance of the sensor is due to the reaction of oxygen ions (O_2^-, O^- and O^{2-}) with molecules of acetone over the ZnO thin film surface which produces CO_2 and H_2O[165]. This phenomenon is also presented in Figure 4. 9. Now, as these reactions takes place, a high level of electron exchange is created due to acetone molecule reacting with oxygen ions which in turn release equal or higher number of electrons. This results in the decreased number of carrier concentrations within the n-type metal oxide thin film and a consequent increase in the resistance of ZnO thin films.

Conclusion

In summary, the acetone sensing characteristics has been studied for ZnO thin film sensors with a bare ZnO thin layer and with 3% doping of gold. Sample S2 shows the enhanced response over the sample S1 which clearly indicates that the doping of gold for an acetone sensor significantly contributes in the gas sensing mechanisms. The doping of gold in ZnO also improves the sensing responses significantly with lowered response and recovery times. Hence it may be concluded that the gold doping of ZnO thin film improves the informative parameters of an acetone vapor sensor.

4.2.3 Doping of Silver (Ag)

ZnO as a sensing layer has been deposited using sol-gel method. The 0.1 M solution has been prepared using zinc acetate dihydrate with ethanol followed by stirring at 60°C with addition of MEA as stabilizing agent. The doping of silver (Ag) has been done by mixing of silver nitrate solution in ethanol at 0.01 M molarity. Now the silver doping has been performed stepwise such that the doping concentration in the final solution comes out to be in terms of v/v as 3%, 6%, 9%, 12%. Now, the thin films have been fabricated over pre-architectured IDE's over silicon wafer with thickness at approximately 430 nm for all the four samples. Then the samples were placed for annealing at 650°C for 6 hours in order to improve the crystallinity. The silver doping of the thin film results in an enhanced response for the ethanol detection as compared to acetone and other oxidizing as well as reducing gases or vapors. The sensitivity for ethanol comes out to be 32 for 9% doped Ag doped ZnO sensor. The samples with doping concentration of 3%, 6%, 9%, 12% has been referred to as S1, S2, S3 and S4 respectively for the current section.

A. Results and Discussion

XRD analysis

The following graph as represented in Figure 4. 15 represents the XRD Graph for all the four samples. The XRD shows the poly-crystallinity patterns of the samples S1, S2, S3 and S4. The diffraction peaks in the XRD spectrum are matched with a pure hexagonal wurtzite structure (JCPDS No. 36-1451) for ZnO. The XRD graph for the ZnO films are established to be highly polycrystalline in nature. The XRD graph with low concentrations show a negligible peak for Ag while the sensor S4 with 12% doping shows a very low diffraction peak at 44.14°C represents the Bragg's angle ($2\boldsymbol{\theta}$) showing the presence of Ag or Ag_2O nanoclusters.

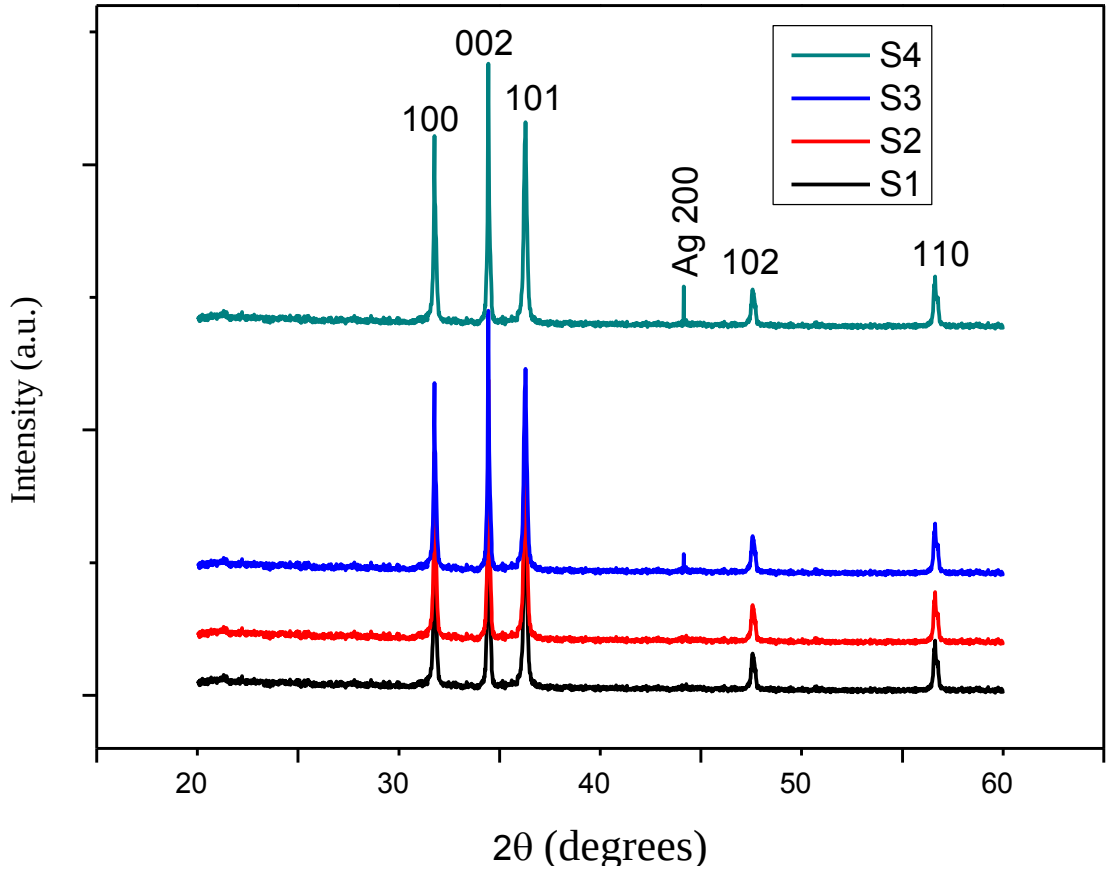

Figure 4. 15: *XRD Graph.*

Surface Morphology

The Figure 4. 16 represents the FESEM images for the Ag doped ZnO for all the four samples. The graph shows relatively no change over the dopant concentration increase in the samples. The SEM image represents high porosity with large surface to volume ratio for the

interaction of gas molecules. Figure 4. 17 represents the TEM image for 9% Ag doped ZnO thin film clearly showing the presence of atoms for both nanoparticles.

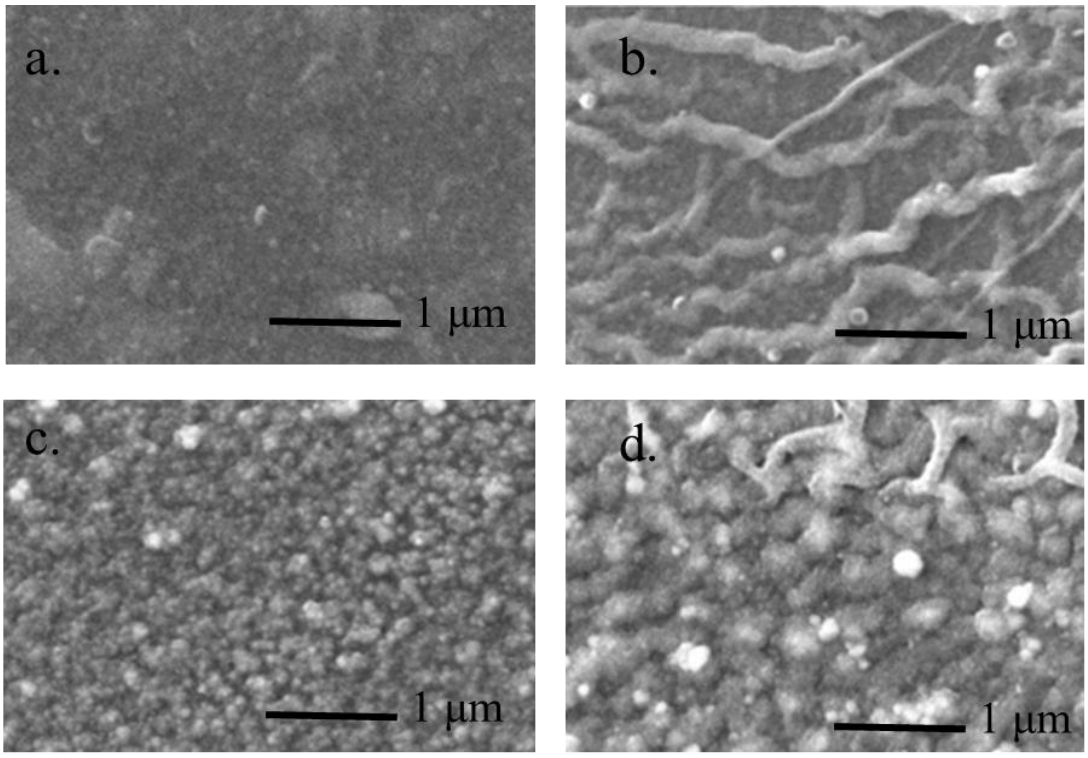

***Figure 4. 16**: SEM Images*

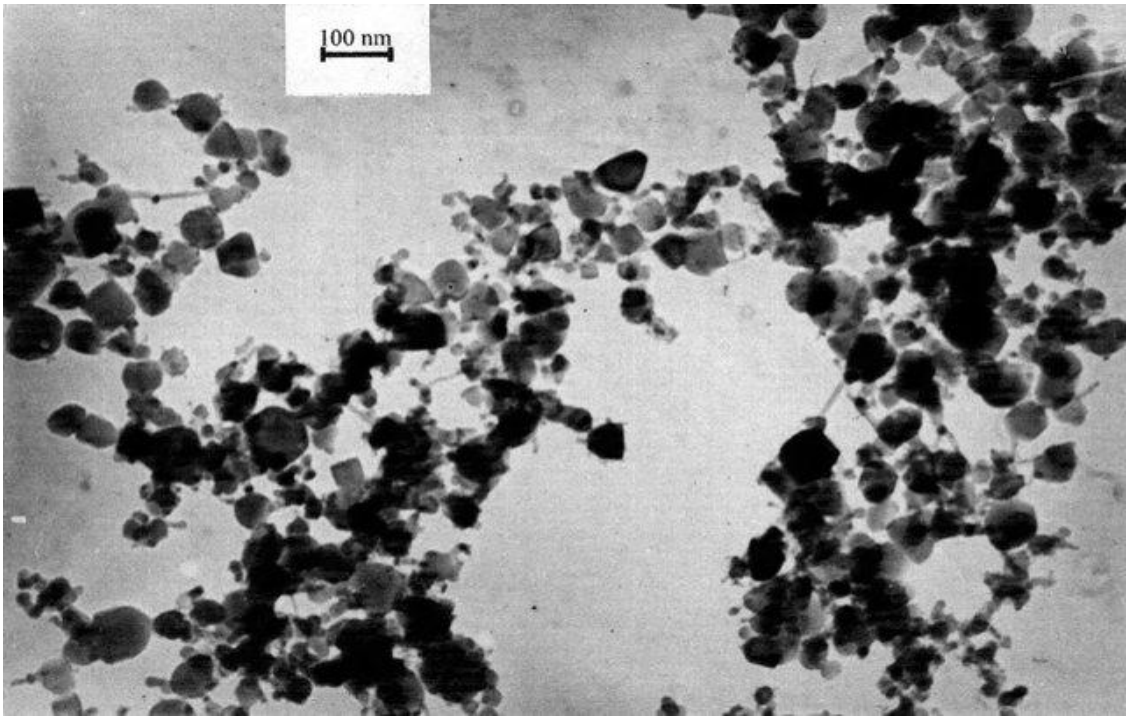

***Figure 4. 17**: TEM Image of sample with 9% Ag doped ZnO.*

B. Gas Sensing Response

All the four prepared sensors are annealed at 250°C for 1 hour in order to desorb the surface of the samples for any gas contamination. Figure 4. 18 shows the sensors responses for all the samples with temperature varying from 180°C to 360°C. The optimal operating temperature for all the sensors is observed in the closed environment at 500 ppm of ethanol vapors which comes out to be equal. The sensing responses for all the sensors increases distinctly initially till attaining the highest sensing responses at an optimal temperature, following with decreasing sensing responses with increasing operating temperatures. Kumar, et al. [143], illustrated this phenomenon by the kinetics and mechanics of gas reaction on the surface of ZnO. As discussed earlier, at lower operating temperatures the gas molecules kinetics is low resulting in lower sensing responses. Also at operating temperatures higher than optimal operating temperature the kinetics of gas molecules is large in such a way that molecules may escape from the active centres of surface before reactions and will affect the quantity of the gas to be adsorbed resulting in lower sensor responses. The sensor response with optimal operating temperature for each sample is shown in Figure 4. 18 where it can be concluded that there is an increase in response for the sensor with increasing doping concentrations but after a certain doping concentration the response starts degrading. This increase may be due to the large surface interactions, oxygen vacancies and open network architectures. Also, the best sensor response at 9% (v/v) Ag doping may be attributed towards an appropriate doping percentage causing the creation of more active adsorption centres. Further. it can be observed that the response time as well as the recovery time are also reduced significantly. This may be observed that there is a dramatic enhancement of the response which may be caused by the enlarged depletion layer, the extremely loosened and small structure, and the additional free electrons and catalysis of Ag nanoparticles [159]. Also, this may be due to the high affinity of molecules of the gas towards Ag nanoparticles present on the sensor layer surface. It is also clear from the results that the overall sensor response, response time, and the recovery time improved significantly. So, the difference can be observed clearly in the responses of sensors, when the samples were annealed at 650°C with the thickness of layer to be 430 nm. The thickness of the ZnO layer has previously been optimised for the oxidizing nature of acetone vapors [75].

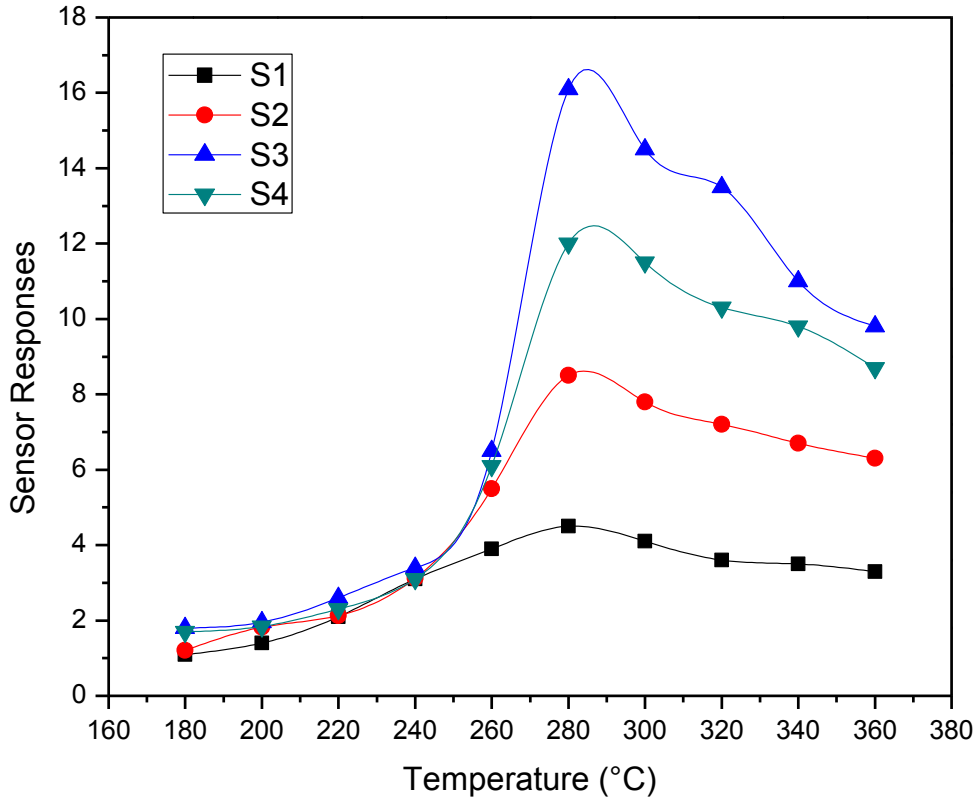

***Figure 4. 18**: Sensor Responses of Samples.*

Figure 4. 19 represents the response taken at regular interval of 48 hours several times with previous standard procedure followed at optimum operating temperature. The graph shown in Figure 4. 19 proves the stability and repeatability of the sensing response of the sample S3 with 1000 ppm concentration of ethanol vapors at optimum operating temperature of 280°C.

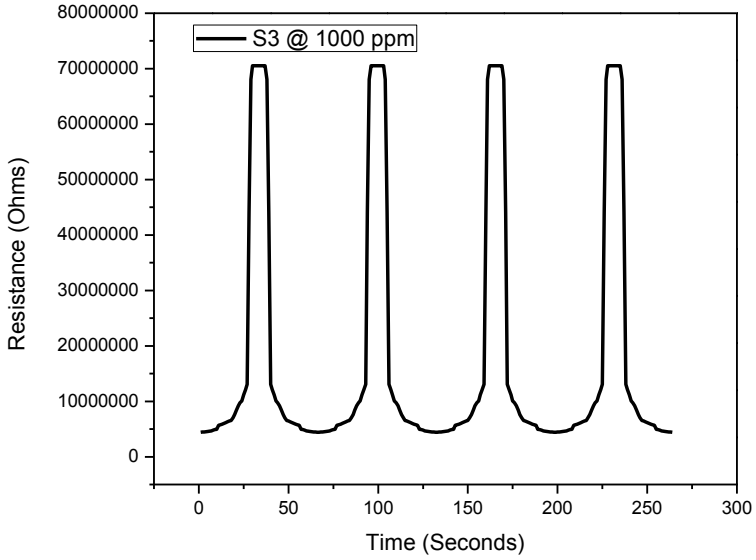

***Figure 4. 19**: Stability and Repeatability for Au doped ZnO.*

Figure 4. 20 shows the response times and recovery times for both the samples giving another important relation between the samples which depicts the decrease in response times and recovery times for the sample with increasing in doping with Ag nanoparticles.

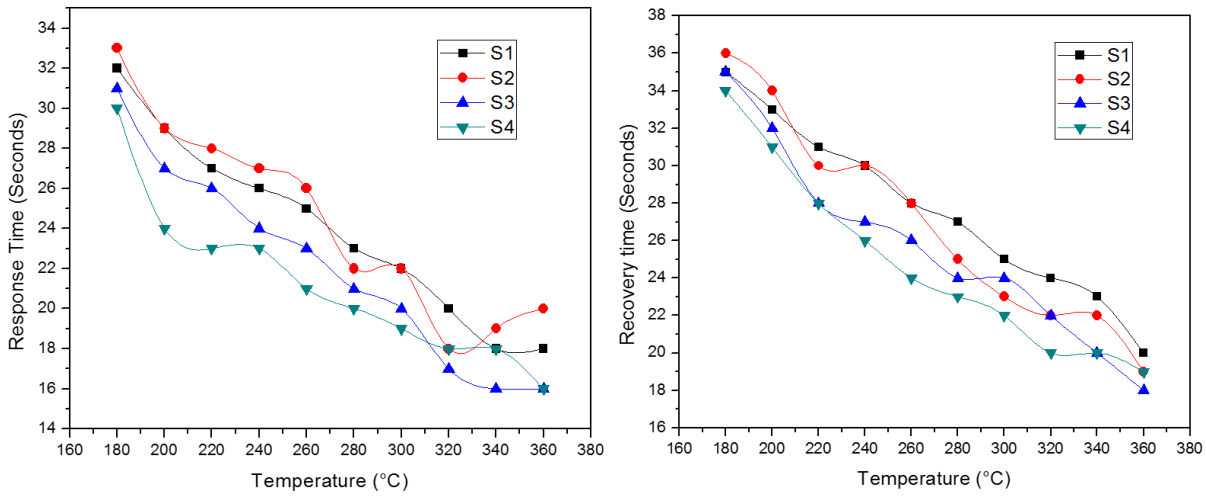

***Figure 4. 20**: Response and Recovery times for S1 and S2.*

Figure 4. 21 represents the sensor response at various concentrations. The concentrations when varied from 500 ppm to 2000 ppm provides the valuable information regarding the sensitivity nature of the sensors towards higher and lower side of the concentrations. This can clearly be seen that the sensor shows linearly increasing sensitivity towards higher concentrations of ethanol. Figure 4. 22 provides the detailed information for the selectivity of the sensor which proves that the doped sensor shows very high sensitivity towards ethanol as compared to the other volatile organic compounds and other gases.

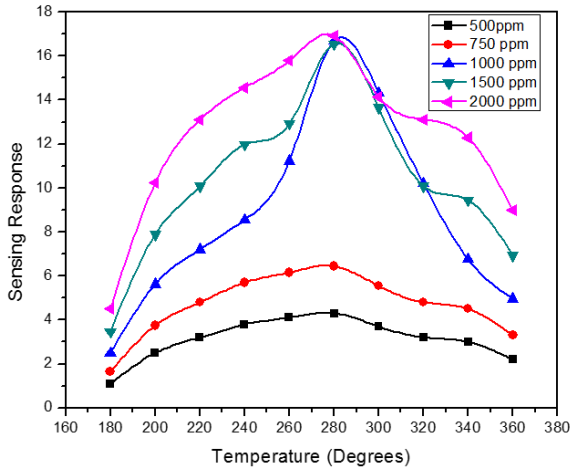

***Figure 4. 21**: Sensing Response at various concentrations.*

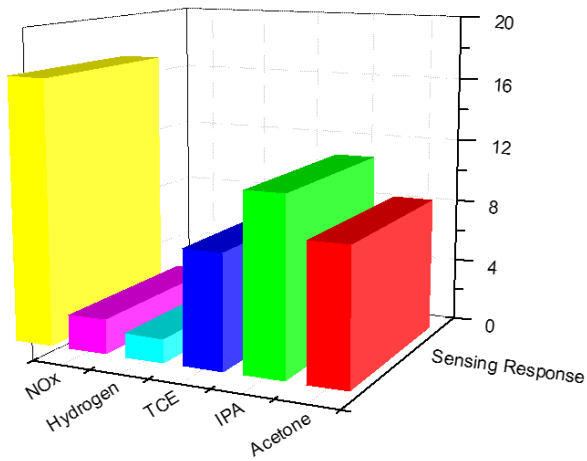

***Figure 4. 22**: Selectivity of Sensor.*

4.3 Summary

In the present chapter, the additives/modifiers/catalysts have been incorporated in the sensing layer of ZnO and studied for the efficient acetone detection. The study have been started with addition of platinum as catalyst deposited by RF sputtering technique which shows the selectivity of the sensor tends towards ethanol. Then the gold nanoparticles are incorporated in the ZnO thin films which attributes for the efficient detection of acetone vapors at low concentrations too. Then Ag/Ag_2O nanoparticles are introduced to the sensing layer of ZnO. The results conclude for Ag-ZnO thin film to be more sensitive towards ethanol as compared to the acetone.

Hence, it may be concluded that Au nanoparticles attribute towards highly sensitive modified ZnO thin film based metal oxide gas sensor.

Chapter 5

Designing & Fabrication of IDE and Micro-Heater

"This chapter presents the designing and fabrication of microheaters and then a proposed architecture of In-plane microheater & IDT/IDE pattern has been simulated and fabricated. The study shows the working of microheater that is fabricated In-plane with IDT/IDE with the improved gas sensitivity."

5.1 Introduction

In recent times, the technology is going down towards nanoscales for the fabrication in electronics with reliable miniaturization of a device over silicon/silicon dioxide substrate using various techniques. As gas sensors are essential in modern industry for regulating environmental safety [166] and other hazards [13, 91, 167], the miniaturization of its packaging is also necessary [168-171]. The gas sensor is required to operate at higher than room temperature, hence the use of the heater is its inevitability [134, 172-175]. Presently, various gas sensors have been fabricated but the mechanism of heating the sensing layer is external or is done with additional layers [176-178]. The Figure 5.1 represents the architecture of present sensors available. The present sensors are having different layers for microheaters and then IDE's. Almost in all microheaters, the designing and fabrication of the architectures are such that the final structure must be small and can be fabricated through CMOS compatible processes with lowest possible power consumption. In general, microheaters are having a hot plate over a membrane fabricated through bulk silicon micromachining. The temperature variations for the microheater are calculated using Joule's heating in a resistor.

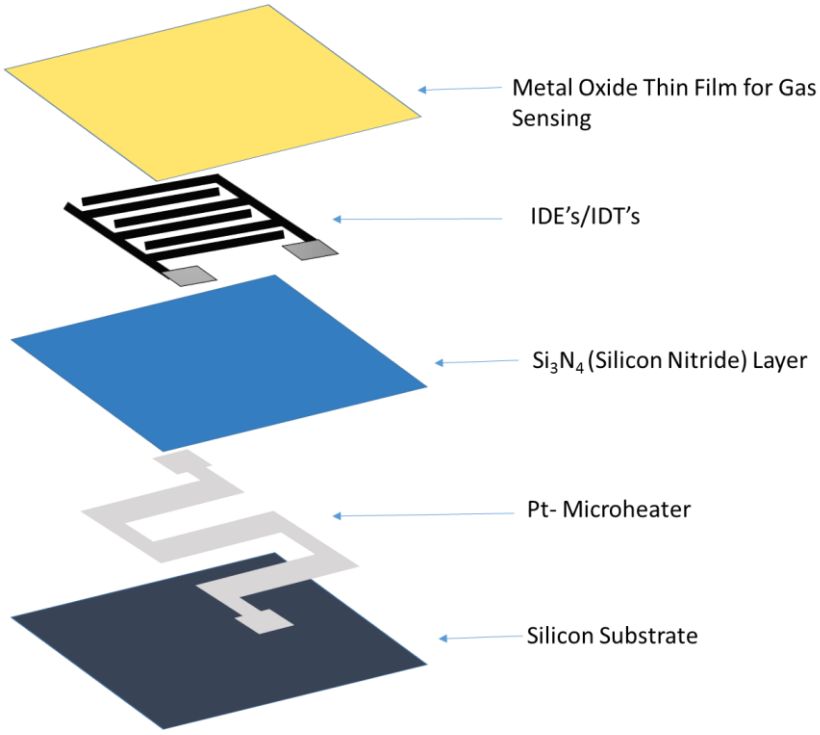

***Figure 5.1**: Chemoresistive gas sensor architecture with microheater and IDE/IDT.*

The objective of designing and fabrication of a microheater for a sensor always remains for low power consumption with maximum as well as a uniform active area for temperature distribution with a target temperature to be in range of 140°C to 350°C. Now the required characteristics that has to be considered while designing a microheater with the substrate geometry are tabulated as follows:

a.) Low Power consumption
b.) Uniform temperature distribution over the sensing layer
c.) Ability to stand with mechanical stress, strain & other constraints
d.) Rapid and stable thermal response time

Hence, the microheater is required to be efficiently designed such that it will influence the sensing properties of a gas sensor directly. Since, a lot of efforts have been made towards the development of a thermally efficient and uniform heating for a sensor with a microheater, the present study proposes for introduction of a new efficient coplanar architecture for IDE's as well as microheaters. Thus reducing the micromachining steps of fabricating a sensor and also reducing the complexity of the circuit with reduction in the effective cost for fabrication of a gas sensor.

5.2 Designing Coplanar IDE and Microheater

A microheater indeed is a very important part for a gas sensor. It is an inevitable aspect for a gas sensor that have to be fabricated within the complete architecture. High temperatures in the range of about 150°C to 400° is required for the operation of a gas sensors. There are various types of geometries that can be fabricated in built with a gas sensor but most of them either lacks in temperature or are power inefficient. Hence such architectures cannot be used for an efficient gas sensing. Since, various geometries have been reported till date for various architectures of microheaters but all of them are fabricated for the gas sensor either externally or in separate layers (as shown in Figure 5.1). Hence in the present study we are discussing some reported geometries and then designing the optimized feasible geometry with coplanar fashion with IDE/IDT. Hence reducing the number of steps involved in fabrication of a gas sensor successively resulting in low cost and energy efficient.

The work started with the study of various feasible architectures for coplanar microheater and IDT while keeping in view the designing parameters in terms of energy efficiency (Power ~ 100-200 mWatt) compatible with CMOS technology.

Platinum (Pt) and polysilicon are mostly used materials for microheaters. Both of these materials are having good electrical properties with stable thermo-mechanical properties including stress as well as strain which severely effects the substrate at higher temperatures. Also the IDE/IDT's are also fabricated using Pt as base material. Hence, further studies we have choosen the Pt as material for microheaters.

The mathematical calculations/modelling simulations wherever performed have been done using the finite element method (FEM) simulator COMSOL® Multiphysics 5.2. The electro-thermal studies have been performed with three dimensional (3-D) builder module for simple microheater and in coplanar architecture with IDE/IDT. Some related geometries reported till date are discussed and studied for coplanar architecture feasibility.

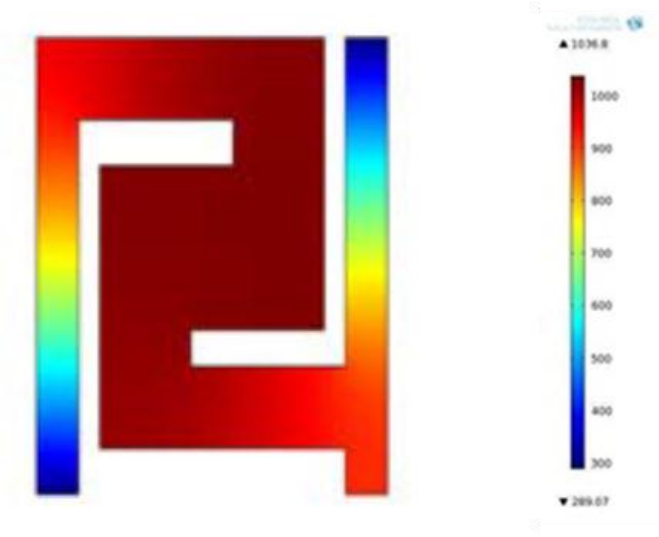

***Figure 5.2**: S-shape geometry.*

As reported in the literature, the simulation results for simple S-shaped microheater geometry is shown in Figure 5.2. The S- shaped geometry is not that much efficient as can be seen through the thermal simulation of the architecture in Figure 5.2 as compared to the architectures in further studies. Also this geometry cannot be integrated with pre-optimised IDE/IDT pattern (as represented in fig 5.1). Hence this geometry is not suitable for coplanar architecture fabrication.

The fan shaped geometry as represented in Figure 5.3, is highly thermally efficient geometry that has been studied for the microheater. But due to its high surface area the geometry becomes low resistive and hence draws high power at provided voltages. Also, this geometry cannot be fabricated in the coplanar fashion with IDE/IDT's. Since it's unobtainability for the

coplanar architectural geometry, the fan shaped geometry is not used further for the present studies.

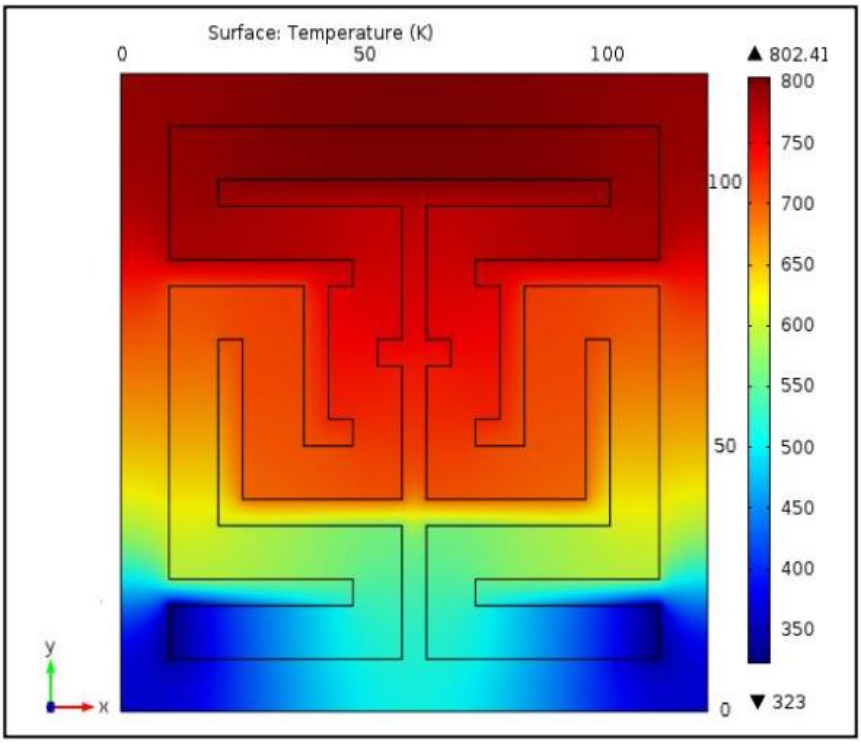

***Figure 5.3**: Fan shaped geometry.*

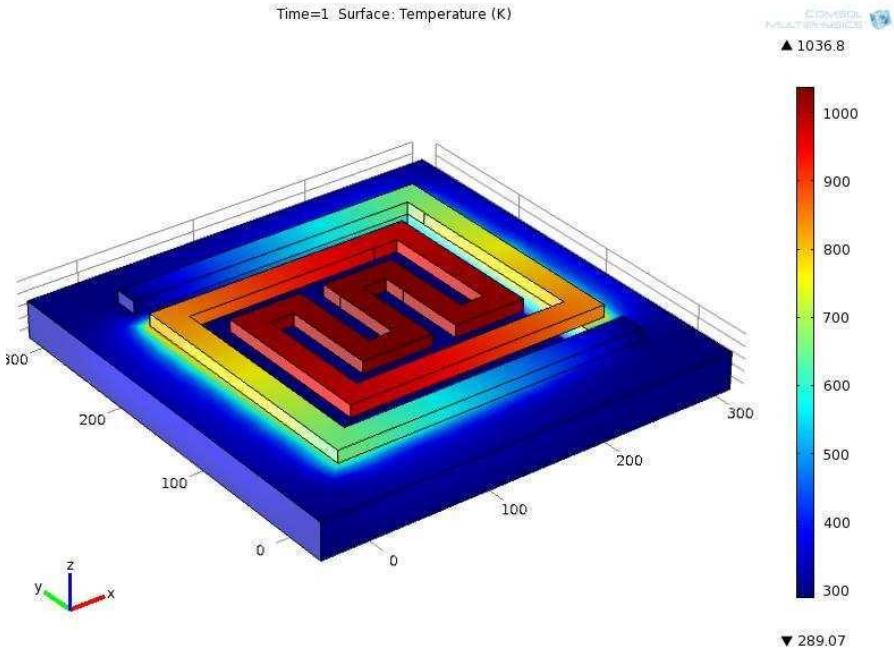

***Figure 5.4**: Spiral geometry.*

The spiral geometry as represented in Figure 5.4, is somehow having larger area for thermally efficiency in uniformity till its outside boundaries. Also, by optimizing the geometry represented in Figure 5.4, the IDE/IDT's can also be integrated in the coplanar fashion. Hence, the present geometry can be used for the fabrication of coplanar architecture of microheater with IDE/IDT by optimization of parameters like length, thickness and width of the Pt-microstrips.

Now, optimizing a geometry linked with optimizing the geometries represented in Figure 5.2 and Figure 5.4, a new S-shaped spiral architecture have been studied and simulated for CMOS compatible parameters [185]. The designing issues are solved mathematically for obtaining the optimum length of the microheater strip that will be feasible for the platinum thickness of 100 nm and can be structured in a coplanar fashion with IDE/IDT in further studies. The resulting structure is as shown in Figure 5.5.

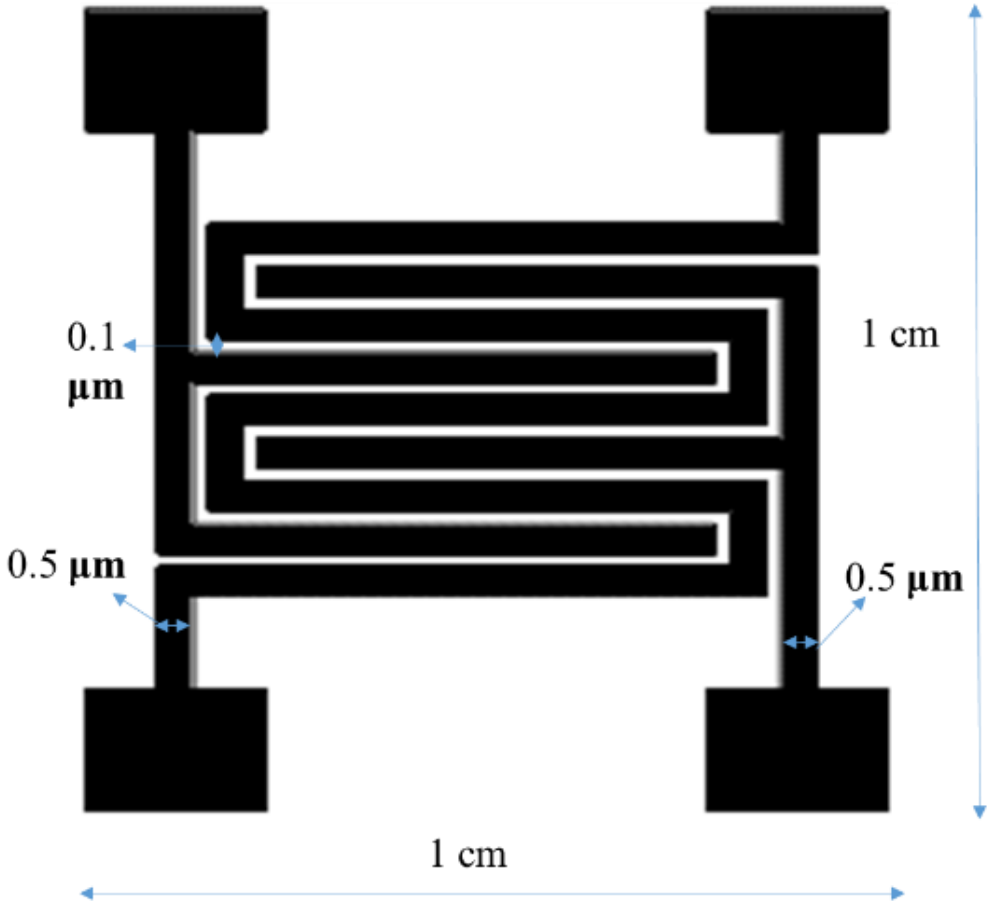

***Figure 5.5**: Optimized coplanar MH & IDT/IDE architecture.*

The resulting geometry is a modified version of the two architectures as represented in Figure 5.2 and Figure 5.4 with co-architecture in-plane IDT/IDE. The total length of the microheater strip comes out to be 5.8 cm while the mathematical simulated results produce the length of the microheater strip to be 5.68 cm for power level of 100 mWatt with voltage 3.3 Volts. The resulting simulated electro-thermal graph of the architecture is shown in Figure 5.6 and the electro-thermal image of the simulated coplanar architecture with thin film of ZnO with thickness of 150 nm is represented by Figure 5.7. The thermal image of the fabricated sensor is represented by the Figure 5.8.

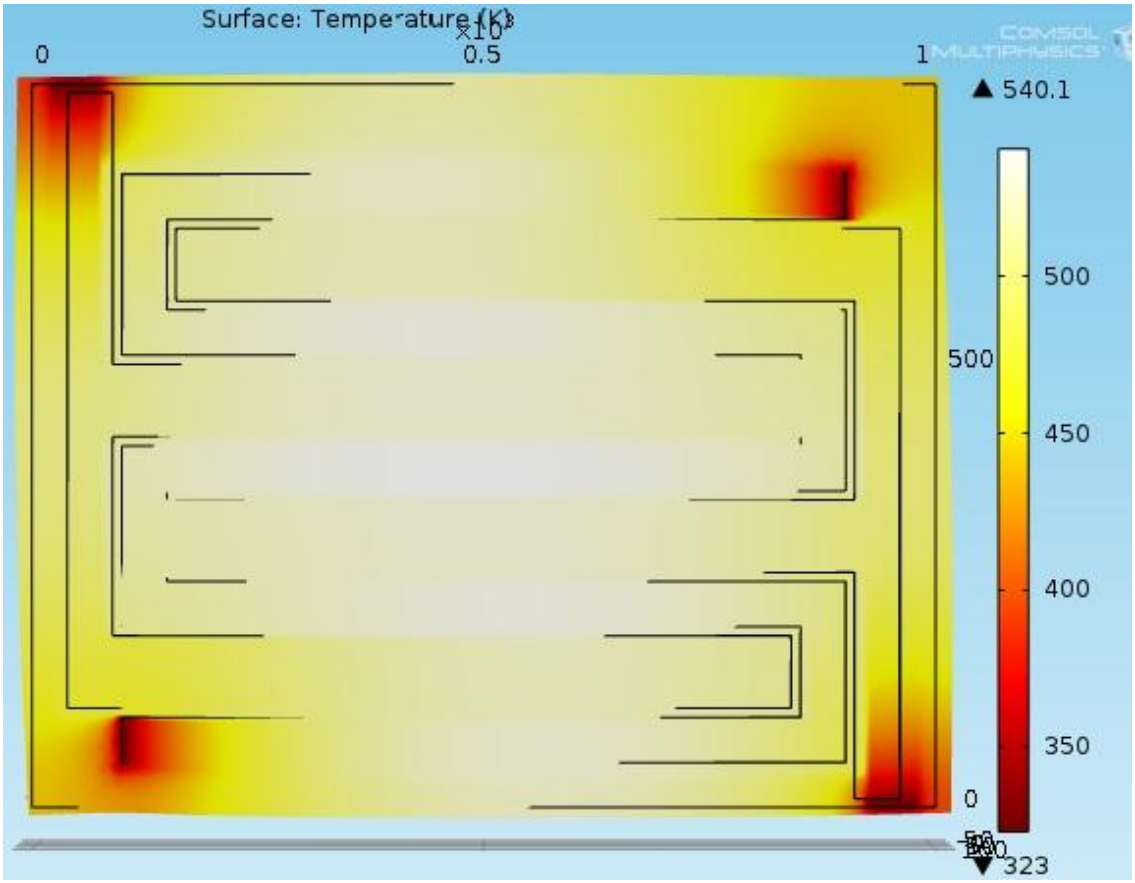

***Figure 5.6**: IDT & MH structure using S-shaped Spiral coplanar geometry.*

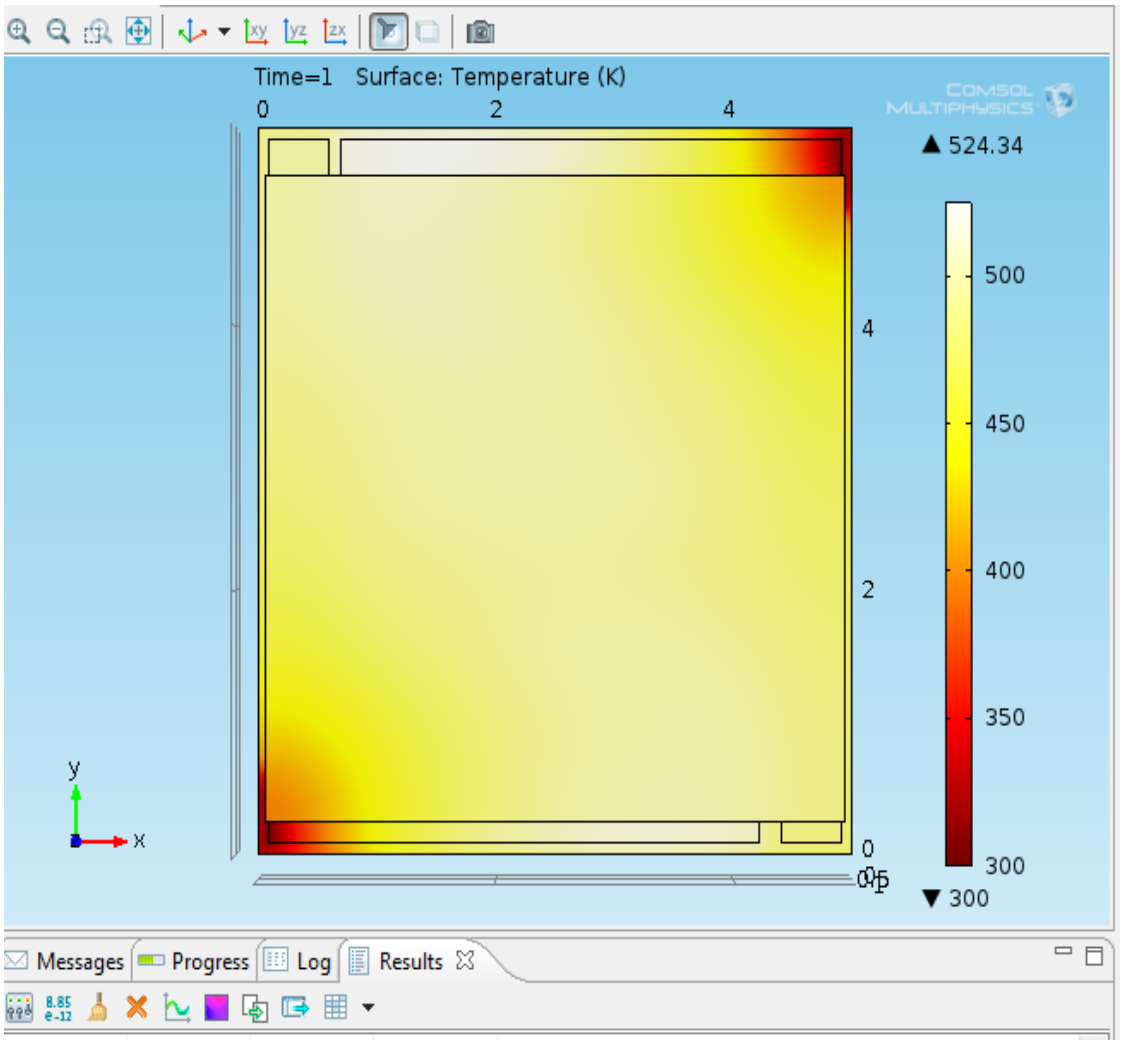

***Figure 5.7**: IDT & MH structure using S-shaped Spiral coplanar geometry with ZnO thin film of thickness 150 nm.*

The presented IDT & MH Structure (Figure 5.7) is the simulated result of the architecture as shown in Figure 5.5 with a thin film layer of 150 nm over the surface of the substrate. The spiral geometry with an integrated IDE/IDT's are here clearly showing a temperature uniformity over the whole surface area of the sensing layer in the simulated results (Figure 5.7) as well as for the fabricated sensor in the thermal imagery as represented by Figure 5.8. The fabricated sensor's thermal imagery also shows the temperature uniformity over the effective surface area for the sensor. The effect of temperature uniformity over the gas sensing results are studied and discussed further in the present chapter.

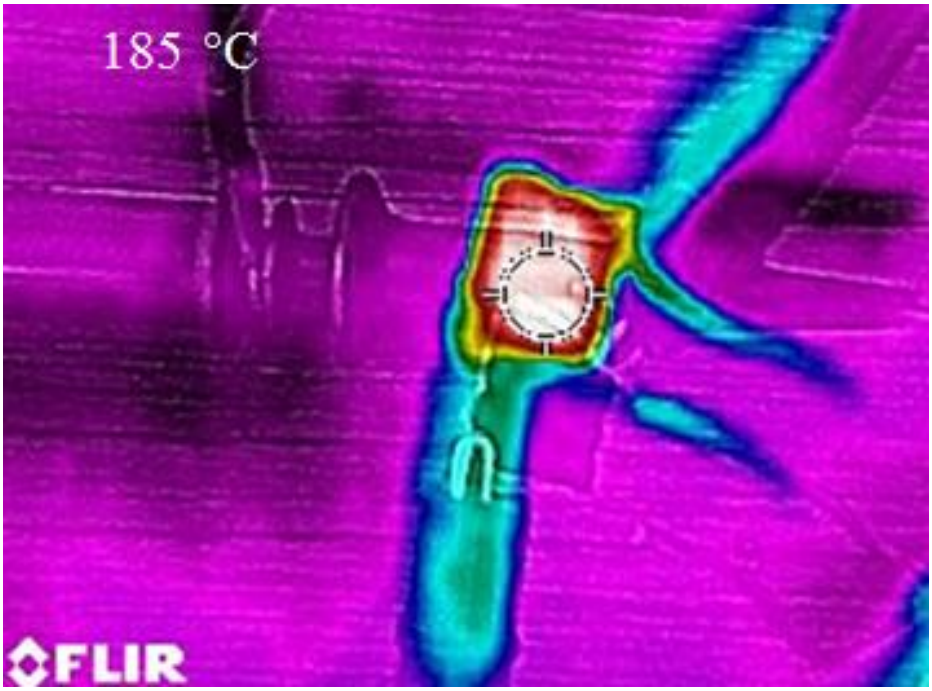

***Figure 5.8**: Thermal Image of the microheating in operation for the fabricated sensor.*

The Coplanar integrated architecture as presented in the images (Figures 5.6, 5.7 and 5.8) have now been mathematically established for the length of the microheater strip with standard power requirements and other parameters as stated below with the following relations:

Typical power requirement for any electronic circuit embedded on board at micrometers level will require ~100 mWatts and the calculated resistance of the fabricated microheater strip comes out to be 112 Ω as measured using a standard Keithley Digital multimeter (DMM 2002).

Now calculating the voltage requirement using the relation,

$$P = \frac{V^2}{R} \quad \text{..... (5.1),}$$

which implies V ~ 3.3 Volts.

Now, calculating the required length for the microheater strip of platinum, where the standard resistivity (ρ) for platinum is = 9.85 $\mu\Omega cm^{-1}$, using the relation:

$$R = \frac{\rho L}{A} \quad \text{..... (5.2),}$$

where, resistance, R = 112 Ω, Height of the strip, H = 0.1 μm, and width of the strip, W = 50 μm, implies the area for the strip, A = H X W = 5 μm^2 which provides the required length of the microheater strip to be approximately 5.68 cm.

Now, the fabricated sample is having a total length, L = 5.8 cm, which approximately matches with the above calculated results.

5.3 Fabrication of IDE and Microheater

5.3.1 Fabrication of Coplanar Microheater and IDE's

As stated by Deshwal and Arora [179], the coplanar architecture, as shown in Figure 5.9.a, has been fabricated over a single oxidized silicon (Si/SiO_2) wafer with dimension 1 cm X 1cm. The fabricated structure is also shown in the Figure 5.9.b.The platinum is used as the material for both heater as well as IDE's. The platinum is deposited over the silicon surface using RF sputtering in optimized environment. Figure 5.5 represents the mask used for the UV-photolithography process for developing the photoresist using ultra violet (UV) rays.

The structure has been fabricated over the surface of the silicon wafer [129] followed by wet/chemical etching method [130]. Figure 5.10 presents a flowchart for the processes involved in the fabrication of the reported architecture. As shown in the flowchart, the fabrication process sequence begins with the deposition of platinum over pre-cleaned oxidized silicon wafers. The cleaning process involves the ultra-sonication of wafer in acetone then in ethanol for 1 hour each. Then the wafers are placed inside the RF sputtering chamber with a distance of ~13 cm from the platinum target. After the sputtering process the deposited platinum is over-layered with a positive photoresist. The photoresist is then covered with a mask of desired shape as shown in Figure 2 and then the sample is exposed to the ultra violet (UV) radiation. Now, the sample is placed in the developer solution where the exposed part of the photoresist is removed. The whole process of photoresist layering and removal of the undesired part, are done in dark room having only mild yellow lights. Now the exposed platinum part over the wafer is etched through wet/chemical etching process.

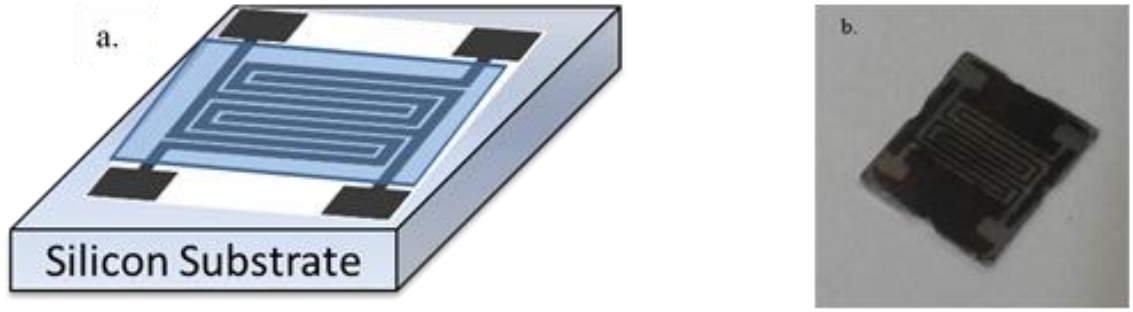

Figure 5.9*: (a) Coplanar architecture of sensor with sensing layer, (b) Fabricated sensor.*

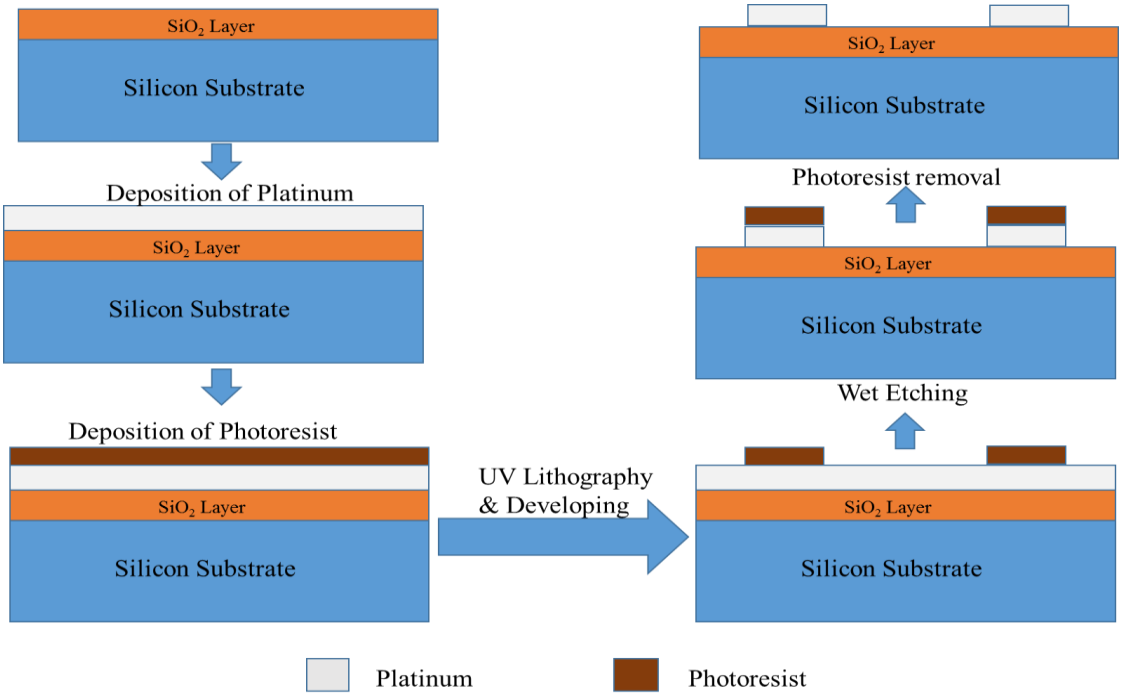

***Figure 5.10**: Flowchart of fabrication process.*

5.4 Application of Coplanar Architecture in Gas Sensors

After preparation of the desired architecture over the oxidized silicon substrate, the ZnO thin films are deposited through sol-gel method with 0.1 M concentration of solution [131, 179]. All the chemicals used are of analytical grade provided by Sigma Aldrich. The solution is prepared using zinc acetate dihydrate and ethanol as staring materials in a desired concentration followed by addition of monoethanolamine (MEA) as stabilizing agent. The solution is refluxed for 30 minutes in open air at a temperature of 80°C [125, 132-134, 179]. Thereafter, the solution is left for 24 hours for ageing process in closed environment. The substrates are cleaned ultrasonically in acetone for 6 hours before the deposition of the ZnO layers. After the cleaning process, ZnO layers are deposited using spin coating technique, which is highly reliable for depositing uniform thin films using centrifuge principle. The substrates are baked at 250°C after each coat. After obtaining the desired thickness, the samples are annealed at 600°C for 8 hours. The indigenously developed Gas Calibrator and Testing Apparatus (GCTA), has been used for calibration of gas and measuring of the sensing response of the sensor. The sensing response (S) is given by [139]:

$$S = \frac{R_a - R_g}{R_g} \quad \text{.....(5.3)}$$

Where R_a is the resistance in air, R_g is the resistance in presence of gas. The response time is defined as the time taken by a sensor in attaining 90% change in total resistance in case of adsorption and in case of desorption, it is defined as the recovery time.

5.4.1 Results and discussions

Electrical characterizations of microheater

The resistance of the microheater has been measured at room temperature and comes out to be 105 Ω. The microheater provides a temperature of 160°C at 3.3 volts ratings for. The contact pads of the microheater and the IDE's are connected to the external system for voltage supply and resistance measurements for the IDE's respectively. These connections are made using aluminium wire-bonding technique attached with crocodile clippers further with the measuring instruments.

5.4.2 Gas sensing properties

Figure 5.11 shows the sensing response of the sensor at an operating temperature of 160°C. The gas sensing response is enhanced as compared to the sensor presented by Lupan, et al. [180] and Mondal, et al. [181] showing a response of 4% and 65% respectively. The fabricated sample shows a higher response of ~11 with a lowered optimum operating temperature of 160°C. This can be attributed towards more uniform heating of the active sensing layer over the substrate as the microheater structure is covering a larger area over the substrate as compared to the existing sensor structures which are provided with an external heating source.

Figure 5.12 represents the optimal operating temperature for the hydrogen gas sensing. This behavior for the sensor may bedue to the fast adsorption and desorption of hydrogen gas molecules onto the sensor surface at higher temperatures. But above a certain temperature the mobility of the gas may be decreasing due to very high vibrational energies inside the gas molecule. Hence the trapping of the gas molecules on the surface of the sensing layer becomes strenuous [182].

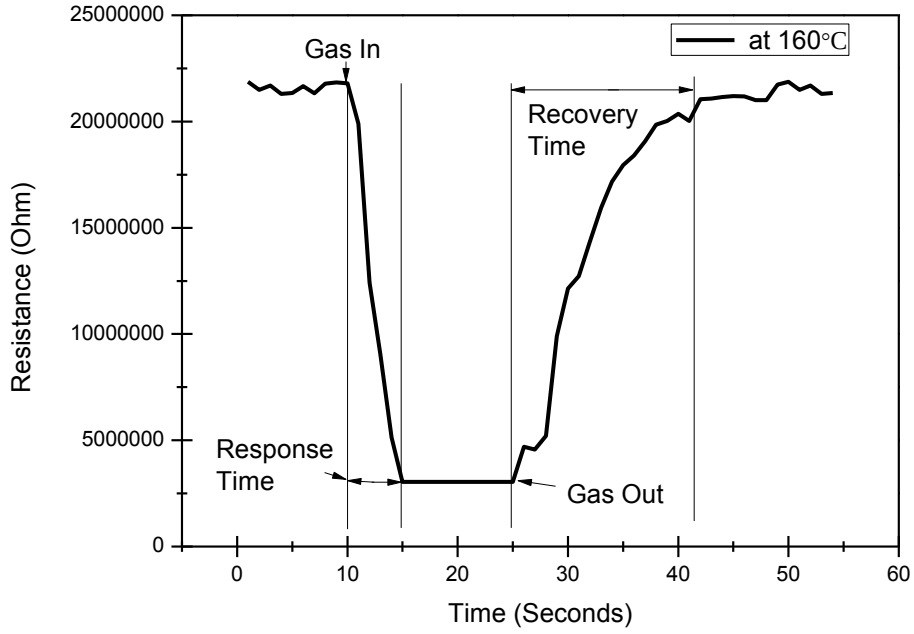

***Figure 5.11**: Gas Sensing Response.*

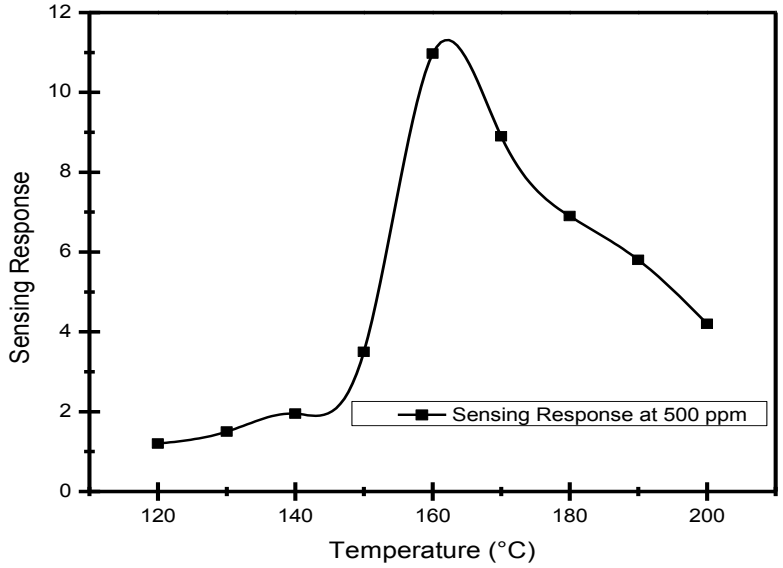

***Figure 5.12:** Sensing response at various Temperatures.*

5.5 Summary

The designed coplanar structure of the microheater and IDE's presents a novel architecture for gas sensor, where the microheater and the IDE's are assembled in a comb like structure. The relative uniformity of the heating is increased over the whole structure of the sensor which helps in increasing the sensing response of the fabricated hydrogen sensor with ZnO thin films as the sensing layer. The present architecture is of 1cm X 1cm in size and the work is going on for reducing the size of the architecture further to the micrometer level.

Conclusions and Future Scope

Conclusions and Future Scope

In this dissertation, the work started with the designing and fabrication of Intergrated Digital Electrodes/Transducers (IDE/IDTs) which are further used for gas sensing application for volatile organic compounds (VOCs). The sensor has been developed for efficient sensitivity by optimizing critical parameters like annealing temperature, thickness for oxidizing gases/vapors and the molarity variations for the sol prepared. Further, the sensor has been studied for enhanced selectivity by addition of the catalysts/dopant/modifier atoms through various methods.

Finally, the gas sensors efficacy is tried to be further improved by implementation of coplanar architecture of IDE/IDT with microheater for the fabricated sensor. The initial attempt to fabricate the coplanar architecture started with analytical studies and simulation using the software tool and then the best architecture has been fabricated. The fabricated structure has been studied for the sensing of reducing gas.

Based on the work carried out in the present thesis, some suggestions for future works includes:

- An efficient and fast acetone sensor has been developed. Hence an effort can be made for its reliability testing and the packaging for commercial applications.
- An effort can be made to investigate the effect of diameter of the nano-clusters in order to optimize their spread or distribution over the sensing layer.
- Further attempts can be made for the improvement of the response time recovery time as well as the low operating temperatures for the fabricated sensor.
- Detection of low concentrations (to the level of few parts per billion (ppb)) shall be attempted for acetone in view of the medico-legal purposes.
- Microheaters must be a wide field of interest, as there are very few researches performed for increasing the uniform heating of the sensing layer which plays a crucial role for high sensitivities.
- An elementary coplanar microheater architecture has been developed which can be further exploited for the various parameters including the thickness of the microheater layer with varying thickness of the microstrips for the heater.

Bibliography

References

[1] C. C. Travis and S. T. Hester Global chemical pollution *Environmental science & technology* 25 pp. 814-819 (1991).

[2] J. M. Gorell, C. Johnson, B. Rybicki, E. Peterson, and R. Richardson The risk of Parkinson's disease with exposure to pesticides, farming, well water, and rural living *Neurology* 50 pp. 1346-1350 (1998).

[3] T. Johns and B. R. Sthapit Biocultural diversity in the sustainability of developing-country food systems *Food and nutrition bulletin* 25 pp. 143-155 (2004).

[4] S. Sharma, S. Kumar, and B. Singh Routing in wireless mesh networks: Three new nature inspired approaches *Wireless Personal Communications* 83 pp. 3157-3179 (2015).

[5] B. Vujičić, N. Cackov, S. Vujičić, and L. Trajković, "Modeling and characterization of traffic in public safety wireless networks," in *Proc. of SPECTS*, 2005.

[6] T. Zhang, S. Mubeen, N. V. Myung, and M. A. Deshusses Recent progress in carbon nanotube-based gas sensors *Nanotechnology* 19 p. 332001 (2008).

[7] P. Mishra, S. Kumar, and D. Singh An approach for finding possible presence of water ice deposits on lunar craters using MiniSAR data *IEEE Journal of Selected Topics in Applied Earth Observations and Remote Sensing* 8 pp. 30-38 (2015).

[8] C. Bisch, X. Mougeot, M.-M. Bé, and A.-M. Nourreddine Development of a system for measuring the shape of β spectra using a semiconductor Si detector *Nuclear Data Sheets* 120 pp. 95-98 (2014).

[9] M. Sharma, A. Kumar, S. Yadav, and Y. Ranga An ultra-wideband printed monopole antenna with dual band-notched characteristics using DGS and SRR *Procedia Technology* 6 pp. 778-783 (2012).

[10] V. Mittal, D. Singh, and L. Saini A critical analysis of EM based fusion of different polarization data for effect on land cover classification *Advances in Space Research* 56 pp. 1094-1105 (2015).

[11] S. Capone, A. Forleo, L. Francioso, R. Rella, P. Siciliano, J. Spadavecchia, *et al.* Solid state gas sensors: state of the art and future activities *Journal of Optoelectronics and Advanced Materials* 5 pp. 1335-1348 (2003).

[12] E. J. Topol, S. R. Steinhubl, and A. Torkamani Digital medical tools and sensors *Jama* 313 pp. 353-354 (2015).

[13] P. Shrivastava, A. Shukla, P. Vepakomma, N. Bhansali, and K. Verma A survey of nature-inspired algorithms for feature selection to identify Parkinson's disease *Computer methods and programs in biomedicine* 139 pp. 171-179 (2017).

[14] A. Agarwal, P. K. Dash, A. K. Singh, S. Sharma, N. Gopalan, P. V. L. Rao, *et al.* Evidence of experimental vertical transmission of emerging novel ECSA genotype of chikungunya virus in Aedes aegypti *PLoS neglected tropical diseases* 8 p. e2990 (2014).

[15] J. D. Keeler, J. P. Havener, D. Godbole, and B. F. I. Ralph, "Virtual emissions monitor for automobile and associated control system," ed: Google Patents, 1997.

[16] D. E. Daniel, *Geotechnical practice for waste disposal*: Springer Science & Business Media, 2012.

[17] P. Tyagi, A. Sharma, M. Tomar, and V. Gupta Metal oxide catalyst assisted SnO 2 thin film based SO 2 gas sensor *Sensors and Actuators B: Chemical* 224 pp. 282-289 (2016).

[18] M. Deshwal and A. Arora Enhanced acetone detection using Au doped ZnO thin film sensor *Journal of Materials Science: Materials in Electronics* pp. 1-6 (2018).

[19] P. Patnaik, *Handbook of environmental analysis: chemical pollutants in air, water, soil, and solid wastes*: Crc Press, 2010.

[20] Z. D.-h. Z. Jian-ping and H. Ju-hua Studies on the enzymatic characteristics of polyphenoloxidase in agaricus bisporus [J] *Food and Machinery* 5 p. 002 (2004).

[21] S. Sheppard The effects of environment and aggregation on the absorption spectra of dyes *Reviews of modern physics* 14 p. 303 (1942).

[22] H. Ibrahim, C. Bindschaedler, E. Doelker, P. Buri, and R. Gurny Aqueous nanodispersions prepared by a salting-out process *International journal of pharmaceutics* 87 pp. 239-246 (1992).

[23] H. B. Singh, D. O'hara, D. Herlth, W. Sachse, D. Blake, J. Bradshaw, *et al.* Acetone in the atmosphere: Distribution, sources, and sinks *Journal of Geophysical Research: Atmospheres* 99 pp. 1805-1819 (1994).
[24] F. P. Labreche and M. S. Goldberg Exposure to organic solvents and breast cancer in women: a hypothesis (1997).
[25] T. Xiao, X.-Y. Wang, Z.-H. Zhao, L. Li, L. Zhang, H.-C. Yao, *et al.* Highly sensitive and selective acetone sensor based on C-doped WO3 for potential diagnosis of diabetes mellitus *Sensors and Actuators B: Chemical* 199 pp. 210-219 (2014).
[26] S. Ampuero and J. Bosset The electronic nose applied to dairy products: a review *Sensors and Actuators B: Chemical* 94 pp. 1-12 (2003).
[27] R. Jaaniso and O. K. Tan, *Semiconductor gas sensors*: Elsevier, 2013.
[28] F. K. Tittel, D. Richter, and A. Fried, "Mid-infrared laser applications in spectroscopy," in *Solid-state mid-infrared laser sources*, ed: Springer, 2003, pp. 458-529.
[29] H. Dubost and L. Abouaf-Marguin Infrared spectra of carbon monoxide trapped in solid argon. Double-doping experiments with H2O, NH3 and N2 *Chemical Physics Letters* 17 pp. 269-273 (1972).
[30] M. Adahchour, J. Beens, R. Vreuls, and U. T. Brinkman Recent developments in comprehensive two-dimensional gas chromatography (GC× GC): I. Introduction and instrumental set-up *TrAC Trends in Analytical Chemistry* 25 pp. 438-454 (2006).
[31] N. H. Snow and G. C. Slack Head-space analysis in modern gas chromatography *TrAC Trends in Analytical Chemistry* 21 pp. 608-617 (2002).
[32] P. Tyagi and V. G. Gupta, "Development of SO2 gas sensor using SnO2 thin film based heterostructures and nanocomposites," Doctrate of Philosophy, Department of Physics & Astrophysics, University of Delhi, University of Delhi, 2017.
[33] A. Paliwal, A. Sharma, M. Tomar, and V. Gupta Room temperature detection of NO2 gas using optical sensor based on surface plasmon resonance technique *Sensors and Actuators B: Chemical* 216 pp. 497-503 (2015).
[34] A. Paliwal, A. Sharma, M. Tomar, and V. Gupta Surface plasmon resonance study on the optical sensing properties of tin oxide (SnO2) films to NH3 gas *Journal of Applied Physics* 119 p. 164502 (2016).
[35] L. Rana, R. Gupta, M. Tomar, and V. Gupta ZnO/ST-quartz SAW resonator: An efficient NO2 gas sensor *Sensors and Actuators B: Chemical* 252 pp. 840-845 (2017).
[36] T. SUZUKI, S. SEKIYAMA, and S. AIZAWA An Electron Microscope Observation of Collagen in Normal Rat Glomeruli *Microscopy* 11 pp. 52-56 (1962).
[37] K. J. Choi and H. W. Jang One-dimensional oxide nanostructures as gas-sensing materials: review and issues *Sensors* 10 pp. 4083-4099 (2010).
[38] A. Cabot, J. Arbiol, J. R. Morante, U. Weimar, N. Barsan, and W. Göpel Analysis of the noble metal catalytic additives introduced by impregnation of as obtained SnO2 sol–gel nanocrystals for gas sensors *Sensors and Actuators B: Chemical* 70 pp. 87-100 (2000).
[39] G. Zhang and M. Liu Effect of particle size and dopant on properties of SnO2-based gas sensors *Sensors and Actuators B: Chemical* 69 pp. 144-152 (2000).
[40] B. B. Rao Zinc oxide ceramic semi-conductor gas sensor for ethanol vapour *Materials Chemistry and Physics* 64 pp. 62-65 (2000).
[41] N. Baik, G. Sakai, N. Miura, and N. Yamazoe Hydrothermally treated sol solution of tin oxide for thin-film gas sensor *Sensors and Actuators B: Chemical* 63 pp. 74-79 (2000).
[42] Z. Ling, C. Leach, and R. Freer Heterojunction gas sensors for environmental NO2 and CO2 monitoring *Journal of the European Ceramic Society* 21 pp. 1977-1980 (2001).
[43] J. Solis, S. Saukko, L. Kish, C. Granqvist, and V. Lantto Semiconductor gas sensors based on nanostructured tungsten oxide *Thin Solid Films* 391 pp. 255-260 (2001).
[44] J. H. Yu and G. M. Choi Selective CO gas detection of CuO-and ZnO-doped SnO2 gas sensor *Sensors and Actuators B: Chemical* 75 pp. 56-61 (2001).
[45] J. Solis, S. Saukko, L. Kish, C. Granqvist, and V. Lantto Nanocrystalline tungsten oxide thick-films with high sensitivity to H2S at room temperature *Sensors and Actuators B: Chemical* 77 pp. 316-321 (2001).

[46] N. Savage, B. Chwieroth, A. Ginwalla, B. R. Patton, S. A. Akbar, and P. K. Dutta Composite n–p semiconducting titanium oxides as gas sensors *Sensors and Actuators B: Chemical* 79 pp. 17-27 (2001).
[47] E. Comini, G. Faglia, G. Sberveglieri, Z. Pan, and Z. L. Wang Stable and highly sensitive gas sensors based on semiconducting oxide nanobelts *Applied Physics Letters* 81 pp. 1869-1871 (2002).
[48] S. Roy and S. Basu Improved zinc oxide film for gas sensor applications *Bulletin of Materials Science* 25 pp. 513-515 (2002).
[49] J. Chang, H. Kuo, I. Leu, and M. Hon The effects of thickness and operation temperature on ZnO: Al thin film CO gas sensor *Sensors and actuators B: Chemical* 84 pp. 258-264 (2002).
[50] W. J. Moon, J. H. Yu, and G. M. Choi The CO and H2 gas selectivity of CuO-doped SnO2–ZnO composite gas sensor *Sensors and Actuators B: Chemical* 87 pp. 464-470 (2002).
[51] J. Tamaki, C. Naruo, Y. Yamamoto, and M. Matsuoka Sensing properties to dilute chlorine gas of indium oxide based thin film sensors prepared by electron beam evaporation *Sensors and Actuators B: Chemical* 83 pp. 190-194 (2002).
[52] G. Neri, A. Bonavita, S. Galvagno, P. Siciliano, and S. Capone CO and NO2 sensing properties of doped-Fe2O3 thin films prepared by LPD *Sensors and Actuators B: Chemical* 82 pp. 40-47 (2002).
[53] D.-S. Lee, Y. T. Kim, J.-S. Huh, and D.-D. Lee Fabrication and characteristics of SnO2 gas sensor array for volatile organic compounds recognition *Thin Solid Films* 416 pp. 271-278 (2002).
[54] N. Barsan and U. Weimar Understanding the fundamental principles of metal oxide based gas sensors; the example of CO sensing with SnO2 sensors in the presence of humidity *Journal of Physics: Condensed Matter* 15 p. R813 (2003).
[55] D. Nicolas-Debarnot and F. Poncin-Epaillard Polyaniline as a new sensitive layer for gas sensors *Analytica Chimica Acta* 475 pp. 1-15 (2003).
[56] N. Yamazoe, G. Sakai, and K. Shimanoe Oxide semiconductor gas sensors *Catalysis Surveys from Asia* 7 pp. 63-75 (2003).
[57] J. Li, Y. Lu, Q. Ye, M. Cinke, J. Han, and M. Meyyappan Carbon nanotube sensors for gas and organic vapor detection *Nano letters* 3 pp. 929-933 (2003).
[58] X.-L. Li, T.-J. Lou, X.-M. Sun, and Y.-D. Li Highly sensitive WO3 hollow-sphere gas sensors *Inorganic chemistry* 43 pp. 5442-5449 (2004).
[59] F. Villalpando-Paez, A. Romero, E. Munoz-Sandoval, L. Martınez, H. Terrones, and M. Terrones Fabrication of vapor and gas sensors using films of aligned CNx nanotubes *Chemical Physics Letters* 386 pp. 137-143 (2004).
[60] X. Niu, W. Du, and W. Du Preparation and gas sensing properties of ZnM2O4 (M= Fe, Co, Cr) *Sensors and actuators B: chemical* 99 pp. 405-409 (2004).
[61] B. Zhu, C. Xie, W. Wang, K. Huang, and J. Hu Improvement in gas sensitivity of ZnO thick film to volatile organic compounds (VOCs) by adding TiO 2 *Materials Letters* 58 pp. 624-629 (2004).
[62] P. Sahay Zinc oxide thin film gas sensor for detection of acetone *Journal of Materials Science* 40 pp. 4383-4385 (2005).
[63] S. T. Shishiyanu, T. S. Shishiyanu, and O. I. Lupan Sensing characteristics of tin-doped ZnO thin films as NO 2 gas sensor *Sensors and Actuators B: Chemical* 107 pp. 379-386 (2005).
[64] K. S. Yoo, S. H. Park, and J. H. Kang Nano-grained thin-film indium tin oxide gas sensors for H2 detection *Sensors and Actuators B: Chemical* 108 pp. 159-164 (2005).
[65] J. Zhang, J. Liu, Q. Peng, X. Wang, and Y. Li Nearly monodisperse Cu2O and CuO nanospheres: preparation and applications for sensitive gas sensors *Chemistry of materials* 18 pp. 867-871 (2006).
[66] L. Zhang, H. Qin, P. Song, J. Hu, and M. Jiang Electric properties and acetone-sensing characteristics of La1− xPbxFeO3 perovskite system *Materials chemistry and physics* 98 pp. 358-362 (2006).
[67] X. Liu, H. Ji, Y. Gu, and M. Xu Preparation and acetone sensitive characteristics of nano-LaFeO3 semiconductor thin films by polymerization complex method *Materials Science and Engineering: B* 133 pp. 98-101 (2006).

[68] J. Zhao, L.-H. Huo, S. Gao, H. Zhao, and J.-G. Zhao Alcohols and acetone sensing properties of SnO2 thin films deposited by dip-coating *Sensors and Actuators B: Chemical* 115 pp. 460-464 (2006).
[69] N. Rezlescu, N. Iftimie, E. Rezlescu, C. Doroftei, and P. Popa Semiconducting gas sensor for acetone based on the fine grained nickel ferrite *Sensors and Actuators B: Chemical* 114 pp. 427-432 (2006).
[70] R. Rella, J. Spadavecchia, M. Manera, S. Capone, A. Taurino, M. Martino, *et al.* Acetone and ethanol solid-state gas sensors based on TiO2 nanoparticles thin film deposited by matrix assisted pulsed laser evaporation *Sensors and Actuators B: Chemical* 127 pp. 426-431 (2007).
[71] G. Zhang, C. Li, F. Cheng, and J. Chen ZnFe2O4 tubes: synthesis and application to gas sensors with high sensitivity and low-energy consumption *Sensors and Actuators B: Chemical* 120 pp. 403-410 (2007).
[72] K.-W. Kim, P.-S. Cho, S.-J. Kim, J.-H. Lee, C.-Y. Kang, J.-S. Kim, *et al.* The selective detection of C2H5OH using SnO2–ZnO thin film gas sensors prepared by combinatorial solution deposition *Sensors and Actuators B: Chemical* 123 pp. 318-324 (2007).
[73] T.-J. Hsueh, C.-L. Hsu, S.-J. Chang, and I.-C. Chen Laterally grown ZnO nanowire ethanol gas sensors *Sensors and Actuators B: Chemical* 126 pp. 473-477 (2007).
[74] C. Ge, C. Xie, and S. Cai Preparation and gas-sensing properties of Ce-doped ZnO thin-film sensors by dip-coating *Materials Science and Engineering: B* 137 pp. 53-58 (2007).
[75] S.-J. Chang, T.-J. Hsueh, I.-C. Chen, S.-F. Hsieh, S.-P. Chang, C.-L. Hsu, *et al.* Highly sensitive ZnO nanowire acetone vapor sensor with Au adsorption *IEEE transactions on nanotechnology* 7 pp. 754-759 (2008).
[76] Q. Qi, T. Zhang, L. Liu, X. Zheng, Q. Yu, Y. Zeng, *et al.* Selective acetone sensor based on dumbbell-like ZnO with rapid response and recovery *Sensors and Actuators B: Chemical* 134 pp. 166-170 (2008).
[77] L. Qin, J. Xu, X. Dong, Q. Pan, Z. Cheng, Q. Xiang, *et al.* The template-free synthesis of square-shaped SnO2 nanowires: the temperature effect and acetone gas sensors *Nanotechnology* 19 p. 185705 (2008).
[78] M.-W. Ahn, K.-S. Park, J.-H. Heo, D.-W. Kim, K. J. Choi, and J.-G. Park On-chip fabrication of ZnO-nanowire gas sensor with high gas sensitivity *Sensors and Actuators B: Chemical* 138 pp. 168-173 (2009).
[79] A. Wisitsoraat, A. Tuantranont, E. Comini, G. Sberveglieri, and W. Wlodarski Characterization of n-type and p-type semiconductor gas sensors based on NiOx doped TiO2 thin films *Thin Solid Films* 517 pp. 2775-2780 (2009).
[80] S. Zhu, D. Zhang, J. Gu, J. Xu, J. Dong, and J. Li Biotemplate fabrication of SnO 2 nanotubular materials by a sonochemical method for gas sensors *Journal of Nanoparticle Research* 12 pp. 1389-1400 (2010).
[81] N. Kakati, S. H. Jee, S. H. Kim, J. Y. Oh, and Y. S. Yoon Thickness dependency of sol-gel derived ZnO thin films on gas sensing behaviors *Thin Solid Films* 519 pp. 494-498 (2010).
[82] R. Pawar, J. Shaikh, A. Moholkar, S. Pawar, J. Kim, J. Patil, *et al.* Surfactant assisted low temperature synthesis of nanocrystalline ZnO and its gas sensing properties *Sensors and Actuators B: Chemical* 151 pp. 212-218 (2010).
[83] Z. Wen and L. Tian-Mo Gas-sensing properties of SnO2–TiO2-based sensor for volatile organic compound gas and its sensing mechanism *Physica B: Condensed Matter* 405 pp. 1345-1348 (2010).
[84] P. Murade, V. Sangawar, G. Chaudhari, V. Kapse, and A. Bajpeyee Acetone gas-sensing performance of Sr-doped nanostructured LaFeO3 semiconductor prepared by citrate sol–gel route *Current Applied Physics* 11 pp. 451-456 (2011).
[85] L. Liu, S. Li, J. Zhuang, L. Wang, J. Zhang, H. Li, *et al.* Improved selective acetone sensing properties of Co-doped ZnO nanofibers by electrospinning *Sensors and actuators B: chemical* 155 pp. 782-788 (2011).
[86] H. Ahn, Y. Wang, S. H. Jee, M. Park, Y. S. Yoon, and D.-J. Kim Enhanced UV activation of electrochemically doped Ni in ZnO nanorods for room temperature acetone sensing *Chemical Physics Letters* 511 pp. 331-335 (2011).

[87] J. Shi, G. Hu, Y. Sun, M. Geng, J. Wu, Y. Liu, *et al.* WO3 nanocrystals: synthesis and application in highly sensitive detection of acetone *Sensors and Actuators B: Chemical* 156 pp. 820-824 (2011).
[88] M. Righettoni, A. Tricoli, S. Gass, A. Schmid, A. Amann, and S. E. Pratsinis Breath acetone monitoring by portable Si: WO3 gas sensors *Analytica chimica acta* 738 pp. 69-75 (2012).
[89] P. Gao, H. Ji, Y. Zhou, and X. Li Selective acetone gas sensors using porous WO3–Cr2O3 thin films prepared by sol–gel method *Thin Solid Films* 520 pp. 3100-3106 (2012).
[90] P. Song, Q. Wang, and Z. Yang Preparation, characterization and acetone sensing properties of Ce-doped SnO2 hollow spheres *Sensors and Actuators B: Chemical* 173 pp. 839-846 (2012).
[91] X.-j. Wang, W. Wang, and Y.-L. Liu Enhanced acetone sensing performance of Au nanoparticles functionalized flower-like ZnO *Sensors and Actuators B: Chemical* 168 pp. 39-45 (2012).
[92] Y. Zhang, W. He, H. Zhao, and P. Li Template-free to fabricate highly sensitive and selective acetone gas sensor based on WO3 microspheres *Vacuum* 95 pp. 30-34 (2013).
[93] J.-S. Do and S.-H. Wang On the sensitivity of conductimetric acetone gas sensor based on polypyrrole and polyaniline conducting polymers *Sensors and Actuators B: Chemical* 185 pp. 39-46 (2013).
[94] H. Shan, C. Liu, L. Liu, S. Li, L. Wang, X. Zhang, *et al.* Highly sensitive acetone sensors based on La-doped α-Fe2O3 nanotubes *Sensors and actuators B: chemical* 184 pp. 243-247 (2013).
[95] C. Shao, Y. Chang, and Y. Long High performance of nanostructured ZnO film gas sensor at room temperature *Sensors and Actuators B: Chemical* 204 pp. 666-672 (2014).
[96] S. Liu, B. Yu, H. Zhang, T. Fei, and T. Zhang Enhancing NO2 gas sensing performances at room temperature based on reduced graphene oxide-ZnO nanoparticles hybrids *Sensors and Actuators B: Chemical* 202 pp. 272-278 (2014).
[97] V. Talwar, O. Singh, and R. C. Singh ZnO assisted polyaniline nanofibers and its application as ammonia gas sensor *Sensors and Actuators B: Chemical* 191 pp. 276-282 (2014).
[98] J. Cheng, B. Wang, M. Zhao, F. Liu, and X. Zhang Nickel-doped tin oxide hollow nanofibers prepared by electrospinning for acetone sensing *Sensors and Actuators B: Chemical* 190 pp. 78-85 (2014).
[99] Z. Hosseini and A. Mortezaali Room temperature H2S gas sensor based on rather aligned ZnO nanorods with flower-like structures *Sensors and Actuators B: Chemical* 207 pp. 865-871 (2015).
[100] X. Zhou, J. Liu, C. Wang, P. Sun, X. Hu, X. Li, *et al.* Highly sensitive acetone gas sensor based on porous ZnFe2O4 nanospheres *Sensors and Actuators B: Chemical* 206 pp. 577-583 (2015).
[101] C. Wang, J. Liu, Q. Yang, P. Sun, Y. Gao, F. Liu, *et al.* Ultrasensitive and low detection limit of acetone gas sensor based on W-doped NiO hierarchical nanostructure *Sensors and Actuators B: Chemical* 220 pp. 59-67 (2015).
[102] G. Korotcenkov, "Surface Modifiers for Metal Oxides in Conductometric Gas Sensors," in *Handbook of Gas Sensor Materials*, ed: Springer, 2013, pp. 273-286.
[103] E. Comini and G. Sberveglieri Metal oxide nanowires as chemical sensors *Materials Today* 13 pp. 36-44 (2010).
[104] G. Korotcenkov and B. Cho Instability of metal oxide-based conductometric gas sensors and approaches to stability improvement (short survey) *Sensors and Actuators B: Chemical* 156 pp. 527-538 (2011).
[105] G. Singh, A. Choudhary, D. Haranath, A. G. Joshi, N. Singh, S. Singh, *et al.* ZnO decorated luminescent graphene as a potential gas sensor at room temperature *Carbon* 50 pp. 385-394 (2012).
[106] S. Benkara, S. Zerkout, and H. Ghamri Synthesis of Sn doped ZnO/TiO2 nanocomposite film and their application to H2 gas sensing properties *Materials Science in Semiconductor Processing* 16 pp. 1271-1279 (2013).
[107] L. Chow, O. Lupan, G. Chai, H. Khallaf, L. Ono, B. R. Cuenya, *et al.* Synthesis and characterization of Cu-doped ZnO one-dimensional structures for miniaturized sensor applications with faster response *Sensors and Actuators A: Physical* 189 pp. 399-408 (2013).
[108] M. Hjiri, L. El Mir, S. Leonardi, A. Pistone, L. Mavilia, and G. Neri Al-doped ZnO for highly sensitive CO gas sensors *Sensors and Actuators B: Chemical* 196 pp. 413-420 (2014).

[109] S. Bai, J. Liu, J. Guo, R. Luo, D. Li, Y. Song, *et al.* Facile preparation of SnO2/NiO composites and enhancement of sensing performance to NO2 *Sensors and Actuators B: Chemical* 249 pp. 22-29 (2017).
[110] L. Li, S. He, M. Liu, C. Zhang, and W. Chen Three-dimensional mesoporous graphene aerogel-supported SnO2 nanocrystals for high-performance NO2 gas sensing at low temperature *Analytical chemistry* 87 pp. 1638-1645 (2015).
[111] M. N. Cardoza-Contreras, J. M. Romo-Herrera, L. A. Ríos, R. García-Gutiérrez, T. Zepeda, and O. E. Contreras Single ZnO nanowire-based gas sensors to detect low concentrations of hydrogen *Sensors* 15 pp. 30539-30544 (2015).
[112] K. Wasa, M. Kitabatake, and H. Adachi, *Thin film materials technology: sputtering of control compound materials*: Springer Science & Business Media, 2004.
[113] L. B. Freund and S. Suresh, *Thin film materials: stress, defect formation and surface evolution*: Cambridge University Press, 2004.
[114] W. Li, H. Jung, N. D. Hoa, D. Kim, S.-K. Hong, and H. Kim Nanocomposite of cobalt oxide nanocrystals and single-walled carbon nanotubes for a gas sensor application *Sensors and Actuators B: Chemical* 150 pp. 160-166 (2010).
[115] R. Waser, T. Schneller, S. Hoffmann-eifert, and P. Ehrhart Advanced chemical deposition techniques-from research to production *Integrated Ferroelectrics* 36 pp. 3-20 (2001).
[116] L. Karakchiev, T. Zima, and N. Lyakhov Low-temperature synthesis of zirconium titanate *Inorganic materials* 37 pp. 386-390 (2001).
[117] M. V. Landau Sol–Gel Process *Handbook of Heterogeneous Catalysis: Online* pp. 119-160 (2008).
[118] P. Chakrabarti Interaction of metal ions with carboxylic and carboxamide groups in protein structures *Protein Engineering, Design and Selection* 4 pp. 49-56 (1990).
[119] Y. Natsume and H. Sakata Zinc oxide films prepared by sol-gel spin-coating *Thin solid films* 372 pp. 30-36 (2000).
[120] S. Sakka and H. Kozuka, *Handbook of sol-gel science and technology. 1. Sol-gel processing* vol. 1: Springer Science & Business Media, 2005.
[121] B. N. Chapman, *Glow discharge processes: sputtering and plasma etching*: Wiley, 1980.
[122] A. Sharma, S. Bahniwal, S. Aggarwal, S. Chopra, and D. Kanjilal Synthesis of copper nanoparticles in polycarbonate by ion implantation *Bulletin of Materials Science* 34 p. 645 (2011).
[123] W. Kern, *Thin film processes II* vol. 2: Elsevier, 2012.
[124] B. D. Cullity and S. R. Stock, *Elements of X-ray Diffraction*: Pearson Education, 2014.
[125] D. Sarid, *Scanning force microscopy: with applications to electric, magnetic, and atomic forces* vol. 5: Oxford University Press on Demand, 1994.
[126] K. S. Suvarna, C. Layton, and J. D. Bancroft, *Bancroft's Theory and Practice of Histological Techniques E-Book*: Elsevier Health Sciences, 2018.
[127] F. C. Jentoft Ultraviolet–visible–near infrared spectroscopy in catalysis: theory, experiment, analysis, and application under reaction conditions *Advances in catalysis* 52 pp. 129-211 (2009).
[128] S. Sze VLSI Technology,(1988) *Google Scholar* p. 131 (1994).
[129] M. J. Zehetbauer and Y. T. Zhu, *Bulk nanostructured materials*: John Wiley & Sons, 2009.
[130] D. Haridas, A. Chowdhuri, K. Sreenivas, and V. Gupta Effect of thickness of platinum catalyst clusters on response of SnO 2 thin film sensor for LPG *Sensors and Actuators B: Chemical* 153 pp. 89-95 (2011).
[131] A. Arora, A. Arora, P. George, V. Dwivedi, and V. Gupta Effect of Different Post Deposition Annealing Treatments on Properties of Zinc Oxide Thin Films *Sensors & Transducers* 117 p. 92 (2010).
[132] J. W. Gardner and P. N. Bartlett, *Electronic noses: principles and applications* vol. 233: Oxford university press New York, 1999.
[133] X. Liu, S. Cheng, H. Liu, S. Hu, D. Zhang, and H. Ning A survey on gas sensing technology *Sensors* 12 pp. 9635-9665 (2012).
[134] A. V. Mamishev, K. Sundara-Rajan, F. Yang, Y. Du, and M. Zahn Interdigital sensors and transducers *Proceedings of the IEEE* 92 pp. 808-845 (2004).

[135] B. J. Lin Deep UV lithography *Journal of Vacuum Science and Technology* 12 pp. 1317-1320 (1975).
[136] P. Köllensperger, W. Karl, M. Ahmad, W. Pike, and M. Green Patterning of platinum (Pt) thin films by chemical wet etching in Aqua Regia *Journal of Micromechanics and Microengineering* 22 p. 067001 (2012).
[137] T. Ivanova, A. Harizanova, T. Koutzarova, and B. Vertruyen Study of ZnO sol–gel films: effect of annealing *Materials letters* 64 pp. 1147-1149 (2010).
[138] D. Bao, H. Gu, and A. Kuang Sol-gel-derived c-axis oriented ZnO thin films *Thin solid films* 312 pp. 37-39 (1998).
[139] A. Arora, P. George, V. Dwivedi, and V. Gupta Post-deposition treatment behaviour of zinc oxide thin films in hydrogen peroxide solution *Materials Science and Technology* 25 pp. 591-594 (2009).
[140] M. Deshwal and A. Arora Enhanced acetone detection using Au doped ZnO thin film sensor *Journal of Materials Science: Materials in Electronics* In Press February 23 (2018).
[141] M. Dutta, S. Mridha, and D. Basak Effect of sol concentration on the properties of ZnO thin films prepared by sol–gel technique *Applied Surface Science* 254 pp. 2743-2747 (2008).
[142] S. Ilican, Y. Caglar, and M. Caglar Preparation and characterization of ZnO thin films deposited by sol-gel spin coating method *Journal of optoelectronics and advanced materials* 10 pp. 2578-2583 (2008).
[143] D. Raoufi and T. Raoufi The effect of heat treatment on the physical properties of sol–gel derived ZnO thin films *Applied Surface Science* 255 pp. 5812-5817 (2009).
[144] A. Katoch, Z. U. Abideen, J.-H. Kim, and S. S. Kim Crystallinity dependent gas-sensing abilities of ZnO hollow fibers *Metals and Materials International* 22 pp. 942-946 (2016).
[145] P. Tyagi, S. Sharma, M. Tomar, F. Singh, and V. Gupta Swift heavy ion irradiated SnO 2 thin film sensor for efficient detection of SO 2 gas *Nuclear Instruments and Methods in Physics Research Section B: Beam Interactions with Materials and Atoms* 379 pp. 219-223 (2016).
[146] Y. Lv, L. Guo, H. Xu, and X. Chu Gas-sensing properties of well-crystalline ZnO nanorods grown by a simple route *Physica E: Low-dimensional Systems and Nanostructures* 36 pp. 102-105 (2007).
[147] A. Sharma, M. Tomar, and V. Gupta WO 3 nanoclusters–SnO 2 film gas sensor heterostructure with enhanced response for NO 2 *Sensors and Actuators B: Chemical* 176 pp. 675-684 (2013).
[148] H. Bian, S. Ma, A. Sun, X. Xu, G. Yang, S. Yan, *et al.* Improvement of acetone gas sensing performance of ZnO nanoparticles *Journal of Alloys and Compounds* 658 pp. 629-635 (2016).
[149] M. Kumar, A. Kumar, and A. Abhyankar SnO 2 based sensors with improved sensitivity and response-recovery time *Ceramics International* 40 pp. 8411-8418 (2014).
[150] N. Al-Hardan, M. Abdullah, A. A. Aziz, H. Ahmad, and L. Low ZnO thin films for VOC sensing applications *Vacuum* 85 pp. 101-106 (2010).
[151] O. Lupan, V. Ursaki, G. Chai, L. Chow, G. Emelchenko, I. Tiginyanu, *et al.* Selective hydrogen gas nanosensor using individual ZnO nanowire with fast response at room temperature *Sensors and Actuators B: Chemical* 144 pp. 56-66 (2010).
[152] J. Xu, J. Han, Y. Zhang, Y. a. Sun, and B. Xie Studies on alcohol sensing mechanism of ZnO based gas sensors *Sensors and Actuators B: Chemical* 132 pp. 334-339 (2008).
[153] H. Xu, X. Liu, D. Cui, M. Li, and M. Jiang A novel method for improving the performance of ZnO gas sensors *Sensors and Actuators B: Chemical* 114 pp. 301-307 (2006).
[154] C. S. Rout, S. H. Krishna, S. Vivekchand, A. Govindaraj, and C. Rao Hydrogen and ethanol sensors based on ZnO nanorods, nanowires and nanotubes *Chemical Physics Letters* 418 pp. 586-590 (2006).
[155] B. Liu and H. C. Zeng Hydrothermal synthesis of ZnO nanorods in the diameter regime of 50 nm *Journal of the American Chemical Society* 125 pp. 4430-4431 (2003).
[156] W. Xu, Z. Ye, D. Ma, H. Lu, L. Zhu, B. Zhao, *et al.* Quasi-aligned ZnO nanotubes grown on Si substrates *Applied Physics Letters* 87 p. 093110 (2005).
[157] L. Liao, H. Lu, J. Li, C. Liu, D. Fu, and Y. Liu The sensitivity of gas sensor based on single ZnO nanowire modulated by helium ion radiation *Applied Physics Letters* 91 p. 173110 (2007).
[158] Y. Li, Y. Bando, T. Sato, and K. Kurashima ZnO nanobelts grown on Si substrate *Applied Physics Letters* 81 pp. 144-146 (2002).

[159] Z. W. Pan, Z. R. Dai, and Z. L. Wang Nanobelts of semiconducting oxides *Science* 291 pp. 1947-1949 (2001).
[160] P. Pawinrat, O. Mekasuwandumrong, and J. Panpranot Synthesis of Au–ZnO and Pt–ZnO nanocomposites by one-step flame spray pyrolysis and its application for photocatalytic degradation of dyes *Catalysis Communications* 10 pp. 1380-1385 (2009).
[161] B. Szyszka and S. Jäger Optical and electrical properties of doped zinc oxide films prepared by ac reactive magnetron sputtering *Journal of non-crystalline solids* 218 pp. 74-80 (1997).
[162] N. Hongsith, C. Viriyaworasakul, P. Mangkorntong, N. Mangkorntong, and S. Choopun Ethanol sensor based on ZnO and Au-doped ZnO nanowires *Ceramics International* 34 pp. 823-826 (2008).
[163] A. Rahm, G. Yang, M. Lorenz, T. Nobis, J. Lenzner, G. Wagner, *et al.* Two-dimensional ZnO: Al nanosheets and nanowalls obtained by Al 2 O 3-assisted carbothermal evaporation *Thin Solid Films* 486 pp. 191-194 (2005).
[164] S. T. Tan, B. Chen, X. Sun, W. Fan, H. S. Kwok, X. Zhang, *et al.* Blueshift of optical band gap in ZnO thin films grown by metal-organic chemical-vapor deposition *Journal of Applied Physics* 98 p. 013505 (2005).
[165] Y. Li, T. Lv, F.-X. Zhao, Q. Wang, X.-X. Lian, and Y.-L. Zou Enhanced acetone-sensing performance of Au/ZnO hybrids synthesized using a solution combustion method *Electronic Materials Letters* 11 pp. 890-895 (2015).
[166] S. Bai, T. Guo, D. Li, R. Luo, A. Chen, and C. C. Liu Intrinsic sensing properties of the flower-like ZnO nanostructures *Sensors and Actuators B: Chemical* 182 pp. 747-754 (2013).
[167] M. Egashira, N. Kanehara, Y. Shimizu, and H. Iwanaga Gas-sensing characteristics of Li+-doped and undoped ZnO whiskers *Sensors and Actuators* 18 pp. 349-360 (1989).
[168] Y. Shimizu, S. Kai, Y. Takao, T. Hyodo, and M. Egashira Correlation between methylmercaptan gas-sensing properties and its surface chemistry of SnO 2-based sensor materials *Sensors and Actuators B: Chemical* 65 pp. 349-357 (2000).
[169] M.-W. Ahn, K.-S. Park, J.-H. Heo, J.-G. Park, D.-W. Kim, K. J. Choi, *et al.* Gas sensing properties of defect-controlled ZnO-nanowire gas sensor *Applied physics letters* 93 p. 263103 (2008).
[170] N. Han, X. Wu, L. Chai, H. Liu, and Y. Chen Counterintuitive sensing mechanism of ZnO nanoparticle based gas sensors *Sensors and Actuators B: Chemical* 150 pp. 230-238 (2010).
[171] N. Al-Hardan, M. Abdullah, and A. A. Aziz Performance of Cr-doped ZnO for acetone sensing *Applied Surface Science* 270 pp. 480-485 (2013).
[172] H. Zhang and W. Chen Tungsten Oxide (WO3) Micro Balls Composed of Curly Nanosheets for Transformer Fault Gas Diagnosis *Journal of Nanoelectronics and Optoelectronics* 12 pp. 1305-1308 (2017).
[173] M. Deshwal and A. Arora Enhanced Sensitivity with Thickness Optimization of ZnO based Acetone Sensor *Indian Journal of Pure and Applied Physics* p. In Press (2018).
[174] Z. Ren, H. Zhao, and Z. Liu Design and Fabrication of Zinc Oxide and Polyethylene Terephthalate Based Nano-Generator for Sensing Applications *Journal of Nanoelectronics and Optoelectronics* 12 pp. 1309-1313 (2017).
[175] K.-N. Lee, D.-S. Lee, S.-W. Jung, Y.-H. Jang, Y.-K. Kim, and W.-K. Seong A high-temperature MEMS heater using suspended silicon structures *Journal of Micromechanics and Microengineering* 19 p. 115011 (2009).
[176] P. Bhattacharyya, P. Basu, B. Mondal, and H. Saha A low power MEMS gas sensor based on nanocrystalline ZnO thin films for sensing methane *Microelectronics Reliability* 48 pp. 1772-1779 (2008).
[177] J.-K. Choi, I.-S. Hwang, S.-J. Kim, J.-S. Park, S.-S. Park, U. Jeong, *et al.* Design of selective gas sensors using electrospun Pd-doped SnO 2 hollow nanofibers *Sensors and Actuators B: Chemical* 150 pp. 191-199 (2010).
[178] M. A. Andio, P. N. Browning, P. A. Morris, and S. A. Akbar Comparison of gas sensor performance of SnO 2 nano-structures on microhotplate platforms *Sensors and Actuators B: Chemical* 165 pp. 13-18 (2012).
[179] K.-Y. Choi, J.-S. Park, K.-B. Park, H. J. Kim, H.-D. Park, and S.-D. Kim Low power micro-gas sensors using mixed SnO 2 nanoparticles and MWCNTs to detect NO 2, NH 3, and xylene

gases for ubiquitous sensor network applications *Sensors and Actuators B: Chemical* 150 pp. 65-72 (2010).
[180] B. Jiang, P. Muralt, P. Heeb, A. J. Santis-Alvarez, M. Nabavi, D. Poulikakos, *et al.* A micro heater platform with fluid channels for testing micro-solid oxide fuel cell components *Sensors and Actuators B: Chemical* 175 pp. 218-224 (2012).
[181] S. Zhang and L. Zhang High Sensitive Formaldehyde Gas Sensing Devices Based on Nickel Oxide Nanowires and Nanodisks *Journal of Nanoelectronics and Optoelectronics* 12 pp. 1355-1359 (2017).
[182] I. Bársony, P. Fürjes, M. Ádám, C. Dücső, Z. Vízváry, J. Zettner, *et al.* Thermal response of microfilament heaters in gas sensing *Sensors and Actuators B: Chemical* 103 pp. 442-447 (2004).
[183] T. Bechtold, E. B. Rudnyi, and J. G. Korvink Dynamic electro-thermal simulation of microsystems—a review *Journal of micromechanics and microengineering* 15 p. R17 (2005).
[184] D. C. Meier, S. Semancik, B. Button, E. Strelcov, and A. Kolmakov Coupling nanowire chemiresistors with MEMS microhotplate gas sensing platforms *Applied Physics Letters* 91 p. 063118 (2007).
[185] S. S. Mondal, "Development of MEMS Based Coplanar Microheater Structures using Finite Element Method," 2013.
[186] M. Deshwal and A. Arora, "A highly sensitive Pt-doped ZnO based Ethanol sensor," in *Emerging Trends in Computing and Communication Technologies (ICETCCT), International Conference on*, 2017, pp. 1-3.
[187] O. Lupan, G. Chai, and L. Chow Novel hydrogen gas sensor based on single ZnO nanorod *Microelectronic Engineering* 85 pp. 2220-2225 (2008).
[188] B. Mondal, S. Maity, S. Das, D. Panda, H. Saha, and A. Kundu Fabrication and packaging of MEMS based platform for hydrogen sensor using ZnO–SnO2 composites *Microsystem Technologies* 22 pp. 2757-2764 (2016).
[189] M. Islam and J. Podder Optical properties of ZnO nano fiber thin films grown by spray pyrolysis of zinc acetate precursor *Crystal Research and Technology* 44 pp. 286-292 (2009).